The Kirchhoff plate equation on surfaces: the surface Hellan–Herrmann–Johnson method

SHAWN W. WALKER

Department of Mathematics, Louisiana State University, Baton Rouge, LA 70803, USA walker@math.lsu.edu

[Received on 13 August 2020; revised on 01 April 2021]

We present a mixed finite element method for approximating a fourth-order elliptic partial differential equation (PDE), the Kirchhoff plate equation, on a surface embedded in \mathbb{R}^3 , with or without boundary. Error estimates are given in mesh-dependent norms that account for the surface approximation and the approximation of the surface PDE. The method is built on the classic Hellan–Herrmann–Johnson method (for flat domains), and convergence is established for C^{k+1} surfaces, with degree k (Lagrangian, parametrically curved) approximation of the surface, for any $k \ge 1$. Mixed boundary conditions are allowed, including clamped, simply-supported and free conditions; if free conditions are present then the surface must be at least $C^{2,1}$. The framework uses tools from differential geometry and is directly related to the seminal work of Dziuk, G. (1988) Finite elements for the Beltrami operator on arbitrary surfaces. *Partial Differential Equations and Calculus of Variations*, vol. 1357 (S. Hildebrandt & R. Leis eds). Berlin, Heidelberg: Springer, pp. 142–155. for approximating the Laplace–Beltrami equation. The analysis here is the first to handle the full surface Hessian operator directly. Numerical examples are given on nontrivial surfaces that demonstrate our convergence estimates. In addition, we show how the surface biharmonic equation can be solved with this method.

Keywords: surface Kirchhoff plate; surface biharmonic; surface finite elements; open surfaces; mesh-dependent norms; geometric consistency error; nonconforming method.

1. Introduction

Physical models involving partial differential equations (PDEs) on surfaces have become quite popular, e.g. surface tension driven droplet motion (Gerbeau & Lelièvre, 2009; Walker *et al.*, 2009; Barrett *et al.*, 2015), surface diffusion (Smereka, 2003; Bänsch *et al.*, 2005), the Stefan problem (Barrett *et al.*, 2010; Davis & Walker, 2015, 2017), elastic bending problems (Timoshenko & Woinowsky-Krieger, 1959; Barrett *et al.*, 2007; Bartels *et al.*, 2017, 2012), biomembranes (Zhong-can & Helfrich, 1989; Du *et al.*, 2004, 2005; Dziuk, 2008; Bonito *et al.*, 2010; Barrett *et al.*, 2016) and other diffusive processes on surfaces (Elliott & Stinner, 2010; Elliott *et al.*, 2012; Elliott & Ranner, 2015). In particular, fourth-order elliptic operators appear in some of these applications, e.g. biomembranes (Elliott & Stinner, 2010; Bonito *et al.*, 2011) and the surface Cahn–Hilliard equation (Elliott & Ranner, 2015).

In this paper we develop and analyze a finite element method (FEM) to solve the surface version of the Kirchhoff plate equation. In addition, we show how the method can be used to solve the surface bi-Laplace (or bi-harmonic) equation. The main object to approximate here is the fourth-order differential operator $\operatorname{div}_{\Gamma} \operatorname{div}_{\Gamma} (\operatorname{hess}_{\Gamma} u) \equiv \nabla_{\alpha} \nabla_{\beta} \nabla^{\alpha} \nabla^{\beta} u$, where $\nabla_{\alpha} (\nabla^{\alpha})$ are covariant (contravariant) derivatives relative to a given surface Γ (see also (A.10), (A.11)). This operator is *not* the same as the surface bi-harmonic operator $(\Delta_{\Gamma})^2 u \equiv \nabla_{\beta} \nabla^{\beta} (\nabla_{\alpha} \nabla^{\alpha} u)$ because of the geometry of the surface, i.e. if the surface has nonzero Gaussian curvature (Eisenhart, 1926; Kreyszig, 1991; do Carmo, 1992).

Moreover, even for surfaces with vanishing Gaussian curvature, these two operators are not equivalent with respect to all types of fourth-order boundary conditions.

It is well known that fourth-order elliptic equations present difficulties for FEMs, even in the flat case. One issue is dealing with the Sobolev space H^2 . Another is correctly capturing fourth-order-type boundary conditions; in fact the classic Babuška paradox illustrates this beautifully (Babuška *et al.*, 1980). Among the various methods for the Kirchhoff plate problem, the Hellan–Herrmann–Johnson (HHJ) mixed method is one of the most powerful (Brezzi & Marini, 1975; Brezzi & Raviart, 1976; Arnold & Brezzi, 1985; Babuška *et al.*, 1980; Brezzi *et al.*, 1980; Comodi, 1989; Blum & Rannacher, 1990; Stenberg, 1991; Krendl *et al.*, 2016; Rafetseder & Zulehner, 2018). It yields stable discretizations of any order and does *not* succumb to the Babuška paradox (Arnold & Walker, 2020). In this paper we extend the HHJ method to surfaces, with or without boundary, and analyze the effect of the approximation of the surface using Lagrange (parametric) elements of any degree.

Numerical approximation of fourth-order elliptic surface PDEs, especially the effect of approximating the geometry, is not as well established as for second-order problems (Dziuk, 1988; Deckelnick et al., 2005; Dziuk & Elliott, 2013). For instance, the geometric consistency error when solving the Laplace–Beltrami equation $-\Delta_{\Gamma}u=f$ on a closed, smooth surface Γ has been analyzed in Dziuk (1988); Demlow & Dziuk (2007); Demlow (2009). The main argument of their analysis is to first approximate the domain Γ with a degree m (Lagrangian) approximation Γ^m with elements of size h; the approximation can be generated using a signed distance function (i.e. closest point map) or interpolation of chart parameterizations. Next, in order to compare approximate solutions obtained on the approximation domain to the exact solution on the exact domain, we need a diffeomorphic mapping $\Psi: \Gamma^m \to \Gamma$. Then, the geometric consistency error is estimated by measuring the change in the metric of the surface from Γ^m to Γ with this mapping. The geometric error reduces to showing the following estimate for the Jacobian of the map: $\|\nabla(\Psi-\mathrm{id}_{\Gamma^m})\|_{L^\infty(\Gamma^m)}=O(h^m)$. Hence, choosing m to equal or exceed the degree of the finite elements used to approximate the solution guarantees optimal approximation order.

The surface biharmonic problem has been solved using surface finite elements via splitting the PDE into two second-order equations, such as in Dziuk & Elliott (2013); Elliott & Ranner (2015) for solving the surface Cahn–Hilliard equation. The geometric consistency error is estimated in a similar way as for the Laplace–Beltrami equation. Of particular relevance to our paper is Larsson & Larson (2017), in which the surface biharmonic problem is discretized more directly using a discontinuous Galerkin (dG) approach (without splitting the equation) and piecewise linear domain approximation of a closed surface. Their analysis also involves estimating the Jacobian, as well as accounting for the geometric error of surface dG operators for the Laplace–Beltrami operator, as well as jump and stabilization terms.

1.1 Main contributions

The surface biharmonic problem. Aside from being the first method to solve the surface Kirchhoff plate problem, which was first (and possibly last) mentioned in Lasiecka *et al.* (2003), it can be used to solve the biharmonic problem on a surface. In the case of flat domains, any method for the Kirchoff plate problem can be used to solve the biharmonic problem with clamped, or periodic, boundary conditions. The same applies to the surface problem, but the Gauss curvature of the surface now appears in the strong form PDE. In Section 7.4 we show a numerical example for the surface biharmonic problem and justify the approximation for small negative Gauss curvature.

Approximation of the surface Hessian. The classic HHJ method (for flat domains) involves the full Hessian of the displacement, in a nonconforming way, and the same is true in our formulation that

utilizes the surface Hessian. Estimating the geometric consistency error when the Hessian is in the PDE is difficult because of the second derivatives of the diffeomorphism $\Psi: \Gamma^m \to \Gamma$ that appear in the analysis (see Ciarlet, 2002, Thm. 4.4.3, and Boffi *et al.*, 2013, pg. 78). For example, let Γ and Γ^m be mapped to a common reference domain using χ and $\tilde{\chi}$, respectively, and note that the Hessian of an arbitrary smooth $v: \Gamma \to \mathbb{R}$ maps as $\nabla_{\alpha} \nabla_{\beta} v = \begin{bmatrix} \partial_{\alpha} \partial_{\beta} \bar{v} - \partial_{\gamma} \bar{v} \Gamma^{\gamma}_{\alpha\beta} \end{bmatrix}$, where $\Gamma^{\gamma}_{\alpha\beta}$ are the Christoffel symbols of the second kind for the induced metric, and $\bar{v} = v \circ \chi$. Since $\Gamma^{\gamma}_{\alpha\beta}$ depend on *second* derivatives of the map then comparing Christoffel symbols for χ and $\tilde{\chi}$ yields $\|\Gamma^{\gamma}_{\alpha\beta} - \Gamma^{\gamma}_{\alpha\beta}\|_{L^{\infty}} = O(h^{m-1})$. Ergo, an improper handling of this term would yield sub-optimal results or no convergence at all for m=1. Another related issue is handling the jump terms (in the mesh dependent 2-norm) when affected by the nonlinear map. A crucial tool that overcomes these issues and is special to the HHJ formulation is a Fortin-like operator (5.8). Moreover, we do not require the diffeomorphism to be the closest point map coming from a signed distance function; interpolants of local charts can be used. Of course one can still use the closest point map.

Surfaces with or without boundary. Our analysis assumes the surface is described by charts that exactly capture the boundary (if there is one). The approximate surface is built by interpolating these maps. For smooth, *closed*, embedded surfaces one can use the closest point map built from a signed distance function to create the approximate surfaces (Dziuk, 1988; Demlow & Dziuk, 2007; Demlow, 2009); this method is very convenient for the analysis. However, it is not so convenient for approximating a surface with boundary. In addition, the order of differentiability of the closest point map is one less than that of the surface, which is a technical annoyance avoided by the use of charts.

Moreover, our analysis allows for a variety of boundary conditions, such as clamped, simply-supported and free. Using the result from Walker (2021) we establish convergence of the surface HHJ scheme even if uniform free boundary conditions are used and the discrete surface is piecewise linear. This is not trivial because of the presence of Killing fields (see Remark 2.2). Our mixed formulation can also handle 'point conditions' (see Section 2.2 and (2.3)).

General error estimates. We make minimal regularity assumptions, in-line with the known regularity for the plate problem with various mixed boundary conditions. Furthermore, if the surface and solution are smooth, we obtain optimal convergence of order r + 1, where r + 1 is the degree of the Lagrange space used, both for the surface approximation and the displacement variable.

Relation with Arnold & Walker (2020). In our prior work we considered the Kirchhoff plate equation on a flat domain with curved boundary, where the geometric error in approximating the curved boundary, using the classic HHJ method with curved triangles, was analyzed. That paper provides a framework, such as mapping theorems and estimates of geometric consistency terms, for the (more general) analysis in this paper. However, we note the following differences: (i) previously, only the elements adjacent to the boundary were curved, which allowed for some minor simplification; (ii) mappings for surfaces create some extra complication over the flat domain case; (iii) since all elements are curved in this paper, extra geometric consistency terms (over our prior work) appear due to the co-normal derivative jumps at internal edges; (iv) free boundary conditions were not considered in the earlier paper; and (v) this paper accounts for the kernel of the discrete (covariant) surface Hessian, which is not as simple as in the flat case.

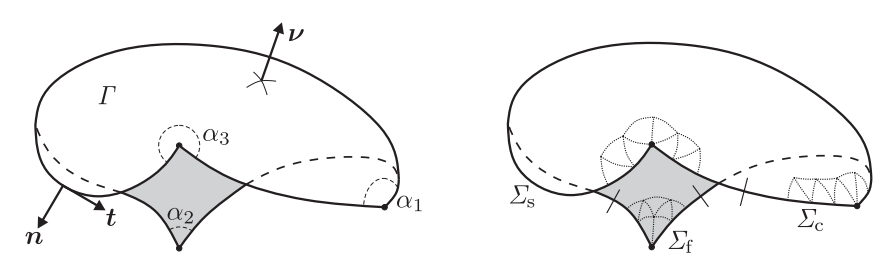


Fig. 1. Illustration of the surface plate domain Γ in \mathbb{R}^3 . The boundary $\Sigma \equiv \partial \Gamma$ decomposes as $\Sigma = \overline{\Sigma_c} \cup \overline{\Sigma_s} \cup \overline{\Sigma_f}$ and has a finite number of corners with interior angles α_i ; the corners may (or may not) lie at the intersection of two boundary components. The boundary Σ has (outer) conormal vector, \boldsymbol{n} , and oriented unit tangent vector, \boldsymbol{t} . The oriented normal vector of Γ is \boldsymbol{v} . Part of the exact, curved surface triangulation \mathcal{T}_h is shown with dotted curves.

1.2 Outline

Section 2 presents the Kirchhoff plate problem on a surface and Section 3 presents the mesh-dependent, mixed formulation that is the surface version of the classic HHJ method. In Section 4 we review parametric surface elements, describe the surface Matrix Piola transform, which is needed for mapping HHJ elements, and derive some change of variable results when mapping the bilinear forms. Section 5 presents the FEM for the mesh-dependent, mixed formulation and verifies the well posedness of the method. Section 6 gives the error analysis. The PDE error is analyzed as in Babuška *et al.* (1980) and Blum & Rannacher (1990) (for the case of a flat domain), where we use mesh-dependent spaces and norms; the geometric error is analyzed in the framework of Dziuk (1988); Dziuk & Elliott (2013) combined with new results we derive here. Section 7 presents numerical results and we conclude in Section 8 with some comments. In the appendix we give an overview of essential differential geometry concepts and provide some technical results.

2. The plate equation on a surface

Let Γ be a smooth, connected, two-dimensional manifold embedded in \mathbb{R}^3 with continuous, piecewise smooth boundary $\partial \Gamma =: \Sigma = \Sigma_c \cup \Sigma_s \cup \Sigma_f$ that consists of clamped (Σ_c) , simply-supported (Σ_s) and free sections (Σ_f) ; see Fig. 1. In some cases the boundary may be empty, giving a closed manifold.

2.1 Sobolev spaces on surfaces

We adopt standard notation for Sobolev spaces on manifolds. For example, the $H^1(\Gamma)$ and $H^2(\Gamma)$ inner products on Γ are written:

$$(w,v)_{H^1(\Gamma)} := \int_{\Gamma} wv + \nabla_{\Gamma} w \cdot \nabla_{\Gamma} v \, \mathrm{dS}, \quad (w,v)_{H^2(\Gamma)} := (w,v)_{H^1(\Gamma)} + \int_{\Gamma} \nabla_{\Gamma} \nabla_{\Gamma} w : \nabla_{\Gamma} \nabla_{\Gamma} v \, \mathrm{dS},$$
 (2.1)

where $\nabla_{\Gamma} v \equiv \operatorname{grad}_{\Gamma} v$ is the surface gradient of v in (A.9) and $\nabla_{\Gamma} \nabla_{\Gamma} w \equiv \operatorname{hess}_{\Gamma} w$ is the surface Hessian of v in (A.10).

REMARK 2.1 We emphasize that $\nabla_{\Gamma}\nabla_{\Gamma}w$ is *not* simply applying the surface gradient ∇_{Γ} to each component of $\nabla_{\Gamma}w$. One must account for the fact that $\nabla_{\Gamma}w$ is tangent to the surface, i.e. $\nabla_{\Gamma}w \in T(\Gamma)$ (tangent space). If $v \in T(\Gamma)$ is a tangential vector field, then $\nabla_{\Gamma}v$ is a tangential tensor field; its explicit

computation requires the Christoffel symbols. See Section A.2 for details of the notation and definitions of the differential operators.

We denote by $\mathring{H}^{\ell}(\Gamma) \subset H^{\ell}(\Gamma)$ the Sobolev space with vanishing boundary conditions up to degree $\ell-1$. We will have special use of the following subspace of $H^2(\Gamma)$: $\mathscr{Y}(\Gamma) := \{w \in H^2(\Gamma) \mid w = 0, \text{ on } \Sigma_c \cup \Sigma_s, \mathbf{n} \cdot \nabla_{\Gamma} w = 0, \text{ on } \Sigma_c \}$, i.e. with clamped and simply-supported boundary conditions.

Next, let $\mathscr{Z}(\Gamma) := \{ w \in \mathscr{Y}(\Gamma) \mid \nabla_{\Gamma} \nabla_{\Gamma} w = \mathbf{0} \}$ be the nullspace of the (covariant) surface Hessian operator on Γ . The maximum dimension of $\mathscr{Z}(\Gamma)$ is three for a two dimensional surface; see (Walker, 2021, Sec. 2.2.2). Furthermore, if $v \in \mathscr{Z}(\Gamma)$ is not constant, then $\nabla_{\Gamma} v$ is a *Killing field* (do Carmo, 1992), (Eisenhart, 1926, eqn. (70.2)), (Petersen, 2006, Prop. 27).

Remark 2.2 Generic manifolds, with nonconstant Gauss curvature, do not have Killing fields. Ergo, even if $\partial \Gamma \equiv \Sigma_{\rm f}$, $\mathscr{Z}(\Gamma)$ may only contain constants. On the other hand, consider the closed 2-sphere. It has three Killing fields corresponding to three independent rotations of the sphere, but none of them come from differentiating a scalar w (so $\mathscr{Z}(\Gamma)$ only contains constants).

Next, consider a small spherical cap with boundary (and free boundary conditions). Two of the Killing fields can be written as a gradient, but the third one is a rotation about a point in the surface so does not correspond to the gradient of a scalar (see do Carmo, 1992, Ch. 4, exer. 3). In this case $\mathscr{Z}(\Gamma)$ is spanned by three basis functions, i.e. two nonconstant functions whose gradients are killing fields and the unit constant function. See Section 7.2 for a numerical example.

2.2 The bending energy on a surface

Owing to the continuous embedding $H^2(\Gamma) \hookrightarrow C^0(\overline{\Gamma})$ point evaluation is well defined. Therefore, set $J = \dim \mathscr{Z}(\Gamma)$ and choose points $\{\mathbf{p}_j\}_{j=1}^J \subset \Gamma$ such that $\{v \in \mathscr{Z}(\Gamma) \mid v(\mathbf{p}_j) = 0, 1 \leqslant j \leqslant J\} \equiv \{0\}$; see Walker (2021, Sec. 2.2.2) for how this can be done. Note that if $J \equiv 0$, then $\{\mathbf{p}_j\}_{j=1}^J \equiv \emptyset$. Moreover, define $\Xi(f) := \left(\sum_{j=1}^J |f(\mathbf{p}_j)|^2\right)^{1/2}$ for all $f \in H^2(\Gamma)$ if J > 0; otherwise, $\Xi(f) \equiv 0$. Then, given $f \in \mathscr{W}^*$ and the duality pairing $\langle \cdot, \cdot \rangle_{\Gamma}$ between \mathscr{W}^* and \mathscr{W} , the 'plate energy' on the surface is given by

$$\mathscr{E}[w] = \frac{1}{2} \left(\mathbf{C} \nabla_{\Gamma} \nabla_{\Gamma} w, \nabla_{\Gamma} \nabla_{\Gamma} w \right)_{\Gamma} - \langle f, w \rangle_{\Gamma}, \text{ for all } w \in \mathscr{W},$$
 (2.2)

where

$$\mathcal{W}(\Gamma) = \{ w \in \mathcal{Y}(\Gamma) \mid \Xi(w) = 0 \}, \tag{2.3}$$

is the space of 'displacements', and C is the constitutive 4-tensor:

$$\mathbf{C}\boldsymbol{\tau} := D\left[(1 - \zeta)\boldsymbol{\tau} + \zeta \operatorname{tr}(\boldsymbol{\tau})\boldsymbol{I} \right], \quad \mathbf{K}\boldsymbol{\tau} := \frac{1}{D} \left[\frac{1}{1 - \zeta} \boldsymbol{\tau} - \frac{\zeta}{1 - \zeta^2} \operatorname{tr}(\boldsymbol{\tau})\boldsymbol{I} \right], \tag{2.4}$$

defined for all symmetric tensors $\tau \in \mathbb{R}^{3\times 3}$, with **K** the inverse of **C** (ζ is *Poisson's ratio*). Note that **C** is a symmetric positive-definite operator on the space $S(\Gamma)$ of symmetric, *tangential* 3×3 tensors, provided $\zeta \in (-1,1)$; for general symmetric 3×3 tensors, **C** is positive definite if $\zeta \in (-1/2,1)$.

The Kirchhoff plate model on a surface follows by minimizing the energy (2.2), which gives the weak formulation is as follows: find $w \in \mathcal{W}$ such that

$$\int_{\Gamma} \boldsymbol{\sigma} : \nabla_{\Gamma} \nabla_{\Gamma} z \, d\mathbf{S} = \langle f, z \rangle_{\Gamma}, \quad \text{for all } z \in \mathcal{W},$$
(2.5)

where $\sigma = \mathbb{C} \, \nabla_{\Gamma} \nabla_{\Gamma} w$. The solvability of (2.5) is guaranteed if $\zeta \in (-1,1)$, because (2.2) is a convex functional with a unique minimizer. Moreover, $(\mathbb{C} \nabla_{\Gamma} \nabla_{\Gamma} w, \nabla_{\Gamma} \nabla_{\Gamma} w)_{\Gamma} \geqslant C_0 \|\nabla_{\Gamma} \nabla_{\Gamma} w\|_{L^2(\Gamma)}^2 \geqslant C_1 \|w\|_{H^2(\Gamma)}^2$, by Poincaré (c.f. (4.7)), so the unique solution of (2.5) follows by the Lax–Milgram lemma (Evans, 1998) with *a priori* estimate $\|w\|_{H^2(\Gamma)} \leqslant C \|f\|_{\mathscr{W}^*}$. The strong form PDE is $\sigma = \mathbb{C} \, \nabla_{\Gamma} \nabla_{\Gamma} w$, and

$$\operatorname{div}_{\Gamma} \operatorname{div}_{\Gamma} \boldsymbol{\sigma} = f, \text{ in } \Gamma \setminus \{\mathbf{p}_{j}\}_{j=1}^{J}, \text{ and } w = 0, \text{ on } \Sigma_{c} \cup \Sigma_{s},$$

$$\boldsymbol{n} \cdot \nabla_{\Gamma} w = 0, \text{ on } \Sigma_{c}, \ \sigma^{\text{nn}} = 0, \text{ on } \Sigma_{s} \cup \Sigma_{f},$$

$$-\boldsymbol{n} \cdot (\operatorname{div}_{\Gamma} \boldsymbol{\sigma}) - \boldsymbol{t} \cdot \nabla_{\Gamma} \sigma^{\text{nt}} = 0, \text{ on } \Sigma_{f}, \quad \Xi(w) = 0,$$

$$(2.6)$$

where $\sigma^{\text{nn}} := \mathbf{n}^T \boldsymbol{\sigma} \mathbf{n}$ ($\sigma^{\text{nt}} := \mathbf{n}^T \boldsymbol{\sigma} \mathbf{t}$) denotes the conormal-conormal (conormal-tangent) component of $\boldsymbol{\sigma}$, the double surface divergence is given in (A.11), and we have the additional corner conditions

$$-\left[\left[\boldsymbol{n}^{T}\boldsymbol{\sigma}\boldsymbol{t}\right]\right]_{p} \equiv -\sigma^{\mathrm{nt}}\Big|_{p^{-}}^{p^{+}} = 0, \text{ at every corner } p \text{ in } \Sigma_{\mathrm{f}}.$$
 (2.7)

3. Mixed formulation of the manifold plate problem

After stating the assumptions on the embedded surface domain Γ we derive the continuous, mesh-dependent formulation of the manifold plate problem in the extrinsic setting.

3.1 Domain assumptions

The surface Γ is taken to be C^{k+1} , where $k\geqslant 1$. If Γ has a boundary $\partial\Gamma:=\Sigma$ we assume Σ is piecewise C^{k+1} with a finite number of corners, with interior angle $\alpha_i\in(0,2\pi]$ of the ith corner measured with respect to the Euclidean metric in \mathbb{R}^3 (see Fig. 1). In particular, Σ is globally continuous and parameterized by a piecewise curve, i.e. $\Sigma=\bigcup_{p\in\mathscr{V}_\Sigma}p\ \cup \bigcup_{\vartheta\in\mathscr{C}_\Sigma}\vartheta$, where \mathscr{V}_Σ is the set of corner vertices and \mathscr{C}_Σ is the set of (open) C^{k+1} curves that make up Σ . Furthermore, as a technical convenience, we assume that Γ is a sub-manifold of Γ^* (also C^{k+1}) with $\overline{\Gamma}\subset\subset\Gamma^*$.

In addition, we assume $\varSigma=\overline{\varSigma_c}\cup\overline{\varSigma_s}\cup\overline{\varSigma_f}$ partitions into three mutually disjoint one-dimensional components \varSigma_c (clamped), \varSigma_s (simply supported) and \varSigma_f (free). Any of the components can be empty, but if $|\varSigma_f|>0$, then we also assume that \varGamma is at least $C^{2,1}$. Each open curve $\vartheta\in\mathscr{C}_{\varSigma}$ belongs to only one of the sets \varSigma_c , \varSigma_s or \varSigma_f , and each curve is maximal such that two distinct curves contained in the same component do not meet at an angle of π . Furthermore, we have the set of corner vertices contained in \varSigma_f :

$$\mathscr{V}_{\Sigma_{\mathrm{f}}} = \{ p \in \mathscr{V}_{\Sigma} \mid p = \overline{\vartheta_{p^{+}}} \cap \overline{\vartheta_{p^{-}}}, \text{ where } \vartheta_{p^{+}}, \vartheta_{p^{-}} \subset \Sigma_{\mathrm{f}}, \vartheta_{p^{+}} \neq \vartheta_{p^{-}} \}. \tag{3.1}$$

3.2 Continuous mesh-dependent formulation

The main difficulty in solving (2.5) numerically is that $\mathcal{W} \subset H^2(\Gamma)$ and so C^1 elements are required for a conforming discretization. This is especially difficult in the case of a surface, e.g. one would need a surface version of the Argyris element (Brenner & Scott, 2008). Thus, we adopt the approach in Brezzi & Raviart (1976); Babuška *et al.* (1980); Arnold & Brezzi (1985); Blum & Rannacher (1990); Arnold & Walker (2020) and use a mesh-dependent version of $H^2(\Gamma)$. We partition Γ with a mesh $\mathcal{T}_h = \{T\}$ of triangles such that $\Gamma = \bigcup_{T \in \mathcal{T}_h} T$, where $h_T := \operatorname{diam}(T)$ and $h := \max_T h_T$, and assume throughout that the mesh is quasi-uniform and shape regular. We also assume the corners of the domain are captured by vertices of the mesh. Note that these triangles are, in general, curved (recall Fig. 1). See Section 4.1 for how this domain partitioning can be created.

Next, we have the *skeleton* of the mesh, i.e. the set of mesh edges $\mathscr{E}_h := \partial \mathscr{T}_h$, which may be curved. Let $\mathscr{E}_{\partial,h} \subset \mathscr{E}_h$ denote the subset of edges that are contained in the boundary Σ and respect the boundary condition partition of Σ . The internal edges are given by $\mathscr{E}_{0,h} := \mathscr{E}_h \setminus \mathscr{E}_{\partial,h}$. The spaces in the following sections are infinite dimensional, but 'mesh dependent'. Thus, we use

The spaces in the following sections are infinite dimensional, but 'mesh dependent'. Thus, we use standard dG notation for writing inner products and norms over the triangulation, e.g. $(f,g)_{\mathscr{T}_h}:=\sum_{T\in\mathscr{T}_h}(f,g)_T$, $\|f\|_{L^p(\mathscr{T}_h)}^p:=\sum_{T\in\mathscr{T}_h}\|f\|_{L^p(T)}^p$, etc. The following scaling/trace estimate is used judiciously (Agmon, 1965, Thm. 3.10):

$$\|v\|_{L^{2}(\partial T)}^{2} \leqslant C\left(h^{-1}\|v\|_{L^{2}(T)}^{2} + h\|\nabla_{\Gamma}v\|_{L^{2}(T)}^{2}\right), \ \forall v \in H^{1}(T), \ T \in \mathcal{T}_{h}. \tag{3.2}$$

3.2.1 Skeleton spaces. We follow Babuška et al. (1980) in defining infinite-dimensional, but mesh-dependent, spaces and norms. A mesh-dependent version of $H^2(\Gamma)$ is given by

$$H_h^2(\Gamma) := \{ v \in H^1(\Gamma) | v|_T \in H^2(T), \text{ for } T \in \mathcal{T}_h \},$$
 (3.3)

with the following seminorm

$$\|v\|_{2,h}^{2} := \|\nabla_{\Gamma}\nabla_{\Gamma}v\|_{L^{2}(\mathscr{T}_{h})}^{2} + h^{-1} \| [\![\boldsymbol{n} \cdot \nabla_{\Gamma}v]\!] \|_{L^{2}(\mathscr{E}_{0,h})}^{2} + h^{-1} \| [\![\boldsymbol{n} \cdot \nabla_{\Gamma}v]\!] \|_{L^{2}(\Sigma_{c})}^{2}, \tag{3.4}$$

where $[\![\eta]\!]$ is the jump in quantity η across mesh edge E, and \mathbf{n} is the unit co-normal on $E \in \mathscr{E}_h$. Hence, if the edge E is shared by two triangles T_1 and T_2 with outward co-normals \mathbf{n}_1 and \mathbf{n}_2 , then $[\![\mathbf{n} \cdot \nabla_{\Gamma} v]\!] = \mathbf{n}_1 \cdot \nabla_{\Gamma} v|_{T_1} + \mathbf{n}_2 \cdot \nabla_{\Gamma} v|_{T_2}$ on E. For E a boundary edge, we set $[\![\eta]\!] = \eta|_E$.

Next, recall that $S(\Gamma)$ is the set of symmetric (extrinsic) tangential tensors on Γ , i.e. $S(\Gamma) := \{ \varphi \in \mathbb{R}^{3\times3} \mid \varphi = \varphi^T, \ \varphi v \equiv 0 \}$, where v is the unit normal vector of Γ (see (A.8)). We shall usually make the abbreviation $S \equiv S(\Gamma)$. For any $\varphi \in H^1(\Gamma; S)$ define

$$\|\varphi\|_{0,h}^{2} := \|\varphi\|_{L^{2}(\Gamma)}^{2} + h \|\mathbf{n}^{T}\varphi\mathbf{n}\|_{L^{2}(\mathcal{E}_{0,h})}^{2} + h \|\mathbf{n}^{T}\varphi\mathbf{n}\|_{L^{2}(\Sigma_{c})}^{2}, \tag{3.5}$$

and define H_h^0 to be the completion: $H_h^0(\Gamma; S) := \overline{H^1(\Gamma; S)}^{\|\cdot\|_{0,h}}$. Following Babuška *et al.* (1980, pg. 1043) and Arnold & Walker (2020, eqn. (2.11)), because of the completion and definition of the norm, $H_h^0(\Gamma; S) \equiv L^2(\Gamma; S) \oplus L^2(\mathscr{E}_h; \mathbb{R})$, i.e. $\varphi \in H_h^0(\Gamma; S)$ is actually $\varphi \equiv (\varphi', \varphi^{\text{nn}})$, where $\varphi' \in L^2(\Gamma; S)$ and $\varphi^{\text{nn}} \in L^2(\mathscr{E}_h)$, with no connection between φ' and φ^{nn} . We also have that $\varphi \in H^1(\Gamma; S) \subset H_h^0(\Gamma; S)$

implies $\mathbf{n}^T \boldsymbol{\varphi}' \mathbf{n}|_{\mathcal{E}_h} = \varphi^{\text{nn}}$ (see Babuška *et al.*, 1980, and Arnold & Walker, 2020). Furthermore, we have a scalar valued function version of $\|\cdot\|_{0,h}$:

$$\|v\|_{0,h}^2 := \|v\|_{L^2(\Gamma)}^2 + h\|v\|_{L^2(\mathscr{E}_h)}^2, \quad \text{for all } v \in H^1(\Gamma), \tag{3.6}$$

which satisfies the estimate: $\|v\|_{0,h}^2 \le C\left(\|v\|_{L^2(\Gamma)}^2 + h^2\|\nabla_{\Gamma}v\|_{L^2(\Gamma)}^2\right)$, for some independent constant C (this follows from (3.2)).

Next, introduce the following skeleton subspaces

$$\mathcal{W}_{h} := \{ w \in H_{h}^{2}(\Gamma) \mid w = 0 \text{ on } \Sigma_{c} \cup \Sigma_{s}, \ \Xi(w) = 0 \} \subset H^{1}(\Gamma),$$

$$\mathcal{Y}_{h} := \{ \boldsymbol{\varphi} \in H_{h}^{0}(\Gamma; \mathbf{S}) \mid \varphi^{\mathrm{nn}} = 0 \text{ on } \Sigma_{s} \cup \Sigma_{f} \},$$

$$(3.7)$$

where \mathcal{W}_h is a mesh-dependent version of (2.3) and \mathcal{V}_h is used for the stress σ ; note that the point condition $\Xi(w) = 0$ makes sense because of the continuous embedding $H_h^2(\Gamma) \hookrightarrow C^0(\overline{\Gamma})$ (see (4.6)). Note that (3.7) imposes essential and natural boundary conditions differently than in (2.3).

3.2.2 Mixed skeleton formulation. The mixed method for the plate equation on an extrinsic manifold is a surface version of the classic HHJ method. Its derivation is essentially the same as for flat domains (Arnold & Walker, 2020, Sec. 2), which we briefly summarize. Start by multiplying the first equation in (2.6) by a test function $v \in \mathcal{W}_h$, integrate over a triangle T, apply integration by parts (twice) and sum over all triangles. This yields the weak form $b_h(\sigma, v) = -\langle f, v \rangle_T$ for all $v \in \mathcal{W}_h$, where

$$b_{h}(\boldsymbol{\varphi}, v) := -\sum_{T \in \mathcal{T}_{h}} (\boldsymbol{\varphi}, \operatorname{hess}_{\Gamma} v)_{T} + \sum_{E \in \mathcal{E}_{h}} \langle \boldsymbol{\varphi}^{\operatorname{nn}}, [\![\boldsymbol{n} \cdot \nabla_{\Gamma} v]\!] \rangle_{E},$$
(3.8)

for all $\varphi \in H_h^0(\Gamma; S)$ and $v \in H_h^2(\Gamma)$. Furthermore, define

$$a(\boldsymbol{\tau}, \boldsymbol{\varphi}) := (\mathbf{K}\boldsymbol{\tau}, \boldsymbol{\varphi})_{\Gamma}, \quad \text{for all } \boldsymbol{\tau}, \boldsymbol{\varphi} \in H_h^0(\Gamma; \mathbf{S}).$$
 (3.9)

Using that $\sigma = \mathbb{C} \nabla_{\Gamma} \nabla_{\Gamma}$, and the continuity of $n \cdot \nabla_{\Gamma} w$, we have $a(\sigma, \varphi) + b_h(\varphi, w) = 0$ for all $\varphi \in \mathscr{V}_h$. Therefore, let $H^1_{\operatorname{cs}}(\Gamma) = \{v \in H^1(\Gamma) \mid v = 0, \text{ on } \Sigma_{\operatorname{c}} \cup \Sigma_{\operatorname{s}} \}$, and assume $f \in (H^1_{\operatorname{cs}}(\Gamma))^*$. Then, the solution $(\sigma, w) \in \mathscr{V}_h \times \mathscr{W}_h$ of (2.5) satisfies the pair of equations:

$$a(\boldsymbol{\sigma}, \boldsymbol{\varphi}) + b_h(\boldsymbol{\varphi}, w) = 0, \qquad \forall \boldsymbol{\varphi} \in \mathcal{V}_h,$$

$$b_h(\boldsymbol{\sigma}, v) = -\langle f, v \rangle_{\Gamma}, \ \forall v \in \mathcal{W}_h,$$
 (3.10)

where $\langle \cdot, \cdot \rangle_{\Gamma}$ is the duality pairing between $(H^1_{cs}(\Gamma))^*$ and $H^1_{cs}(\Gamma)$. In the case of polygonal domains in \mathbb{R}^2 this method has been analyzed by numerous authors with different techniques. The mesh-dependent analysis we give is based on techniques in Babuška *et al.* (1980); Blum & Rannacher (1990), which were generalized to piecewise curved domains in Arnold & Walker (2020). The equivalence of (3.10) for flat domains is described in Babuška *et al.* (1980), (Blum & Rannacher, 1990, Sec. 3) and Arnold & Walker (2020); the equivalence in the case of surfaces is similar.

4. Domain approximation and mappings

Given an embedded manifold Γ , with or without boundary, we assume we have access to an atlas of charts $\{(U_i, \chi_i)\}$ that parameterizes Γ , and that we can generate a piecewise linear triangulation, with some mesh size h, which interpolates Γ at the vertices. Furthermore, we assume h is sufficiently small so that the triangulation lies within a 'tubular neighborhood' of Γ where the closest point map is well defined; see Dziuk (1988); Demlow & Dziuk (2007); Demlow (2009); Dziuk & Elliott (2013) for more discussion on these basic issues. The following sections review the basic theory of curved elements and describe how tangential tensors transform under a diffeomorphism, followed by a transformation rule for the forms in (3.8) and (3.9).

4.1 Curved triangulations

We review the parametric approach to approximating a manifold with a curvilinear triangulation \mathcal{T}_h^m of order $m \ge 1$. We start with a conforming, shape-regular, piecewise linear triangulation \mathcal{T}_h^1 of a polyhedral domain Γ^1 that interpolates Γ at the vertices; furthermore, the boundary vertices of Γ^1 (namely Σ^1) lie on the boundary of Γ . Let $\mathcal{T}_{\partial,h}^1$ be the set of triangles with one side on Σ^1 and, for convenience, assume the triangulation satisfies the following property.

PROPERTY 1 Each triangle in \mathcal{T}_h^1 has at most two vertices on the boundary and so has at most one edge contained in Σ^1 .

We assume \mathscr{T}_h^1 is homeomorphic to an exact triangulation \mathscr{T}_h of Γ in the following sense. For each $T^1 \in \mathscr{T}_h^1$ there is a chart (U, χ) , and a straight-edged triangle $T' \subset U$, such that the following holds.

- (i) $T^1 = (\pi^1 \chi)(T')$, where π^1 is the standard continuous linear, nodal Lagrange interpolation operator with the usual approximation properties.
- (ii) There is a unique $T \in \mathcal{T}_h$ such that $T = \chi(T')$.

With the above considerations one can generate another atlas of charts $\{(\widehat{T}, \chi_T)\}_{T \in \mathcal{T}_h}$, where for each $T \in \mathcal{T}_h$, $T = \chi_T(\widehat{T})$, where \widehat{T} is the standard reference triangle. Thus, we can define a family of curved triangulations, \mathcal{T}_h^m , for $m \ge 1$ (all homeomorphic to \mathcal{T}_h) by

$$\mathscr{T}_h^m = \{ T^m \mid T^m = (\widehat{\mathscr{I}}^m \chi_T)(\widehat{T}), \text{ for some unique } T \in \mathscr{T}_h \}, \tag{4.1}$$

where $\widehat{\mathscr{I}}^m:C^0(\widehat{T})\to\mathscr{P}_m(\widehat{T})$ is any degree m Lagrange interpolation operator on \widehat{T} that yields a globally continuous interpolant $\mathscr{I}_h^m:C^0(\Gamma^1)\to C^0(\Gamma^1)$ in the following sense. For any $f\in C^0(\Gamma^1)$ define \mathscr{I}_h^m element-wise by $\mathscr{I}_h^m f|_{T^1}:=\left[\widehat{\mathscr{I}}^m(f|_{T^1}\circ(\widehat{\mathscr{I}}^1\chi_T))\right]\circ(\widehat{\mathscr{I}}^1\chi_T)^{-1}$. Thus, \mathscr{I}_h^m has the usual approximation properties, (Lenoir, 1986; Brenner & Scott, 2008). Later, we use a specific choice for \mathscr{I}_h^m given by (5.2).

Therefore, \mathscr{T}_h^m is a conforming, shape-regular triangulation that approximates Γ by $\Gamma^m:=\bigcup_{T^m\in\mathscr{T}_h^m}\overline{T^m}$, for all $m\geqslant 1$ (where \overline{G} is the closure of the set G). We also denote by \mathscr{E}_h^m the set of edges of the triangulation \mathscr{T}_h^m , which is partitioned into interior edges $\mathscr{E}_{0,h}^m$ and boundary edges $\mathscr{E}_{\partial,h}^m$. Thus $\Sigma^m:=\bigcup_{E^m\in\mathscr{E}_{0,h}^m}\overline{E^m}$ is an mth order approximation of Σ .

Next, for each $T^1 \in \mathscr{T}_h^1$, we define the mapping $\mathbf{F}: \Gamma^1 \to \Gamma$ through the diffeomorphism $\mathbf{F}_T \equiv \mathbf{F}|_{T^1} := \mathbf{\chi}_T \circ (\mathscr{I}_h^1 \mathbf{\chi}_T)^{-1}$, as well as the map $\mathbf{F}^m : \Gamma^1 \to \Gamma^m$ by $\mathbf{F}^m := \mathscr{I}_h^m \mathbf{F}$, i.e. the map

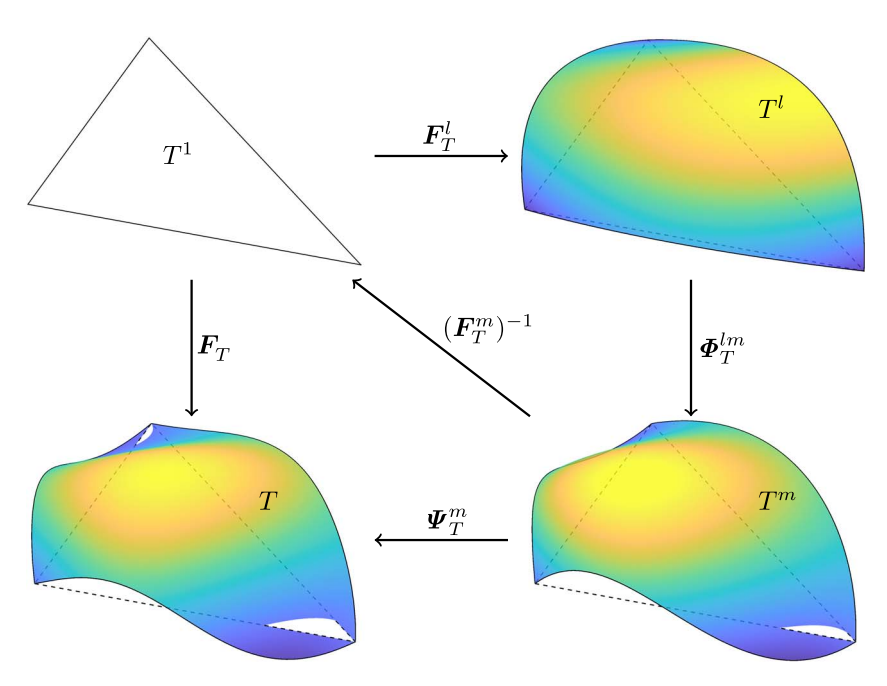


Fig. 2. Illustration of the mappings between approximate triangles T^1 and T^m , and the exact curved triangle T. The dashed triangle is T^1 .

is defined by specifying the images of the Lagrange nodes of degree m on T^1 . Note that $F_T^1 \equiv \mathrm{id}_{T^1}$. Moreover, we define maps (see Fig. 2) between approximate domains, of degrees l and m by

$$\boldsymbol{\Phi}^{lm}|_{T} = \boldsymbol{\Phi}_{T}^{lm} : T^{l} \to T^{m}$$
, where $\boldsymbol{\Phi}_{T}^{lm} := \boldsymbol{F}_{T}^{m} \circ (\boldsymbol{F}_{T}^{l})^{-1}$, so $\boldsymbol{\Phi}_{T}^{1m} \equiv \boldsymbol{F}_{T}^{m}$. (4.2)

We also require a map from the approximate domain Γ^m to the exact domain Γ . Specifically, given a triangle $T^m \in \mathscr{T}_h^m$, we define a diffeomorphism $\Psi^m_T: T^m \to T \in \mathscr{T}_h$ by $\Psi^m_T:= F_T \circ (F_T^m)^{-1}$, so then $\mathscr{T}_h \equiv \{\Psi^m_T(T^m)\}_{T^m \in \mathscr{T}_h^m}$. The Ψ^m_T may be pieced together to give a global map $\Psi^m: \Gamma^m \to \Gamma$.

The notation Γ and Γ^m is inconvenient because the exact domain has no superscript, but the polynomial approximation does. Thus, for convenience in later statements, we will abuse notation and make the identification $\Gamma^\infty \equiv \Gamma$, $\mathcal{T}_h^\infty \equiv \mathcal{T}_h$, $\Phi^{l\infty} \equiv \Psi^l$, $F_T^\infty \equiv \Psi^l$, etc. This is motivated by the fact that for most C^∞ surfaces Γ , the polynomial approximate domain Γ^m , with triangulation \mathcal{T}_h^m , would converge to Γ as $m \to \infty$ with h fixed. Of course we do not claim (in general) that Γ^m converges Γ , for fixed h, as $m \to \infty$, especially when Γ is not C^∞ .

The main approximation properties for these maps are summarized in the next theorem.

THEOREM 4.1 Suppose Γ is a C^{k+1} surface for some fixed $k \ge 1$, i.e. Γ is parameterized by an atlas of charts $\{(U_i, \chi_i)\}$ and $\chi_i \in C^{k+1}(U_i)$ for all i. Then, for all $1 \le l \le m \le k$ and $m = \infty$ (see notation

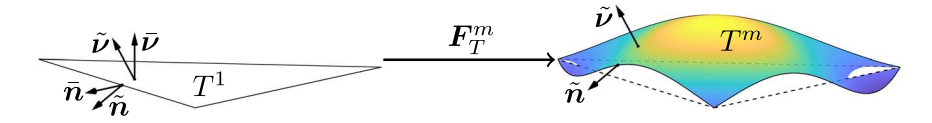


Fig. 3. Mapping unit vectors on T^m back to T^1 . We sometimes abuse notation and write $\tilde{v} \equiv \tilde{v} \circ F_T^m$, etc.

above), the maps F_T^m , F_T^l described above satisfy

$$\|\nabla_{T^{1}}^{s}(\boldsymbol{F}_{T}^{l} - \mathrm{id}_{T^{1}})\|_{L^{\infty}(T^{1})} \leqslant Ch^{2-s}, \text{ for } s = 0, 1, 2,$$

$$\|\nabla_{T^{1}}^{s}(\boldsymbol{F}_{T}^{m} - \boldsymbol{F}_{T}^{l})\|_{L^{\infty}(T^{1})} \leqslant Ch^{l+1-s}, \text{ for } 0 \leqslant s \leqslant l+1,$$

$$1 - Ch \leqslant \|[\nabla_{T^{1}}\boldsymbol{F}_{T}^{l}]^{-1}\|_{L^{\infty}(T^{1})} \leqslant 1 + Ch, \quad \|[\nabla_{T^{1}}\boldsymbol{F}_{T}^{l}]^{-1} - \boldsymbol{I}\|_{L^{\infty}(T^{1})} \leqslant Ch,$$

$$(4.3)$$

where all constants depend on $\max_i \|\nabla^j \chi_i\|_{L^{\infty}(U_i)}$, for j = 0, 1, ..., l + 1.

Next, recall the tangent t, co-normal n and surface normal vectors v from Fig. 1 and let $\tilde{\cdot}$, $\hat{\cdot}$ or $\bar{\cdot}$ denote quantities defined on T^s , or using F_T^s , for s=m,l, or 1, respectively; e.g. \tilde{v} is the surface normal of T^m (see Fig. 3). Then, the following estimate holds:

$$\|\tilde{\boldsymbol{t}} \circ \boldsymbol{F}_T^m - \hat{\boldsymbol{t}} \circ \boldsymbol{F}_T^l\|_{L^{\infty}(T^1)} + \|\tilde{\boldsymbol{n}} \circ \boldsymbol{F}_T^m - \hat{\boldsymbol{n}} \circ \boldsymbol{F}_T^l\|_{L^{\infty}(T^1)} + \|\tilde{\boldsymbol{v}} \circ \boldsymbol{F}_T^m - \hat{\boldsymbol{v}} \circ \boldsymbol{F}_T^l\|_{L^{\infty}(T^1)} \leqslant Ch^l. \tag{4.4}$$

We close with some results on how the mesh-dependent norms $\|\cdot\|_{0,h}$ and $\|\cdot\|_{2,h}$ transform between different domain approximations Γ^l and Γ^m . Thus, let $\|\cdot\|_{2,h,m}$, $\|\cdot\|_{0,h,m}$ denote the norms in (3.4), (3.6), but defined on Γ^m . The proof of Proposition 4.2 is a straightforward application of basic mapping arguments and estimating Jacobians.

PROPOSITION 4.2 Let $v \in H_h^2(\Gamma^m)$ and define $\hat{v} = v \circ \Phi \in H_h^2(\Gamma^l)$, $\Phi|_T := \Phi_T^{lm}$ for any choice of $l, m \in \{1, 2, ..., k, \infty\}$. Then,

$$\begin{split} \|\nabla_{\Gamma^{m}}\nabla_{\Gamma^{m}}v\|_{L^{2}(\mathcal{T}_{h}^{m})} & \leq C\left(\|\nabla_{\Gamma^{l}}\nabla_{\Gamma^{l}}\hat{v}\|_{L^{2}(\mathcal{T}_{h}^{l})} + h^{\min(l,m)-1}\|\nabla_{\Gamma^{l}}\hat{v}\|_{L^{2}(\Gamma^{l})}\right), \\ \|v\|_{2,h,m} & \leq C\left(\|\hat{v}\|_{2,h,l} + h^{\min(l,m)-1}\|\nabla_{\Gamma^{l}}\hat{v}\|_{L^{2}(\Gamma^{l})}\right), \end{split} \tag{4.5}$$

for some constant C > 0 depending only on the domain.

PROPOSITION 4.3 Let $1 \le m \le k$ and $m = \infty$. For all $v \in H_h^2(\Gamma^m)$ there holds

$$\|v\|_{L^{\infty}(\Gamma^{m})} \leq C_{\inf} \left(\|v\|_{H^{1}(\Gamma^{m})}^{2} + \|\nabla_{\Gamma^{m}}\nabla_{\Gamma^{m}}v\|_{L^{2}(\mathcal{T}_{h}^{m})}^{2} \right)^{1/2},$$

$$\|\nabla_{\Gamma^{m}}v\|_{L^{2}(\partial\Gamma^{m})} \leq C_{\operatorname{tr}} \left(\|\nabla_{\Gamma^{m}}v\|_{L^{2}(\Gamma^{m})}^{2} + \|\nabla_{\Gamma^{m}}\nabla_{\Gamma^{m}}v\|_{L^{2}(\mathcal{T}_{h}^{m})}^{2} \right)^{1/2},$$

$$(4.6)$$

for constants C_{\inf} , $C_{\operatorname{tr}} > 0$ independent of h. Moreover, $\|\cdot\|_{2,h,m}$ is a norm on \mathcal{W}_h^m , and for h > 0 sufficiently small (depending only on Γ), there is a constant $C_P > 0$, depending only on Γ and

independent of h, such that

$$\|v\|_{L^{2}(\Gamma^{m})} + \|\nabla_{\Gamma^{m}}v\|_{L^{2}(\Gamma^{m})} \leqslant C_{\mathbf{P}}\|v\|_{2,h,m}, \text{ for all } v \in \mathcal{W}_{h}^{m}. \tag{4.7}$$

Proof. When m=1, the proof is given in (Walker, 2021, Thm. 4.2). For m>1 the m=1 case is combined with (4.5).

Proposition 4.4 Assume the hypothesis of Proposition 4.2, and let $u \in H^1(\Gamma^m)$ and define $\hat{u} = u \circ \Phi \in H^1(\Gamma^l)$. Then, for h > 0 sufficiently small,

$$C_0^{-1} \|\hat{u}\|_{0,h,l} \le \|u\|_{0,h,m} \le C_0 \|\hat{u}\|_{0,h,l},\tag{4.8}$$

and

$$C_2^{-1} \|\hat{v}\|_{2,h,l} \leqslant \|v\|_{2,h,m} \leqslant C_2 \|\hat{v}\|_{2,h,l}, \text{ for all } v \in \mathcal{W}_h^m, \tag{4.9}$$

where $C_0, C_2 > 0$ depend only on Γ .

Proof. Inequality (4.8) follows by standard mapping arguments, and (4.9) follows by combining (4.5) and (4.7).

4.2 The Piola transform

Recall the space of tangential, tensor-valued functions $H_h^0(\Gamma^m; S^m)$ (see Section 3.2.1), where $S^m \equiv S^m(\Gamma^m)$ is the space of symmetric, tangential tensors on Γ^m . Note that the tangent space on Γ^m is element-wise defined through the mesh \mathcal{T}_h^m . We require a transformation rule that relates functions in $H_h^0(\Gamma^m; S^m)$ to $H_h^0(\Gamma^l; S^l)$ (with $m \neq l$), such that *conormal-conormal continuity* is preserved; this is crucial to ensure that the HHJ finite element space in (5.4) is continuous. We first recall the matrix Piola transform from Arnold & Walker (2020).

DEFINITION 4.5 (Standard matrix Piola transform). Let $\Phi: \mathscr{D} \to \widetilde{\mathscr{D}}$ be an orientation-preserving diffeomorphism between domains in \mathbb{R}^n . Given $\varphi: \mathscr{D} \to \mathbb{R}^{n \times n}$ we define its *matrix Piola transform* $\widetilde{\varphi}: \widetilde{\mathscr{D}} \to \mathbb{R}^{n \times n}$ by

$$\tilde{\boldsymbol{\varphi}}(\tilde{\mathbf{x}}) = (\det \boldsymbol{B})^{-2} \boldsymbol{B} \boldsymbol{\varphi}(\mathbf{x}) \boldsymbol{B}^{T} = (\det \nabla \boldsymbol{\Phi})^{-2} (\partial_{i} \boldsymbol{\Phi}) \varphi^{ij}(\mathbf{x}) (\partial_{i} \boldsymbol{\Phi})^{T}, \tag{4.10}$$

where $\tilde{\mathbf{x}} = \boldsymbol{\Phi}(\mathbf{x})$, and $\boldsymbol{B} = \boldsymbol{B}(\mathbf{x}) = \nabla \boldsymbol{\Phi}(\mathbf{x})$.

Note that (4.10) is analogous to the Piola transform for H(div) functions. This suggests the following surface version.

DEFINITION 4.6 (Surface matrix Piola transform). Let Γ be a two-dimensional surface that is locally parameterized by the chart (U, χ) , i.e. $\Theta := \chi(U) \subset \Gamma$. Given the contravariant tensor $\varphi^{\mathfrak{ab}} : U \to S$, we define its extrinsic *surface matrix Piola transform* $\tilde{\varphi} : \Theta \to S$, via the chart, by

$$\tilde{\boldsymbol{\varphi}}(\tilde{\mathbf{x}}) = g^{-1} \mathbf{e}_{\alpha} \varphi^{\alpha \beta}(\mathbf{x}) \mathbf{e}_{\beta}, \tag{4.11}$$

 $\text{ where } \tilde{\mathbf{x}} = \mathbf{\chi}(\mathbf{x}), \, \mathbf{e}_{\alpha} := \partial_{\alpha} \mathbf{\chi}, \, g_{\alpha\beta} := \mathbf{e}_{\alpha} \cdot \mathbf{e}_{\beta} \text{ and } g := \det g_{\mathfrak{a}\mathfrak{b}}.$

Moreover, let $J = (\nabla_{T^1} F_T^m) \bar{P}_{\star} \in \mathbb{R}^{3 \times 2}$ where ∇_{T^1} is the surface gradient on $T^1 \in \mathcal{T}_h^1$, $(\nabla_{T^1} F_T^m) \in \mathbb{R}^{3 \times 3}$ and $\bar{P}_{\star} \in \mathbb{R}^{3 \times 2}$ is the projection and restriction onto the tangent space of T^1 . Given an extrinsic tensor $\bar{\varphi} : \Gamma^1 \to S^1$ on the piecewise linear surface Γ^1 we map it (element-wise) to a tensor $\tilde{\varphi} : \Gamma^m \to S^m$, for any m, using the map $\tilde{\mathbf{x}} = F_T^m(\bar{\mathbf{x}})$ and

$$\tilde{\boldsymbol{\varphi}}(\tilde{\mathbf{x}}) = \operatorname{Piola}(\tilde{\boldsymbol{\varphi}})(\bar{\mathbf{x}}) := \det(\boldsymbol{Q})^{-1} \boldsymbol{J} \bar{\boldsymbol{P}}_{\perp}^{T} \tilde{\boldsymbol{\varphi}}(\bar{\mathbf{x}}) \bar{\boldsymbol{P}}_{\perp} \boldsymbol{J}^{T}, \tag{4.12}$$

where $Q = J^T J$. The inverse Piola transform is given by

$$\bar{\boldsymbol{\varphi}}(\bar{\mathbf{x}}) = \operatorname{Piola}^{-1}(\tilde{\boldsymbol{\varphi}})(\tilde{\mathbf{x}}) := \det(\boldsymbol{Q}) \bar{\boldsymbol{P}}_{\bullet} \boldsymbol{Q}^{-1} \boldsymbol{J}^{T} \tilde{\boldsymbol{\varphi}}(\tilde{\mathbf{x}}) \boldsymbol{J} \boldsymbol{Q}^{-1} \bar{\boldsymbol{P}}_{\bullet}^{T}. \tag{4.13}$$

Note that (4.11) is similar to the definition of S in (A.8), except for the g^{-1} factor.

REMARK 4.1 A tangential tensor $\bar{\varphi}$ defined on Γ^l is mapped to a tensor $\tilde{\varphi}$ on Γ^m , for $m \neq l$, through the map Φ^{lm} (see (4.2)). To see this more explicitly suppose $\bar{\varphi}:\Gamma^l\to S^l$. Then, given a chart for one triangle $T^l\subset \Gamma^l$, with metric $\bar{g}_{\mathfrak{a}\mathfrak{b}}$, there is a unique contravariant tensor $\varphi^{\mathfrak{a}\mathfrak{b}}$ such that $\bar{\varphi}$ and $\varphi^{\mathfrak{a}\mathfrak{b}}$ satisfy (4.11). Furthermore, using the chart for the corresponding triangle $T^m\subset \Gamma^m$, there is a unique $\tilde{\varphi}:\Gamma^m\to S^m$ that satisfies (4.11) with a different metric $\tilde{g}_{\mathfrak{a}\mathfrak{b}}$. We adopt this approach throughout the paper.

A simple consequence of Definition 4.6 is the following.

PROPOSITION 4.7 Adopt the hypothesis of Definition 4.6 and recall F_T^m from Section 4.1. Let $\tilde{\chi} := \mathscr{I}_h^m \chi_T$, $\bar{\chi} := \mathscr{I}_h^1 \chi_T$ (note that $\tilde{\chi} = F_T^m \circ \bar{\chi}$), and let \tilde{n} (\bar{n}) be the unit conormal on ∂T^m (∂T^1); likewise, let \tilde{t} (\bar{t}) be the unit tangent vector of ∂T^m (∂T^1). Moreover, let $\tilde{\varphi} \in H^1(\Gamma^m; S^m)$, $\bar{\varphi} \in H^1(\Gamma^1; S^1)$, be related through (4.11) using $\tilde{\chi}$ and $\bar{\chi}$. Then, denoting the surface gradient on T^1 by ∇_{T^1} , we have

$$\tilde{\varphi}^{\mathrm{nn}} \circ F_T^m = \bar{\varphi}^{\mathrm{nn}} \left| (\nabla_{T^1} F_T^m) \bar{t} \right|^{-2}. \tag{4.14}$$

Proof. Noting $\tilde{\varphi}^{nn} \equiv \tilde{\boldsymbol{n}}^T \tilde{\boldsymbol{\varphi}} \tilde{\boldsymbol{n}}, \bar{\varphi}^{nn} \equiv \bar{\boldsymbol{n}}^T \bar{\boldsymbol{\varphi}} \bar{\boldsymbol{n}}$, and applying (A.14), gives

$$\tilde{\varphi}^{\mathrm{nn}} \circ \tilde{\chi} = |t^{\mu} \tilde{\mathbf{e}}_{\mu}|^{-2} n_{\alpha} \varphi^{\alpha \beta} n_{\beta}, \quad \bar{\varphi}^{\mathrm{nn}} \circ \bar{\chi} = |t^{\mu} \bar{\mathbf{e}}_{\mu}|^{-2} n_{\alpha} \varphi^{\alpha \beta} n_{\beta}.$$

Since $\tilde{\mathbf{e}}_{\omega} = (\nabla_{T^1} \mathbf{F}_T^m) \bar{\mathbf{e}}_{\omega}$, for all ω , and $\bar{\mathbf{t}} = t^{\mu} \bar{\mathbf{e}}_{\mu} |t^{\mu} \bar{\mathbf{e}}_{\mu}|^{-1}$, we have $|(\nabla_{T^1} \mathbf{F}_T^m) \bar{\mathbf{t}}|^2 = |t^{\mu} \bar{\mathbf{e}}_{\mu}|^{-2} |t^{\mu} \tilde{\mathbf{e}}_{\mu}|^2$. Combining these results yields the assertion.

Since F^m is piecewise smooth and continuous with respect to the mesh \mathscr{T}_h^1 it follows that $(\nabla_{T^1}F_T^m)\bar{t}$ is single-valued at interelement edges, so $\tilde{\varphi}$ is conormal-conormal continuous if and only if $\bar{\varphi}$ is. So, by completion, any $\tilde{\varphi} \equiv (\tilde{\varphi}', \tilde{\varphi}^{nn}) \in H_h^0(\Gamma^m; S^m)$ transforms to $\bar{\varphi} \equiv (\bar{\varphi}', \bar{\varphi}^{nn}) \in H_h^0(\Gamma^l; S^l)$ as follows: $\tilde{\varphi}'$ and $\bar{\varphi}'$ are related through the Piola transform (see Remark 4.1) while $\tilde{\varphi}^{nn}$ and $\bar{\varphi}^{nn}$ are related through (4.14). The following norm equivalence is immediate from (4.8):

$$\|\tilde{\boldsymbol{\varphi}}\|_{0,h,m} \approx \|\bar{\boldsymbol{\varphi}}\|_{0,h,l}, \ \forall \ \tilde{\boldsymbol{\varphi}} \in H_h^0(\Gamma^m; \mathbf{S}^m), \ \text{ for all } \ 1 \leqslant l,m \leqslant k, \infty.$$

$$(4.15)$$

4.3 *Mapping forms*

The following result is essential for analyzing the geometric error when approximating the solution on an approximate domain and also for deriving the discrete inf-sup condition on curved elements.

Theorem 4.8 Let $1 \leq l \leq k$ such that l < m, for $1 < m \leq k$, or $m = \infty$, and recall the mapping discussion in Section 4.1. Let $\tilde{\sigma} \in H_h^0(\Gamma^m; \mathbb{S}^m)$, $\hat{\sigma} \in H_h^0(\Gamma^l; \mathbb{S}^l)$ and $\bar{\sigma} \in H_h^0(\Gamma^1; \mathbb{S}^1)$ and assume they are related through (4.11) in the sense of Remark 4.1. Make the same assumption for $\tilde{\varphi}$, $\hat{\varphi}$, $\bar{\varphi}$. In addition, let $\tilde{v} \in H_h^2(\Gamma^m)$, $\hat{v} \in H_h^2(\Gamma^l)$, $\bar{v} \in H_h^2(\Gamma^1)$, where $\tilde{v}|_T \circ \Phi_T^{1m} = \bar{v}$ and $\hat{v}|_T \circ \Phi_T^{1l} = \bar{v}$. Then, there holds

$$a^{m}(\tilde{\boldsymbol{\sigma}}, \tilde{\boldsymbol{\varphi}}) = a^{l}(\hat{\boldsymbol{\sigma}}, \hat{\boldsymbol{\varphi}}) + O(h^{l}) \|\hat{\boldsymbol{\sigma}}\|_{L^{2}(\Gamma^{l})} \|\hat{\boldsymbol{\varphi}}\|_{L^{2}(\Gamma^{l})}, \tag{4.16}$$

$$b_{h}^{m}\left(\tilde{\boldsymbol{\varphi}},\tilde{\boldsymbol{v}}\right) = b_{h}^{l}\left(\hat{\boldsymbol{\varphi}},\hat{\boldsymbol{v}}\right) + O(h^{l})\|\hat{\boldsymbol{\varphi}}\|_{0,h,l}\left(\|\hat{\boldsymbol{v}}\|_{2,h,l} + |\hat{\boldsymbol{v}}|_{H^{1}(\Gamma^{l})}\right) \\ - b_{h}^{1}\left(\bar{\boldsymbol{\varphi}},\left(\boldsymbol{F}^{m} - \boldsymbol{F}^{l}\right) \cdot \mathbf{P}_{0}\nabla_{\Gamma^{1}}\bar{\boldsymbol{v}}\right) + \sum_{E^{1} \in \mathscr{E}_{a,h}^{1}} \left\langle\bar{\boldsymbol{\varphi}}^{nn},\beta\bar{\boldsymbol{t}}\cdot\nabla_{T^{1}}\mathscr{I}_{h}^{1,1}\bar{\boldsymbol{v}}\right\rangle_{E^{1}},$$

$$(4.17)$$

where $\mathscr{I}_h^{1,1}$ is the Lagrange interpolation operator onto piecewise linear on Γ^1 , $P_0: L^2(\Gamma^1) \to L^2(\Gamma^1)$ is the projection onto piecewise constants and $\beta = [(\tilde{t} - \hat{t}) \times v] \cdot \tilde{t}$, $|\beta| = O(h^l)$ and $v \equiv v \circ F_T$ is the unit normal vector of T (see Theorem 4.1).

Proof. From (3.9) we have a^m ($\tilde{\sigma}, \tilde{\varphi}$) = $(\mathbf{K}\tilde{\sigma}, \tilde{\varphi})_{\Gamma^m} = \sum_{T^m \in \mathscr{T}_h^m} (\mathbf{K}\tilde{\sigma}, \tilde{\varphi})_{T^m}$. Consider a single element T^m , the map F_T^m and associated element T^1 . Now apply a global rigid motion that maps T^m to $T^{m'}$ and T^1 to $T^{1'}$ such that $T^{1'} \subset \mathbb{R}^2$. Moreover, let $\tilde{\sigma}', \tilde{\varphi}'$ be the corresponding mapped tensors using (4.10). Clearly, from (2.4), $(\mathbf{K}\tilde{\sigma}, \tilde{\varphi})_{T^m} = (\mathbf{K}\tilde{\sigma}', \tilde{\varphi}')_{T^{m'}}$. Let $F_T^{m'}: T^{1'} \to T^{m'}$ be the corresponding rotated map, which can be viewed as a parametrization of $T^{m'}$ (see Appendix A.3 for more details). For ease of notation let us momentarily drop the ' notation.

Treating F_T^m as a parametrization (4.11) implies

$$(\mathbf{K}\tilde{\boldsymbol{\sigma}}, \tilde{\boldsymbol{\varphi}})_{T^m} = \left(\tilde{g}^{-3/2}\tilde{K}_{\gamma\omega\alpha\beta}\bar{\sigma}^{\alpha\beta}, \bar{\varphi}^{\gamma\omega}\right)_{T^1},\tag{4.18}$$

where $\tilde{K}_{\gamma\omega\alpha\beta} = D^{-1}\left[(1-\zeta)^{-1}\tilde{g}_{\gamma\alpha}\tilde{g}_{\omega\beta} - \zeta(1-\zeta^2)^{-1}\tilde{g}_{\gamma\omega}\tilde{g}_{\alpha\beta}\right]$, with the metric given by $\tilde{g}_{\mathfrak{a}\mathfrak{b}} \equiv \tilde{\mathbf{g}} = \tilde{\mathbf{J}}^T\tilde{\mathbf{J}}$, where $\tilde{\mathbf{J}}$ is the 3 × 2 Jacobian matrix given by $\tilde{\mathbf{J}} = [\partial_1 \mathbf{F}_T^m, \partial_2 \mathbf{F}_T^m]$. Similarly, $(\mathbf{K}\hat{\boldsymbol{\sigma}}, \hat{\boldsymbol{\phi}})_{T^l} = \left(\hat{g}^{-3/2}\widehat{K}_{\gamma\omega\alpha\beta}\bar{\sigma}^{\alpha\beta}, \bar{\varphi}^{\gamma\omega}\right)_{T^l}$, where $\hat{g}, \widehat{K}_{\gamma\omega\alpha\beta}$ come from using \mathbf{F}_T^l . We then arrive at

$$\left| (\mathbf{K}\tilde{\boldsymbol{\sigma}}, \tilde{\boldsymbol{\varphi}})_{T^m} - \left(\mathbf{K}\hat{\boldsymbol{\sigma}}, \hat{\boldsymbol{\varphi}} \right)_{T^l} \right| \leqslant Ch^l \|\hat{\boldsymbol{\sigma}}\|_{L^2(T^l)} \|\hat{\boldsymbol{\varphi}}\|_{L^2(T^l)}, \tag{4.19}$$

where we used that $\|\widetilde{K}_{\gamma\omega\alpha\beta} - \widehat{K}_{\gamma\omega\alpha\beta}\|_{L^{\infty}(T^1)} \leq Ch^l$, which follows from (4.3). Since (4.19) also holds for the unrotated elements, summing over all elements yields (4.16).

As for (4.17) we start with (3.8) and write it as

$$b_h^m(\tilde{\boldsymbol{\varphi}}, \tilde{\boldsymbol{v}}) = -\sum_{T^m \in \mathcal{T}_h^m} \left[\left(\tilde{\boldsymbol{\varphi}}, \nabla_{T^m} \nabla_{T^m} \tilde{\boldsymbol{v}} \right)_{T^m} - \left\langle \tilde{\boldsymbol{\varphi}}^{nn}, \tilde{\boldsymbol{n}} \cdot \nabla_{T^m} \tilde{\boldsymbol{v}} \right\rangle_{\partial T^m} \right], \tag{4.20}$$

noting that $\tilde{n}^T \tilde{\varphi} \tilde{n} \equiv \tilde{\varphi}^{nn}$. We proceed as before, i.e. consider a single element T^m , the map F_T^m and associated element T^1 . Again, we apply a global rotation and drop the ' notation. Mapping the first term in (4.20) from T^m to T^1 we see that

$$\left(\tilde{\boldsymbol{\varphi}}, \nabla_{T^m} \nabla_{T^m} \tilde{\boldsymbol{v}}\right)_{T^m} = \left(\tilde{\boldsymbol{g}}^{-1/2} \bar{\boldsymbol{\varphi}}^{\alpha\beta}, \left[\partial_{\alpha} \partial_{\beta} \bar{\boldsymbol{v}} - \partial_{\gamma} \bar{\boldsymbol{v}} \widetilde{\Gamma_{\alpha\beta}^{\gamma}}\right]\right)_{T^1},\tag{4.21}$$

where $\widetilde{\Gamma_{\alpha\beta}^{\gamma}}$ are the Christoffel symbols of the second kind (depending on the induced metric \tilde{g}). By using the parametrization we have $\widetilde{\varGamma_{\alpha\beta}^{\gamma}} = (\tilde{\mathbf{g}}^{-1}\tilde{\mathbf{J}}^T\mathbf{a}_i)^{\gamma}\partial_{\alpha}\partial_{\beta}(\mathbf{F}_T^m\cdot\mathbf{a}_i)$, where $\tilde{g}^{\mathfrak{a}\mathfrak{b}}$ is the inverse metric, and $\{a_1, a_2, a_3\}$ are the canonical basis vectors in \mathbb{R}^3 . Using the estimates in (4.3) for F_T^m we can express (4.21) as

$$\begin{split} \left(\tilde{\boldsymbol{\varphi}}, \nabla_{T^{m}} \nabla_{T^{m}} \tilde{\boldsymbol{v}}\right)_{T^{m}} &= \left(\bar{\boldsymbol{\varphi}}^{\alpha \beta}, \partial_{\alpha} \partial_{\beta} \bar{\boldsymbol{v}}\right)_{T^{1}} + \left((\tilde{\boldsymbol{g}}^{-1/2} - 1) \bar{\boldsymbol{\varphi}}^{\alpha \beta}, \partial_{\alpha} \partial_{\beta} \bar{\boldsymbol{v}}\right)_{T^{1}} \\ &- \left(\bar{\boldsymbol{\varphi}}^{\alpha \beta}, \partial_{\gamma} \bar{\boldsymbol{v}} \delta_{i}^{\gamma} \partial_{\alpha} \partial_{\beta} (\boldsymbol{F}_{T}^{m} \cdot \mathbf{a}_{i})\right)_{T^{1}} - \left(\bar{\boldsymbol{\varphi}}^{\alpha \beta}, \partial_{\gamma} \bar{\boldsymbol{v}} (\tilde{\boldsymbol{q}}_{i}^{\gamma} - \delta_{i}^{\gamma}) \partial_{\alpha} \partial_{\beta} (\boldsymbol{F}_{T}^{m} \cdot \mathbf{a}_{i})\right)_{T^{1}}, \\ &(4.22) \end{split}$$

where we introduced $\tilde{q}_i^{\gamma} = \tilde{g}^{-1/2} (\tilde{g}^{-1} \tilde{J}^T \mathbf{a}_i)^{\gamma}$ and $\delta_i^{\gamma} = 1$ if $i = \gamma$ and zero otherwise for $1 \leqslant \gamma \leqslant 2$, $1 \leqslant i \leqslant 3$. A similar result holds for $(\hat{\boldsymbol{\varphi}}, \nabla_{T^l} \nabla_{T^l} \hat{\boldsymbol{\nabla}}_{T^l} \hat{$ with $\hat{\boldsymbol{g}} = \hat{\boldsymbol{J}}^T \hat{\boldsymbol{J}}$, for $\hat{\boldsymbol{J}} = [\partial_1 \boldsymbol{F}_T^l, \partial_2 \boldsymbol{F}_T^l]$. Next, let $A_1 := (\tilde{\boldsymbol{\varphi}}, \nabla_{T^m} \nabla_{T^m} \tilde{\boldsymbol{v}})_{T^m} - (\hat{\boldsymbol{\varphi}}, \nabla_{T^l} \nabla_{T^l} \hat{\boldsymbol{v}})_{T^l}$ and expand:

$$\begin{split} A_{1} &= -\left(\bar{\varphi}^{\alpha\beta}\,\partial_{\gamma}\bar{\boldsymbol{v}}, \delta_{i}^{\gamma}\,\partial_{\alpha}\partial_{\beta}([\boldsymbol{F}_{T}^{m}-\boldsymbol{F}_{T}^{l}]\cdot\boldsymbol{a}_{i})\right)_{T^{1}} + \left((\tilde{g}^{-1/2}-\hat{g}^{-1/2})\bar{\varphi}^{\alpha\beta},\,\partial_{\alpha}\partial_{\beta}\bar{\boldsymbol{v}}\right)_{T^{1}} \\ &- \left(\bar{\varphi}^{\alpha\beta},\,\partial_{\gamma}\bar{\boldsymbol{v}}(\tilde{q}_{i}^{\gamma}-\hat{q}_{i}^{\gamma})\partial_{\alpha}\partial_{\beta}(\boldsymbol{F}_{T}^{m}\cdot\boldsymbol{a}_{i})\right)_{T^{1}} - \left(\bar{\varphi}^{\alpha\beta},\,\partial_{\gamma}\bar{\boldsymbol{v}}(\hat{q}_{i}^{\gamma}-\delta_{i}^{\gamma})\partial_{\alpha}\partial_{\beta}([\boldsymbol{F}_{T}^{m}-\boldsymbol{F}_{T}^{l}]\cdot\boldsymbol{a}_{i})\right)_{T^{1}}. \end{split} \tag{4.23}$$

Note that $\|\tilde{g}^{-1/2} - \hat{g}^{-1/2}\|_{L^{\infty}(T^1)} \leqslant Ch^l$, $\|\tilde{q}_i^{\gamma} - \hat{q}_i^{\gamma}\|_{L^{\infty}(T^1)} \leqslant Ch^l$ and $\|\hat{q}_i^{\gamma} - \delta_i^{\gamma}\|_{L^{\infty}(T^1)} \leqslant Ch$, for all $T^1 \in \mathscr{T}_h^1$ using (4.3). Thus, the last three terms in (4.23) are $O(h^l) \|\hat{\boldsymbol{\varphi}}\|_{L^2(T^l)} \|\nabla_{T^l} \hat{\boldsymbol{v}}\|_{H^1(T^l)}$. Furthermore, letting $Q_{\alpha\beta}^{\gamma} := \delta_i^{\gamma} \partial_{\alpha} \partial_{\beta} ([\mathbf{F}_T^m - \mathbf{F}_T^l] \cdot \mathbf{a}_i)$, and using the piecewise projection $P_0|_{T^1} : L^2(T^1) \to \mathbb{R}$ onto constants, we have that

$$\begin{split}
\left(\bar{\varphi}^{\alpha\beta}\,\partial_{\gamma}\bar{v},Q_{\alpha\beta}^{\gamma}\right)_{T^{1}} &= \left(\bar{\varphi}^{\alpha\beta}P_{0}\partial_{\gamma}\bar{v},Q_{\alpha\beta}^{\gamma}\right)_{T^{1}} + \left(\bar{\varphi}^{\alpha\beta}[\partial_{\gamma}\bar{v}-P_{0}\partial_{\gamma}\bar{v}],Q_{\alpha\beta}^{\gamma}\right)_{T^{1}} \\
&\leq \left(\bar{\varphi}^{\alpha\beta}P_{0}\partial_{\gamma}\bar{v},Q_{\alpha\beta}^{\gamma}\right)_{T^{1}} + Ch^{l}\|\hat{\boldsymbol{\varphi}}\|_{L^{2}(T^{l})}\|\nabla_{T^{l}}\hat{v}\|_{H^{1}(T^{l})},
\end{split} \tag{4.24}$$

where we used the approximation property of P_0 , and $\|Q_{\alpha\beta}^{\gamma}\|_{L^{\infty}(T^1)} \leqslant Ch^{l-1}$, for all $T^1 \in \mathscr{T}_h^1$. Note that $\left(\bar{\varphi}^{\alpha\beta}P_0\partial_{\gamma}\bar{v},Q_{\alpha\beta}^{\gamma}\right)_{T^1}=\left(\bar{\pmb{\varphi}},\nabla_{T^1}\nabla_{T^1}[(\pmb{F}_T^m-\pmb{F}_T^l)\cdot P_0\nabla_{T^1}\bar{v}]\right)_{T^1}$, and the same result holds in the unrotated coordinates. Therefore,

$$(\tilde{\boldsymbol{\varphi}}, \nabla_{T^m} \nabla_{T^m} \tilde{\boldsymbol{v}})_{T^m} = (\hat{\boldsymbol{\varphi}}, \nabla_{T^l} \nabla_{T^l} \hat{\boldsymbol{v}})_{T^l} + O(h^l) \|\hat{\boldsymbol{\varphi}}\|_{L^2(T^l)} \|\nabla_{T^l} \hat{\boldsymbol{v}}\|_{H^1(T^l)}$$

$$- (\bar{\boldsymbol{\varphi}}, \nabla_{T^1} \nabla_{T^1} [(\boldsymbol{F}_T^m - \boldsymbol{F}_T^l) \cdot P_0 \nabla_{T^1} \bar{\boldsymbol{v}}])_{T^1}.$$

$$(4.25)$$

Next, consider the second term in (4.20). Again, we focus on a single element T^m , map it to T^1 and apply a global rotation to obtain $T^{m'}$ and $T^{1'} \subset \{x_3 = 0\}$. Let \bar{t}', \bar{n}' in \mathbb{R}^3 be the oriented unit tangent and conormal vectors of $\partial T^{1'}$, which point in the plane $\{x_3 = 0\}$. It behooves us to introduce $\bar{P}_{\star}^T = [I_2, \mathbf{0}]$ so that $\bar{P}_{\star}^T \bar{n}' \in \mathbb{R}^2$. We now drop the 'notation for simplicity.

Let $\tilde{\boldsymbol{n}}$ be the conormal of ∂T^m , and let us abuse notation with $\tilde{\boldsymbol{n}} \equiv \tilde{\boldsymbol{n}} \circ \boldsymbol{F}_T^m$. By (4.14) $\tilde{\varphi}^{nn} \circ \boldsymbol{F}_T^m = \bar{\varphi}^{nn} |\tilde{\boldsymbol{J}}\boldsymbol{t}|^{-2}$; note that the arc-length measure on ∂T^m is given by $\mathrm{d}\,\mathrm{s}(\tilde{g}) = |\tilde{\boldsymbol{J}}\boldsymbol{t}|\mathrm{d}\,\bar{\mathrm{s}}$, where $\mathrm{d}\,\bar{\mathrm{s}}$ is the arc-length measure on ∂T^1 . Applying a change of variable yields

$$\langle \tilde{\varphi}^{\text{nn}}, \tilde{\boldsymbol{n}} \cdot \nabla_{T^m} \tilde{\boldsymbol{v}} \rangle_{\partial T^m} = \langle |\tilde{\boldsymbol{J}} \tilde{\boldsymbol{t}}|^{-1} \bar{\varphi}^{\text{nn}}, \tilde{\boldsymbol{n}} \cdot \tilde{\boldsymbol{J}} \tilde{\boldsymbol{g}}^{-1} \bar{\boldsymbol{P}}_{\star}^{T} \nabla_{T^1} \bar{\boldsymbol{v}} \rangle_{\partial T^1}, \tag{4.26}$$

where we used (4.14), (A.9) and $\nabla_{T^1} \bar{v} \in \mathbb{R}^3$. A similar result holds for $\langle \hat{\varphi}^{nn}, \hat{\boldsymbol{n}} \cdot \nabla_{T^l} \hat{v} \rangle_{\partial T^l}$ by replacing m with l in (4.26), and replacing $\tilde{\boldsymbol{g}}$ with $\hat{\boldsymbol{g}}$, etc.

Define $A_2 := \langle \tilde{\varphi}^{\text{nn}}, \tilde{\boldsymbol{n}} \cdot \nabla_{T^m} \tilde{\boldsymbol{v}} \rangle_{\partial T^m} - \langle \hat{\varphi}^{\text{nn}}, \hat{\boldsymbol{n}} \cdot \nabla_{T^l} \hat{\boldsymbol{v}} \rangle_{\partial T^l}$ and expand:

$$A_{2} = \left\langle \left(|\tilde{\boldsymbol{J}}\boldsymbol{\bar{t}}|^{-1} - |\hat{\boldsymbol{J}}\boldsymbol{\bar{t}}|^{-1} \right) \bar{\varphi}^{\text{nn}}, \boldsymbol{\bar{n}} \cdot \nabla_{T^{1}} \bar{v} \right\rangle_{\partial T^{1}} + \left\langle \left(|\tilde{\boldsymbol{J}}\boldsymbol{\bar{t}}|^{-1} - |\hat{\boldsymbol{J}}\boldsymbol{\bar{t}}|^{-1} \right) \bar{\varphi}^{\text{nn}}, (\tilde{\boldsymbol{n}}^{T} \tilde{\boldsymbol{J}} \tilde{\boldsymbol{g}}^{-1} \boldsymbol{\bar{P}_{\star}}^{T} - \tilde{\boldsymbol{n}}^{T}) \nabla_{T^{1}} \bar{v} \right\rangle_{\partial T^{1}} + \left\langle (|\tilde{\boldsymbol{J}}\boldsymbol{\bar{t}}|^{-1} - 1) \bar{\varphi}^{\text{nn}}, \boldsymbol{z}^{T} \nabla_{T^{1}} \bar{v} \right\rangle_{\partial T^{1}} + \left\langle \bar{\varphi}^{\text{nn}}, \boldsymbol{z}^{T} \nabla_{T^{1}} \bar{v} \right\rangle_{\partial T^{1}},$$

$$(4.27)$$

where $\mathbb{R}^3 \ni z^T = \tilde{\boldsymbol{n}}^T \tilde{\boldsymbol{J}} \tilde{\boldsymbol{g}}^{-1} \bar{\boldsymbol{P}}_{\star}^T - \hat{\boldsymbol{n}}^T \hat{\boldsymbol{J}} \hat{\boldsymbol{g}}^{-1} \bar{\boldsymbol{P}}_{\star}^T$. Let $\alpha = |\tilde{\boldsymbol{J}} \bar{\boldsymbol{t}}|^{-1} - |\hat{\boldsymbol{J}} \bar{\boldsymbol{t}}|^{-1}$ and note that from (4.3), $|\alpha| = O(h^l)$ and $||\hat{\boldsymbol{J}} \bar{\boldsymbol{t}}|^{-1} - 1| = O(h)$. Using (A.17) we get

$$A_{2} = \left\langle \alpha \bar{\varphi}^{\text{nn}}, \bar{\boldsymbol{n}} \cdot \nabla_{T^{1}} \bar{v} \right\rangle_{\partial T^{1}} + O(h^{l+1}) \|\bar{\varphi}^{\text{nn}}\|_{L^{2}(\partial T^{1})} \|\nabla_{T^{1}} \bar{v}\|_{L^{2}(\partial T^{1})}$$

$$+ \left\langle \bar{\varphi}^{\text{nn}}, \beta \bar{\boldsymbol{t}} \cdot \nabla_{T^{1}} \bar{v} \right\rangle_{\partial T^{1}} - \left\langle \bar{\varphi}^{\text{nn}}, [\bar{\boldsymbol{n}} \cdot \nabla_{T^{1}} (\boldsymbol{F}_{T}^{m} - \boldsymbol{F}_{T}^{l})] \cdot \nabla_{T^{1}} \bar{v} \right\rangle_{\partial T^{1}},$$

$$(4.28)$$

where β was defined earlier. By the approximation properties of $\mathscr{I}_h^{1,1}$, and using (3.2), we have

$$h^{1/2} \|\nabla_{T^{1}} \bar{v} - \nabla_{T^{1}} \mathscr{I}_{h}^{1,1} \bar{v}\|_{L^{2}(\partial T^{1})} \leqslant C \Big(\|\nabla_{T^{1}} (\bar{v} - \mathscr{I}_{h}^{1,1} \bar{v})\|_{L^{2}(T^{1})} + h \|\nabla_{T^{1}} \nabla_{T^{1}} (\bar{v} - \mathscr{I}_{h}^{1,1} \bar{v})\|_{L^{2}(T^{1})} \Big) \leqslant C h \|\nabla_{T^{1}} \nabla_{T^{1}} \bar{v}\|_{L^{2}(T^{1})},$$

$$(4.29)$$

and similarly $h^{1/2} \|\nabla_{T^1} \bar{v} - P_0 \nabla_{T^1} \bar{v}\|_{L^2(\partial T^1)} \le Ch \|\nabla_{T^1} \nabla_{T^1} \bar{v}\|_{L^2(T^1)}$. Applying (3.2) to $\|\nabla_{T^1} \bar{v}\|_{L^2(\partial T^1)}$ in (4.28) and combining with the above estimates yield

$$A_{2} = \left\langle \alpha \bar{\varphi}^{\text{nn}}, \bar{\boldsymbol{n}} \cdot \nabla_{T^{1}} \bar{\boldsymbol{v}} \right\rangle_{\partial T^{1}} + O(h^{l}) (h^{1/2} \| \bar{\varphi}^{\text{nn}} \|_{L^{2}(\partial T^{1})}) \| \nabla_{T^{1}} \bar{\boldsymbol{v}} \|_{H^{1}(T^{1})}$$

$$+ \left\langle \bar{\varphi}^{\text{nn}}, \beta \bar{\boldsymbol{t}} \cdot \nabla_{T^{1}} \mathscr{I}_{h}^{1,1} \bar{\boldsymbol{v}} \right\rangle_{\partial T^{1}} - \left\langle \bar{\varphi}^{\text{nn}}, \bar{\boldsymbol{n}} \cdot \nabla_{T^{1}} [(\boldsymbol{F}_{T}^{m} - \boldsymbol{F}_{T}^{l}) \cdot \mathbf{P}_{0} \nabla_{T^{1}} \bar{\boldsymbol{v}}] \right\rangle_{\partial T^{1}}.$$

$$(4.30)$$

This estimate also holds for the unrotated element, and for all $T^1 \in \mathcal{T}_h^1$.

Now note that the mapped tangent vectors, and the mapped normal vector \mathbf{v} , is continuous across edges in \mathcal{E}_h^1 , which implies that α and β are *continuous* across edges. Since $\bar{\varphi}^{nn}$ is also continuous, and setting $\alpha_{E^1} := \alpha|_{E^1}$, this implies that

$$\begin{split} &\sum_{T^{1} \in \mathscr{T}_{h}^{1}} \left[\left\langle \alpha \bar{\varphi}^{\text{nn}}, \bar{\boldsymbol{n}} \cdot \nabla_{T^{1}} \bar{\boldsymbol{v}} \right\rangle_{\partial T^{1}} + \left\langle \bar{\varphi}^{\text{nn}}, \beta \bar{\boldsymbol{t}} \cdot \nabla_{T^{1}} \mathscr{I}_{h}^{1,1} \bar{\boldsymbol{v}} \right\rangle_{\partial T^{1}} \right] \\ &= \sum_{E^{1} \in \mathscr{E}_{h}^{1}} \left\langle \alpha_{E^{1}} \bar{\varphi}^{\text{nn}}, \left[\bar{\boldsymbol{n}} \cdot \nabla_{T^{1}} \bar{\boldsymbol{v}} \right] \right\rangle_{E^{1}} + \sum_{E^{1} \in \mathscr{E}_{\partial,h}^{1}} \left\langle \bar{\varphi}^{\text{nn}}, \beta \bar{\boldsymbol{t}} \cdot \nabla_{T^{1}} \mathscr{I}_{h}^{1,1} \bar{\boldsymbol{v}} \right\rangle_{E^{1}} \\ &\leq O(h^{l}) \sum_{E^{1} \in \mathscr{E}_{h}^{1}} h^{1/2} \|\bar{\varphi}^{\text{nn}}\|_{L^{2}(E^{1})} h^{-1/2} \| \left[\bar{\boldsymbol{n}} \cdot \nabla_{T^{1}} \bar{\boldsymbol{v}} \right] \|_{L^{2}(E^{1})} + \sum_{E^{1} \in \mathscr{E}_{\partial,h}^{1}} \left\langle \bar{\varphi}^{\text{nn}}, \beta \bar{\boldsymbol{t}} \cdot \nabla_{T^{1}} \mathscr{I}_{h}^{1,1} \bar{\boldsymbol{v}} \right\rangle_{E^{1}}, \end{split} \tag{4.31}$$

where the internal edge terms in the second sum cancel out. Combining the above results and summing over all $T^m \in \mathcal{T}_h^m$ prove (4.17).

A simple consequence of Theorem 4.8 is

$$b_h^m(\boldsymbol{\varphi}, \mathbf{v}) = b_h^l(\hat{\boldsymbol{\varphi}}, \hat{\mathbf{v}}) + O(h^{l-1}) \|\hat{\boldsymbol{\varphi}}\|_{0, h, l} \|\hat{\mathbf{v}}\|_{2, h, l}. \tag{4.32}$$

5. Finite element approximation

5.1 Curved Lagrange spaces

Let $r \ge 0$ be an integer and $m \ge 1$ be an integer or ∞ . The (continuous) Lagrange finite element space of degree r+1 is defined on Γ^m via the mapping F_T^m :

$$W_h^{m,r+1} \equiv W_h^{m,r+1}(\Gamma^m) := \{ v \in H_h^2(\Gamma^m) \, | \, v|_T \circ F_T^m \in \mathcal{P}_{r+1}(T^1), \, \forall T \in \mathcal{T}_h^m \}, \tag{5.1}$$

where we will usually suppress the r+1 superscript, i.e. we make the abbreviation $W_h^{m,r+1} \equiv W_h^m$. For the case $m=\infty$ (the exact domain) we simply write W_h .

Again, owing to the continuous embedding $H_h^2(\Gamma^1) \hookrightarrow C^0(\overline{\Gamma^1})$ (see (4.6)), we can define the Lagrange interpolation operator $\mathscr{I}_h^1: H_h^2(\Gamma^1) \to W_h^1$, Babuška *et al.* (1980) defined on each element

$$T^1 \in \mathscr{T}_h^1$$
 by

$$(\mathscr{I}_{h}^{1}v)(\mathbf{x}) - v(\mathbf{x}) = 0, \quad \forall \text{ vertices } \mathbf{x} \text{ of } T^{1},$$

$$\int_{E^{1}} (\mathscr{I}_{h}^{1}v - v)q \, \mathrm{d}s = 0, \quad \forall q \in \mathscr{P}_{r-1}(E^{1}), \ \forall E^{1} \in \partial T^{1},$$

$$\int_{T^{1}} (\mathscr{I}_{h}^{1}v - v)q \, \mathrm{d}S = 0, \quad \forall q \in \mathscr{P}_{r-2}(T^{1}).$$

$$(5.2)$$

Then, given $v \in H_h^2(\Gamma^m)$, we define the global interpolation operator, $\mathscr{I}_h^m: H_h^2(\Gamma^m) \to W_h^m$, elementwise through $\mathscr{I}_h^m v\big|_{T^m} \circ F_T^m := \mathscr{I}_h^1(v \circ F_T^m)$. Note that $v \circ F^m \in C^0(\Gamma^1)$ because $v \in C^0(\Gamma^m)$ and F^m is continuous over Γ^1 . The approximation properties of \mathscr{I}_h^m are standard. We also denote $\mathscr{I}_h^{m,s}$ to be the above Lagrange interpolant on Γ^m onto continuous piecewise polynomials of degree s, and we make the following abbreviation $\mathscr{I}_h^{m,r+1} \equiv \mathscr{I}_h^m$.

5.2 The HHJ curved finite element space

We start with a space of tangential, tensor-valued functions defined on curved surfaces, with special continuity properties and state the conforming finite element space V_h^m for $\mathcal{V}_h^m \subset H_h^0(\Gamma^m; \mathbf{S}^m)$ in (3.10), where $\mathbf{S}^m = \mathbf{S}^m(\Gamma^m)$ is the space of symmetric, tangential tensors on Γ^m . In addition, we define an interpolation operator for this space while accounting for the effect of curved surface elements.

For p > 3/2 let

$$\mathcal{M}_{nn}^{m}(\Gamma^{m}) := \{ \boldsymbol{\varphi} \in L^{2}(\Gamma^{m}; \mathbf{S}^{m}) \mid \boldsymbol{\varphi}|_{T^{m}} \in W^{1,p}(T^{m}; \mathbf{S}^{m}) \ \forall T^{m} \in \mathcal{T}_{h}^{m},$$
with $\boldsymbol{\varphi}$ conormal-conormal continuous}, (5.3)

where the *conormal-conormal continuity* condition holds at inter-element boundaries, i.e. for any pair of triangles (T_a^m, T_b^m) that share an edge $E^m = \overline{T_a^m} \cap \overline{T_b^m}$, we have $\boldsymbol{n}_a^T \boldsymbol{\varphi} \boldsymbol{n}_a|_{E^m} = \boldsymbol{n}_b^T \boldsymbol{\varphi} \boldsymbol{n}_b|_{E^m}$, where $\boldsymbol{n}_a \ (\boldsymbol{n}_b)$ is the outer conormal of $\partial T_a^m \ (\partial T_b^m)$; note that, in general, $\boldsymbol{n}_a \neq -\boldsymbol{n}_b \ (\text{on } E^m)$ unless $m = \infty$. Clearly, $\mathcal{M}_{\text{nn}}^m(\Gamma^m) \subset H_h^0(\Gamma^m; \mathbf{S}^m)$ with $\boldsymbol{\varphi}^{\text{nn}} \equiv \boldsymbol{n}^T \boldsymbol{\varphi}' \boldsymbol{n}$ on each mesh edge. We assume p > 3/2 for simplicity to ensure that the trace of a function in $\mathcal{M}_{\text{nn}}^m(\Gamma^m)$ onto the mesh skeleton \mathcal{E}_b^m is in $L^2(\mathcal{E}_b^m)$.

We can use (4.11) to build the global, conforming, HHJ finite element space (on curved elements) by mapping from a reference element (see Section 4.2 for details), i.e. $V_h^m \equiv V_h^m(\Gamma^m) \subset \mathscr{M}_{nn}^m(\Gamma^m)$ is defined by

$$V_h^m(\Gamma^m) := \{ \boldsymbol{\varphi} \in \mathcal{M}_{\mathrm{nn}}^m(\Gamma^m) \mid \boldsymbol{\varphi}|_{T^m} \circ \boldsymbol{F}_T^m := \operatorname{Piola}(\bar{\boldsymbol{\varphi}}), \bar{\boldsymbol{\varphi}} \in \mathcal{P}_r(T^1; \boldsymbol{\mathsf{S}}^1), \ \forall T^m \in \mathcal{T}_h^m \}, \quad (5.4)$$

using the Piola transform in (4.12). Note that V_h^m is isomorphic to V_h^1 , for $1 \le m \le k$ and $m = \infty$. Note that, by (3.2) and an inverse inequality, we have the following equivalence

$$\|\boldsymbol{\varphi}\|_{0,h,m} \approx \|\boldsymbol{\varphi}\|_{L^2(\Gamma^m)}, \ \forall \ \boldsymbol{\varphi} \in V_h^m. \tag{5.5}$$

Next, we define the following tensor-valued interpolation operator $\Pi_h^1: \mathscr{M}_{nn}^1(\Gamma^1) \to V_h^1$ Brezzi & Raviart (1976); Babuška *et al.* (1980) defined on each element $T^1 \in \mathscr{T}_h^1$ by

$$\int_{E^{1}} \mathbf{n}^{T} \left[\Pi_{h}^{1} \boldsymbol{\varphi} - \boldsymbol{\varphi} \right] \mathbf{n} \, q \, \mathrm{d}s = 0, \quad \forall q \in \mathscr{P}_{r}(E^{1}), \ \forall E^{1} \in \partial T^{1},
\int_{T^{1}} \left[\Pi_{h}^{1} \boldsymbol{\varphi} - \boldsymbol{\varphi} \right] : \boldsymbol{\eta} \, \mathrm{d}S = 0, \quad \forall \boldsymbol{\eta} \in \mathscr{P}_{r-1}(T^{1}; \mathbb{S}).$$
(5.6)

Recall Theorem 4.8 and Definition 4.6. Given $\varphi \in \mathscr{M}^m_{\mathrm{nn}}(\Gamma^m)$ we define the global interpolation operator, $\Pi^m_h : \mathscr{M}^m_{\mathrm{nn}}(\Gamma^m) \to V^m_h$, element-wise through

$$\Pi_h^m \boldsymbol{\varphi} \big|_{T^m} \circ \boldsymbol{F}_T^m = \text{Piola}(\Pi_h^1 \bar{\boldsymbol{\varphi}})(\bar{\mathbf{x}}), \text{ with } \mathbf{x} = \boldsymbol{F}_T^m(\bar{\mathbf{x}}), \tag{5.7}$$

where $\bar{\boldsymbol{\varphi}}(\bar{\mathbf{x}}) := \text{Piola}^{-1}(\boldsymbol{\varphi})(\mathbf{x})$ (i.e. see (4.13)). The operator Π_h^m clearly extends to $H_h^0(\Gamma^m; \mathbf{S}^m)$, as well as $W^{1,1}(\Gamma^m; \mathbf{S}^m)$, and satisfies many basic approximation results, which can be found in Arnold & Walker (2020, Supp. Mater.). Note that the degrees of freedom for V_h^1 are given by (5.6), (Brezzi & Raviart, 1976, Lem. 3), (Li, 2018).

On affine elements we have a Fortin-like property involving $b_h^1(\cdot,\cdot)$ (Brezzi & Raviart, 1976; Babuška *et al.*, 1980; Blum & Rannacher, 1990):

$$b_h^1 \left(\boldsymbol{\varphi} - \boldsymbol{\Pi}_h^1 \boldsymbol{\varphi}, \boldsymbol{\theta}_h \boldsymbol{v}_h \right) = 0, \quad \forall \boldsymbol{\varphi} \in H_h^0(\boldsymbol{\Gamma}^1; \mathbf{S}^1), \quad \boldsymbol{v}_h \in W_h^1,$$

$$b_h^1 \left(\boldsymbol{\varphi}_h, (\boldsymbol{v} - \boldsymbol{\mathcal{I}}_h^1 \boldsymbol{v}) \boldsymbol{\theta}_h \right) = 0, \quad \forall \boldsymbol{\varphi}_h \in V_h^1, \quad \boldsymbol{v} \in H_h^2(\boldsymbol{\Gamma}^1), \tag{5.8}$$

which holds for *any* piecewise constant function θ_h defined on \mathcal{T}_h^1 (Brezzi & Raviart, 1976; Babuška *et al.*, 1980; Blum & Rannacher, 1990). However, (5.8) does not hold on curved elements, but instead we have the following result.

LEMMA 5.1 Let $1 \le m \le k$, or $m = \infty$, and set $r \ge 0$ to be the degree of HHJ space V_h^m , and r + 1 to be the degree of the Lagrange space W_h^m . Moreover, assume V_h^m and W_h^m impose *no essential* boundary conditions. Then, the following estimates hold:

$$\left|b_{h}^{m}\left(\boldsymbol{\varphi}_{h}, v - \mathscr{I}_{h}^{m}v\right)\right| \leqslant C\|\boldsymbol{\varphi}_{h}\|_{L^{2}(\Gamma^{m})}\left(\|\nabla_{\Gamma^{m}}(v - \mathscr{I}_{h}^{m}v)\|_{L^{2}(\Gamma^{m})} + h\|\nabla_{\Gamma^{m}}\nabla_{\Gamma^{m}}(v - \mathscr{I}_{h}^{m}v)\|_{L^{2}(\mathscr{T}_{h}^{m})}\right),$$

$$\left|b_{h}^{m}\left(\boldsymbol{\varphi} - \Pi_{h}^{m}\boldsymbol{\varphi}, v_{h}\right)\right| \leqslant C\|\boldsymbol{\varphi} - \Pi_{h}^{m}\boldsymbol{\varphi}\|_{H_{h}^{0}(\Gamma^{m})}\|\nabla_{\Gamma^{m}}v_{h}\|_{L^{2}(\Gamma^{m})},$$
(5.9)

for all $\varphi \in H_h^0(\Gamma^m; \mathbb{S}^m)$, $v_h \in W_h^m$, and all $\varphi_h \in V_h^m$, $v \in H_h^2(\Gamma^m)$, where C is an independent constant. Note that C = 0 if m = 1.

Proof. The result follows by setting l=1 in (4.17), using (4.3) and (5.8), and equivalence of norms. In other words, for the first estimate in (5.9), replace v with $v-\mathscr{I}_h^m v$ in (4.17), set $\varphi=\varphi_h\in V_h^m$, use

20 S. W. WALKER

(5.8), and (5.5) to get

$$\left|b_h^m\left(\boldsymbol{\varphi}_h,\boldsymbol{v}-\boldsymbol{\mathcal{I}}_h^m\boldsymbol{v}\right)\right|\leqslant C\|\bar{\boldsymbol{\varphi}}_h\|_{L^2(\Gamma^1)}\left(\|\nabla_{\Gamma^1}(\bar{\boldsymbol{v}}-\boldsymbol{\mathcal{I}}_h^1\bar{\boldsymbol{v}})\|_{L^2(\Gamma^1)}+h\|\nabla_{\Gamma^1}\nabla_{\Gamma^1}(\bar{\boldsymbol{v}}-\boldsymbol{\mathcal{I}}_h^1\bar{\boldsymbol{v}})\|_{L^2(\boldsymbol{\mathcal{I}}_h^1)}\right),\tag{5.10}$$

then use equivalence of norms: (4.9), (4.15). For the second estimate replace φ with $\varphi - \Pi_h^m \varphi$ in (4.17), set $v = v_h \in W_h^m$, use (5.8), and an inverse inequality to get

$$\left| b_h^m \left(\varphi - \Pi_h^m \varphi, v_h \right) \right| \leqslant C \| \bar{\varphi} - \Pi_h^1 \bar{\varphi} \|_{0,h,1} \| \nabla_{\Gamma^1} \bar{v}_h \|_{L^2(\Gamma^1)}, \tag{5.11}$$

followed by equivalence of norms.

5.3 The HHJ mixed formulation

We pose (3.10) on Γ^m with continuous skeleton spaces denoted $\mathcal{V}_h^m \equiv \mathcal{V}_h^m(\Gamma^m)$ and $\mathcal{W}_h^m \equiv \mathcal{W}_h^m(\Gamma^m)$. Fixing the polynomial degree $r \ge 0$ the conforming finite element spaces are

$$V_h^m \subset \mathcal{V}_h^m, \qquad W_h^m \subset \mathcal{W}_h^m,$$
 (5.12)

where we abuse notation by now *enforcing essential boundary conditions* directly in the definitions of V_h^m and W_h^m . The conforming finite element approximation to (3.10) is as follows. Let $H_{\rm cs}^1(\Gamma^m)=\{v\in H^1(\Gamma^m)\mid v=0, \text{ on } \Sigma_{\rm c}^m\cup \Sigma_{\rm s}^m\}$. Given $f\in (H^1_{\rm cs}(\Gamma^m))^*$ find $\sigma_h\in V_h^m$, $w_h\in W_h^m$ such that

$$a^{m}\left(\boldsymbol{\sigma}_{h},\boldsymbol{\varphi}\right) + b_{h}^{m}\left(\boldsymbol{\varphi},w_{h}\right) = 0, \ \forall \boldsymbol{\varphi} \in V_{h}^{m},$$

$$b_{h}^{m}\left(\boldsymbol{\sigma}_{h},v\right) = -\langle f,v\rangle_{\Gamma^{m}}, \ \forall v \in W_{h}^{m}.$$

$$(5.13)$$

The well posedness of (5.13) is established in the next section, i.e. we prove the classic Ladyzhenskaya-Babuška-Brezzi (LBB) conditions (Boffi *et al.*, 2013). With this, we have the following *a priori* estimate:

$$\|w_h\|_{2,h,m} + \|\sigma_h\|_{0,h,m} \leqslant C\|f\|_{(H^1_{c_n}(\Gamma^m))^*}. \tag{5.14}$$

Note that LBB conditions for (5.13), for the case m = 1, were originally shown in Blum & Rannacher (1990) for flat domains.

5.3.1 Well posedness. Obviously, we have

$$a^{m}\left(\boldsymbol{\sigma},\boldsymbol{\varphi}\right) \leqslant A_{0}\|\boldsymbol{\sigma}\|_{L^{2}(\Gamma^{m})}\|\boldsymbol{\varphi}\|_{L^{2}(\Gamma^{m})}, \quad |b_{h}^{m}\left(\boldsymbol{\varphi},v\right)| \leqslant B_{0}\|\boldsymbol{\varphi}\|_{0,h,m}\|v\|_{2,h,m}, \tag{5.15}$$

for all $\sigma, \varphi \in H_h^0(\Gamma^m; S) \supset V_h^m$, $v \in H_h^2(\Gamma^m) \supset W_h^m$, and we have coercivity of $a^m(\cdot, \cdot)$, which is a curved element version of Babuška *et al.* (1980, Thm. 2).

LEMMA 5.2 Assume the domain Γ^m is piecewise C^{k+1} consisting of curved elements as described in Section 4. Then there is a constant $\alpha_0 > 0$, independent of h and m, such that

$$a^{m}\left(\boldsymbol{\sigma},\boldsymbol{\sigma}\right) \geqslant \min(|\mathbf{K}|) \|\boldsymbol{\sigma}\|_{L^{2}\left(\Gamma^{m}\right)}^{2} \geqslant \alpha_{0} \|\boldsymbol{\sigma}\|_{0,h,m}^{2}, \ \forall \boldsymbol{\sigma} \in V_{h}^{m}, \ \forall h > 0, \tag{5.16}$$

where α_0 depends on **K**.

Proof. Clearly,
$$a^m(\sigma, \sigma) \geqslant C_0 \|\sigma\|_{L^2(\Gamma^m)}^2$$
, where C_0 depends on $K_{\gamma\omega\alpha\beta}$. Furthermore, by (5.5), $\|\sigma\|_{L^2(\Gamma^m)} \geqslant C^{-1} \|\sigma\|_{0,h,m}$, so then $\alpha_0 := C_0/C^2$.

5.3.2 *Inf-sup*. The stability of the surface HHJ method, as well as its convergence, depends crucially on the following choice of surface approximation: let $\widetilde{F}_T^m: T^1 \to T^m$, for all $T^1 \in \mathcal{T}_h^1$ and $1 \le m \le k$, be given by

$$\boldsymbol{F}_{T}^{m} \equiv \widetilde{\boldsymbol{F}_{T}^{m}} := \mathscr{I}_{h}^{1,m} \boldsymbol{F}_{T} \equiv \mathscr{I}_{h}^{1,m} \boldsymbol{\Psi}_{T}^{1}, \tag{5.17}$$

where $\mathscr{I}_h^{1,m}$ is the Lagrange interpolation operator in (5.2) onto degree m polynomials; we simplify the notation by writing $F_T^m \equiv \widetilde{F_T^m}$. This choice is necessary to guarantee optimal convergence of the HHJ method when m = r + 1. If m > r + 1, the standard Lagrange interpolant can be used.

Next, we have a surface finite element version of the inf-sup condition in Blum & Rannacher (1990, Lem. 5.1).

LEMMA 5.3 Assume the surface $\Gamma^m \subset \mathbb{R}^3$, with $1 \le m \le k$ or $m = \infty$ consists of curved elements as described in Section 4 and satisfying (5.17). Then, for any degree $r \ge 0$, there is a constant $\beta_0 > 0$, independent of h and m, such that for all h sufficiently small,

$$\sup_{\boldsymbol{\varphi} \in V^m} \frac{|b_h^m(\boldsymbol{\varphi}, \boldsymbol{v})|}{\|\boldsymbol{\varphi}\|_{0,h,m}} \geqslant \beta_0 \|\boldsymbol{v}\|_{2,h,m}, \quad \forall \boldsymbol{v} \in W_h^m, \ \forall h > 0.$$
 (5.18)

Proof. We start with the case m = 1, which is addressed in Lemma A.3:

$$\sup_{\bar{\boldsymbol{\varphi}} \in V_{\iota}^{1}} \frac{\left| b_{h}^{1}(\bar{\boldsymbol{\varphi}}, \bar{\boldsymbol{v}}) \right|}{\|\bar{\boldsymbol{\varphi}}\|_{0,h,1}} \geqslant C_{0} \|\bar{\boldsymbol{v}}\|_{2,h,1}, \quad \forall \bar{\boldsymbol{v}} \in W_{h}^{1}, \, \forall h > 0, \tag{5.19}$$

on the piecewise linear domain Γ^1 with triangulation \mathcal{T}_h^1 , and holds for any degree $r \ge 0$ of the HHJ space.

Next, we recall the mapped variables introduced in Theorem 4.8. Because of boundary conditions, the choice of surface parametrization (5.17) and the Fortin property (5.8), the identity (4.17) reduces to

$$b_h^m(\tilde{\boldsymbol{\varphi}}, \tilde{\boldsymbol{v}}) = b_h^1(\tilde{\boldsymbol{\varphi}}, \tilde{\boldsymbol{v}}) + O(h) \|\tilde{\boldsymbol{\varphi}}\|_{0,h,1} (\|\tilde{\boldsymbol{v}}\|_{2,h,1} + |\tilde{\boldsymbol{v}}|_{H^1(\Gamma^1)}), \tag{5.20}$$

where we set l=1. From (4.15) we have that $\|\tilde{\varphi}\|_{0,h,1} \approx \|\tilde{\varphi}\|_{0,h,m}$. Then, combining (4.7) with (5.20), we get

$$\frac{\left|b_{h}^{m}(\tilde{\boldsymbol{\varphi}},\tilde{\boldsymbol{v}})\right|}{\|\tilde{\boldsymbol{\varphi}}\|_{0,h,m}} \geqslant C_{1} \frac{\left|b_{h}^{1}(\bar{\boldsymbol{\varphi}},\bar{\boldsymbol{v}})\right|}{\|\bar{\boldsymbol{\varphi}}\|_{0,h,1}} - C_{1}h\|\bar{\boldsymbol{v}}\|_{2,h,1}. \tag{5.21}$$

Taking the supremum, using (5.19), and the equivalence of norms (4.9), proves (5.18) when h is sufficiently small.

REMARK 5.1 By (4.7), (5.18) holds with $\|v\|_{2,h,m}$ replaced by $|v|_{H^1(\Gamma^m)}$ with a different inf-sup constant.

Therefore, (5.15), (5.16) and (5.18) imply by the standard theory of mixed methods that (5.13) is well posed in the mesh-dependent norms.

6. Error analysis

We prove convergence of the surface HHJ method while accounting for the approximation of the surface using curved elements (see Section 4). The main difficulties are dealing with higher derivatives of the nonlinear map and handling the jump terms in the mesh dependent norms when affected by a nonlinear map. The key ingredients here are Theorem 4.1, (5.8) and (5.17).

In deriving the error estimates we make the following regularity hypothesis, which assumes the Kirchhoff plate regularity for the flat domains (taken from Blum & Rannacher, 1980, Thm. 2, and Blum & Rannacher, 1990, Table 1) also applies to the surface case.

Hypothesis 1 (Regularity). Let $H^1_{\mathrm{cs}}(\Gamma) = \{v \in H^1(\Gamma) \mid v = 0, \text{ on } \Sigma_{\mathrm{c}} \cup \Sigma_{\mathrm{s}}\}$, and let $f \in (H^1_{\mathrm{cs}}(\Gamma))^*$. Assume Γ satisfies the assumptions in Section 3.1, with $k \geqslant t-1$, where $t \in [3,\infty)$ is the assumed measure of elliptic regularity in the following sense. The weak solution $w \in \mathcal{W}$ of (2.5) satisfies $w \in W^{t,p}(\Gamma)$ for some value of $p \in (p_0,2]$, where $3/2 \leqslant p_0 < 2$ depends on the angles at the corners of Γ . For technical reasons we assume p > 3/2 here (recall (5.3)). Note that $\sigma = \mathbb{C} \nabla_{\Gamma} \nabla_{\Gamma} w \in W^{t-2,p}(\Gamma; \mathbb{S})$.

6.1 Estimate the PDE error

First, we derive an error estimate that ignores the geometric error, i.e. the continuous and discrete problems are posed on the exact domain.

THEOREM 6.1 Adopt Hypothesis 1 and note that $\sigma = \mathbb{C} \nabla_{\Gamma} \nabla_{\Gamma} w$ and $w \in \mathcal{W}$ also satisfy (3.10) on the true domain Γ . Furthermore, let $r \ge 0$ be the degree of V_h , and let $\sigma_h \in V_h$, $w_h \in W_h$ be the discrete solution of (5.13) on Γ . Then, we obtain

$$\|\sigma - \sigma_h\|_{0,h} + \|\nabla_{\Gamma}(w - w_h)\|_{L^2(\Gamma)} \leqslant Ch^{\min(r+2,t-1)-2/p},$$
when $r \geqslant 1$: $\|w - w_h\|_{2,h} \leqslant Ch^{\min(r+1,t-1)-2/p},$
when $r = 0$: $\|\nabla_{\Gamma}(w - w_h)\|_{L^2(\Gamma)} \leqslant Ch,$

$$(6.1)$$

where C > 0 depends on f, the domain Γ and the shape regularity of the mesh.

Proof. With coercivity and the inf-sup condition in hand, the proof is a standard application of error estimates for mixed methods, so we omit the details. See Arnold & Walker (2020, Supp. Mat.) for a proof in the case of flat domains.

The above result generalizes (Blum & Rannacher, 1990, Thm. 5.1) to surfaces.

6.2 Estimate the geometric error

Next, we approximate the domain using curved surface elements.

Lemma 6.2 Recall the map $\Psi^m: \Gamma^m \to \Gamma$, with $\Psi^m_T:= \Psi^m|_T$, from Section 4.1, and adopt (5.17) and the hypothesis of 6.1. Let $\hat{\sigma}_h \in V_h^m$, $\hat{w}_h \in W_h^m$ be the discrete solution of (5.13), with f replaced by $\tilde{f}:=f\circ \Psi^m\mu_h$, where μ_h is the change in area when mapping from Γ to Γ^m . Take (σ_h,w_h) from Theorem 6.1, and let $\tilde{\sigma}_h \in V_h^m$, $\tilde{w}_h \in W_h^m$ be the mapped discrete solutions onto Γ^m using (4.11). In other words, $\sigma_h \circ \Psi^m$ and $\tilde{\sigma}_h$ are related through the matrix Piola transform (recall Remark 4.1), and $\tilde{w}_h = w_h \circ \Psi^m$, element-wise. Similarly, we map the test functions $\varphi_h \in V_h$, $v_h \in W_h$ to $\hat{\varphi}_h \in V_h^m$, $\hat{v}_h \in W_h^m$. Then, we obtain the error equations for the geometric error:

$$a^{m}\left(\widetilde{\boldsymbol{\sigma}}_{h}-\hat{\boldsymbol{\sigma}}_{h},\widehat{\boldsymbol{\varphi}}_{h}\right)+b_{h}^{m}\left(\widehat{\boldsymbol{\varphi}}_{h},\widetilde{\boldsymbol{w}}_{h}-\hat{\boldsymbol{w}}_{h}\right)+b_{h}^{m}\left(\widetilde{\boldsymbol{\sigma}}_{h}-\hat{\boldsymbol{\sigma}}_{h},\widehat{\boldsymbol{v}}_{h}\right)=\mathrm{E}_{0}(\widehat{\boldsymbol{\varphi}}_{h},\widehat{\boldsymbol{v}}_{h}),\tag{6.2}$$

for all $(\hat{v}_h, \hat{\boldsymbol{\varphi}}_h) \in W_h^m \times V_h^m$, where

$$|\mathcal{E}_{0}(\hat{\boldsymbol{\varphi}}_{h}, \hat{\boldsymbol{v}}_{h})| \leq Ch^{q} \left(\|\hat{\boldsymbol{\varphi}}_{h}\|_{0, h, m} + \|\hat{\boldsymbol{v}}_{h}\|_{2, h, m} \right) \|f\|_{(H^{1}(\Gamma))^{*}}, \tag{6.3}$$

where q = m when m = r + 1, otherwise q = m - 1.

Proof. We will need $\bar{\sigma}_h$, $\bar{\phi}_h \in V_h^1$, \bar{w}_h , $\bar{v}_h \in W_h^1$ as in Theorem 4.8; recall the notation from Theorem 4.1. Applying (4.17) with m, l replaced by ∞ , m, respectively, we get

$$b_{h}(\boldsymbol{\varphi}_{h}, v_{h}) = b_{h}^{m}(\hat{\boldsymbol{\varphi}}_{h}, \hat{v}_{h}) + O(h^{m}) \|\hat{\boldsymbol{\varphi}}_{h}\|_{0, h, m} (\|\hat{v}_{h}\|_{2, h, m} + |\hat{v}_{h}|_{H^{1}(\Gamma^{m})}) - b_{h}^{1}(\bar{\boldsymbol{\varphi}}_{h}, (\boldsymbol{F} - \boldsymbol{F}^{m}) \cdot P_{0} \nabla_{T^{1}} \bar{v}_{h}),$$

$$(6.4)$$

where we note the boundary conditions (either \bar{v}_h or $\bar{\varphi}^{nn}$ vanishes on $\partial \Gamma^1$). Recalling (5.17), i.e. $F^m := \mathscr{I}_h^{1,m} F$, if m = r+1, the Fortin property (5.8) yields $b_h^1 \left(\bar{\varphi}_h, (F-F^m) \cdot \mathrm{P}_0 \nabla_{T^1} \bar{v}_h \right) = 0$. If $m \neq r+1$ then a straightforward estimate shows $b_h^1 \left(\bar{\varphi}_h, (F-F^m) \cdot \mathrm{P}_0 \nabla_{T^1} \bar{v}_h \right) \leqslant C h^{m-1} \|\hat{\varphi}_h\|_{0,h,m} \|\hat{v}_h\|_{2,h,m}$, where we used equivalence of norms (4.9), (4.15).

Therefore, using (4.16) and (4.32), the first line in (5.13) (with $m = \infty$) maps to

$$a^{m}\left(\widetilde{\boldsymbol{\sigma}}_{h},\widehat{\boldsymbol{\varphi}}_{h}\right)+b_{h}^{m}\left(\widehat{\boldsymbol{\varphi}}_{h},\widetilde{\boldsymbol{w}}_{h}\right)=\mathbf{I}_{1},\ \forall\widehat{\boldsymbol{\varphi}}_{h}\in\boldsymbol{V}_{h}^{m},\tag{6.5}$$

where $1 \le m \le k$ and C > 0 is a constant depending only on Γ such that

$$|I_1| \leqslant Ch^q \|\hat{\boldsymbol{\phi}}_h\|_{L^2(\Gamma^m)} \left(\|\tilde{\boldsymbol{\sigma}}_h\|_{L^2(\Gamma^m)} + \|\tilde{w}_h\|_{2,h,m} \right), \tag{6.6}$$

where q was defined earlier. The second equation in (5.13) (with $m = \infty$) maps to

$$b_h^m\left(\widetilde{\boldsymbol{\sigma}}_h, \widehat{\boldsymbol{v}}_h\right) = -\left\langle f \circ \boldsymbol{\Psi}^m \boldsymbol{\mu}_h, \widehat{\boldsymbol{v}}_h \right\rangle_{\Gamma^m} + \mathbf{I}_2, \quad \forall \widehat{\boldsymbol{v}}_h \in W_h^m, \tag{6.7}$$

where, for some constant C > 0 depending only on Γ ,

$$|I_2| \leqslant Ch^q \|\widetilde{\sigma}_h\|_{L^2(\Gamma^m)} \|\hat{v}_h\|_{2.h.m}.$$
 (6.8)

Then, subtracting (5.13) (with $1 \le m \le k$) for the solution $(\hat{\sigma}_h, \hat{w}_h)$ from the above equations, combining everything, noting the *a priori* estimate (5.14), and the fact that $\|\tilde{f}\|_{(H^1_{cs}(\Gamma^m))^*} \le C\|f\|_{(H^1_{cs}(\Gamma))^*}$, gives (6.2) and (6.3).

THEOREM 6.3 Adopt the hypothesis of Lemma 6.2. Then, the following error estimate holds

$$\|\tilde{\boldsymbol{\sigma}}_{h} - \hat{\boldsymbol{\sigma}}_{h}\|_{0,h,m} + \|\tilde{w}_{h} - \hat{w}_{h}\|_{2,h,m} \leqslant Ch^{q} \|f\|_{(H_{\infty}^{1}(\Gamma))^{*}}, \tag{6.9}$$

for some uniform constant C > 0.

Proof. From (6.2), choose $\hat{v}_h = 0$ and use Lemma 5.3 to get

$$\beta_{0} \|\tilde{w}_{h} - \hat{w}_{h}\|_{2,h,m} \leq \sup_{\hat{\boldsymbol{\varphi}}_{h} \in V_{h}^{m}} \frac{|b_{h}^{m} \left(\hat{\boldsymbol{\varphi}}_{h}, \tilde{w}_{h} - \hat{w}_{h}\right)|}{\|\hat{\boldsymbol{\varphi}}_{h}\|_{0,h,m}} \leq \sup_{\hat{\boldsymbol{\varphi}}_{h} \in V_{h}^{m}} \frac{|a^{m} \left(\tilde{\boldsymbol{\sigma}}_{h} - \hat{\boldsymbol{\sigma}}_{h}, \hat{\boldsymbol{\varphi}}_{h}\right)| + |\mathbf{E}_{0}(\hat{\boldsymbol{\varphi}}_{h}, 0)|}{\|\hat{\boldsymbol{\varphi}}_{h}\|_{0,h,m}}$$

$$\leq CA_{0} \|\tilde{\boldsymbol{\sigma}}_{h} - \hat{\boldsymbol{\sigma}}_{h}\|_{0,h,m} + Ch^{q} \|f\|_{(H^{1}(\Gamma))^{*}}, \tag{6.10}$$

where we used the norm equivalence (4.15). Next, choose $\hat{\varphi}_h = \tilde{\sigma}_h - \hat{\sigma}_h$ and $\hat{v}_h = -(\tilde{w}_h - \hat{w}_h)$ in (6.2) to get

$$\begin{split} \alpha_{0} \| \widetilde{\boldsymbol{\sigma}}_{h} - \widehat{\boldsymbol{\sigma}}_{h} \|_{L^{2}(\Gamma^{m})}^{2} & \leq a^{m} \left(\widetilde{\boldsymbol{\sigma}}_{h} - \widehat{\boldsymbol{\sigma}}_{h}, \widetilde{\boldsymbol{\sigma}}_{h} - \widehat{\boldsymbol{\sigma}}_{h} \right) \\ & \leq C h^{q} \left(\| \widetilde{\boldsymbol{\sigma}}_{h} - \widehat{\boldsymbol{\sigma}}_{h} \|_{0,h,m} + \| \widetilde{\boldsymbol{w}}_{h} - \widehat{\boldsymbol{w}}_{h} \|_{2,h,m} \right) \| f \|_{(H_{cs}^{1}(\Gamma))^{*}} \\ & \leq C h^{q} \left(\| \widetilde{\boldsymbol{\sigma}}_{h} - \widehat{\boldsymbol{\sigma}}_{h} \|_{0,h,m} + C h^{q} \| f \|_{(H_{cs}^{1}(\Gamma))^{*}} \right) \| f \|_{(H_{cs}^{1}(\Gamma))^{*}} \\ & \leq C (h^{q})^{2} \| f \|_{(H_{cs}^{1}(\Gamma))^{*}}^{2} + C h^{q} \| \widetilde{\boldsymbol{\sigma}}_{h} - \widehat{\boldsymbol{\sigma}}_{h} \|_{L^{2}(\Gamma^{m})} \| f \|_{(H_{cs}^{1}(\Gamma))^{*}} \\ & \leq C (h^{q})^{2} \| f \|_{(H_{cs}^{1}(\Gamma))^{*}}^{2} + \frac{\alpha_{0}}{2} \| \widetilde{\boldsymbol{\sigma}}_{h} - \widehat{\boldsymbol{\sigma}}_{h} \|_{L^{2}(\Gamma^{m})}^{2}, \end{split}$$

$$(6.11)$$

where we used (6.10), norm equivalence (5.5) and a weighted Cauchy inequality. Then, by combining the above results, we get the assertion.

6.3 Estimate the total error

We will combine Theorem 6.1 and Theorem 6.3 to get the total error.

THEOREM 6.4 (general error estimate). Adopt the hypotheses of Theorem 6.1 and Lemma 6.2. If $m \ge r + 1$, then

$$\|\boldsymbol{\sigma} - \hat{\boldsymbol{\sigma}}_{h} \circ (\boldsymbol{\Psi}^{m})^{-1}\|_{0,h} + \|\nabla_{\Gamma}(w - \hat{w}_{h} \circ (\boldsymbol{\Psi}^{m})^{-1})\|_{L^{2}(\Gamma)} \leqslant Ch^{\min(r+2,t-1)-2/p},$$

$$r \geqslant 1: \|w - \hat{w}_{h} \circ (\boldsymbol{\Psi}^{m})^{-1}\|_{2,h} \leqslant Ch^{\min(r+1,t-1)-2/p},$$

$$r = 0: \|\nabla_{\Gamma}(w - \hat{w}_{h} \circ (\boldsymbol{\Psi}^{m})^{-1})\|_{L^{2}(\Gamma)} \leqslant Ch,$$
(6.12)

where C > 0 depends on f, the domain Γ and the shape regularity of the mesh.

Proof. By the triangle inequality and using the properties of the map Ψ^m we have

$$\|\boldsymbol{\sigma} - \hat{\boldsymbol{\sigma}}_{h} \circ (\boldsymbol{\Psi}^{m})^{-1}\|_{0,h} \leq \|\boldsymbol{\sigma} - \widetilde{\boldsymbol{\sigma}}_{h} \circ (\boldsymbol{\Psi}^{m})^{-1}\|_{0,h} + \|\widetilde{\boldsymbol{\sigma}}_{h} \circ (\boldsymbol{\Psi}^{m})^{-1} - \hat{\boldsymbol{\sigma}}_{h} \circ (\boldsymbol{\Psi}^{m})^{-1}\|_{0,h}$$

$$\leq \|\boldsymbol{\sigma} - \boldsymbol{\sigma}_{h}\|_{0,h} + \|\boldsymbol{\sigma}_{h} - \widetilde{\boldsymbol{\sigma}}_{h} \circ (\boldsymbol{\Psi}^{m})^{-1}\|_{0,h} + C\|\widetilde{\boldsymbol{\sigma}}_{h} - \hat{\boldsymbol{\sigma}}_{h}\|_{0,h,m}. \tag{6.13}$$

Focusing on the middle term the Piola transform in (4.12) yields

$$\|\boldsymbol{\sigma}_{h} - \widetilde{\boldsymbol{\sigma}}_{h} \circ (\boldsymbol{\Psi}^{m})^{-1}\|_{0,h} \leqslant C\|\boldsymbol{\sigma}_{h} \circ \boldsymbol{F} - \widetilde{\boldsymbol{\sigma}}_{h} \circ \boldsymbol{F}^{m}\|_{0,h,1} \leqslant Ch^{r+1}\|\widetilde{\boldsymbol{\sigma}}_{h}\|_{0,h,m} \leqslant Ch^{r+1}\|f\|_{(H_{cs}^{1}(\Gamma))^{*}},$$
(6.14)

where we use the approximation properties in (4.3). Whence,

$$\|\boldsymbol{\sigma} - \hat{\boldsymbol{\sigma}}_h \circ (\boldsymbol{\Psi}^m)^{-1}\|_{0,h} \leqslant C \max\left(h^{r+1}, h^{\min(r+2,t-1)-2/p}\right),$$
 (6.15)

where C > 0 depends on f. Taking a similar approach for the other terms involving $w - \hat{w}_h \circ (\Psi^m)^{-1}$ delivers the estimates.

COROLLARY 6.5 Adopt the hypothesis of Theorem 6.4, but assume Γ , Σ are smooth, and the data and solution (σ, w) are smooth. If $r \ge 0$ is the degree of V_h then

$$\|\boldsymbol{\sigma} - \hat{\boldsymbol{\sigma}}_h \circ (\boldsymbol{\Psi}^m)^{-1}\|_{0,h} + \|\nabla_{\Gamma} (w - \hat{w}_h \circ (\boldsymbol{\Psi}^m)^{-1})\|_{L^2(\Gamma)} + h\|w - \hat{w}_h \circ (\boldsymbol{\Psi}^m)^{-1}\|_{2,h} \leqslant Ch^{r+1},$$
(6.16)

where C > 0 depends on w, the domain Γ and the shape regularity of the mesh.

REMARK 6.1 From Theorem 6.3, if m < r + 1, the error is sub-optimal, i.e., is $O(h^{m-1})$ for a smooth solution. However, the numerical experiments in Section 7 have better rates. When m < r + 1 the worst case error for $\hat{\sigma}_h$ is $O(h^{m-1/2})$ and for \hat{w}_h (in H^1) is $O(h^m)$.

6.4 Inhomogeneous boundary conditions

We now explain how to extend the above theory to handle nonvanishing boundary conditions. First, construct a function $g \in W^{t,p}(\Gamma)$, such that the displacement satisfies w = g on $\Sigma_c \cup \Sigma_s$, $\partial_n w = \partial_n g$ on Σ_c , and $\Xi(w - g) = 0$. Next, construct a function $\rho \in W^{t-2,p}(\Gamma; S)$, such that the conormal-conormal moment satisfies $\mathbf{n}^T \sigma \mathbf{n} = \mathbf{n}^T \rho \mathbf{n}$ on $\Sigma_s \cup \Sigma_f$, where $t \geqslant 3$, $3/2 (recall Hypothesis 1). In addition, let <math>\zeta_f$ in $W^{t-3,p}(\Sigma_f)$ and $\zeta_p \in \mathbb{R}$, for all $p \in \mathscr{V}_{\Sigma_f}$ (recall (3.1)) such that

$$-\boldsymbol{n} \cdot (\operatorname{div}_{\Gamma} \boldsymbol{\sigma}) - \boldsymbol{t} \cdot \nabla_{\Gamma} (\boldsymbol{n}^{T} \boldsymbol{\sigma} \boldsymbol{t}) = \varsigma_{f}, \text{ on } \Sigma_{f},$$

$$- \left[\boldsymbol{n}^{T} \boldsymbol{\sigma} \boldsymbol{t} \right]_{p} = \varsigma_{p}, \text{ for all } p \in \mathscr{V}_{\Sigma_{f}}.$$
(6.17)

Then (3.10) is replaced by the problem of determining $(\sigma, w) = (\mathring{\sigma} + \rho, \mathring{w} + g)$, with $\mathring{\sigma} \in \mathscr{V}_h$, $\mathring{w} \in \mathscr{W}_h$ (i.e. with homogeneous boundary conditions) such that

$$a\left(\mathring{\boldsymbol{\sigma}},\boldsymbol{\varphi}\right) + b_{h}\left(\boldsymbol{\varphi},\mathring{\boldsymbol{w}}\right) = -a\left(\boldsymbol{\rho},\boldsymbol{\varphi}\right) - b_{h}\left(\boldsymbol{\varphi},g\right) + \left(\boldsymbol{\varphi}^{\mathrm{nn}},\boldsymbol{n}\cdot\nabla_{\Gamma}g\right)_{\Sigma_{\mathrm{c}}}, \quad \forall \boldsymbol{\varphi} \in \mathscr{V}_{h},$$

$$b_{h}\left(\mathring{\boldsymbol{\sigma}},v\right) = -\left\langle f,v\right\rangle_{\Gamma} - b_{h}\left(\boldsymbol{\rho},v\right) - \left(\varsigma_{\mathrm{f}},v\right)_{\Sigma_{\mathrm{f}}} - \sum_{p \in \mathscr{V}_{\Sigma_{\mathrm{c}}}} \varsigma_{p}v(p), \ \forall v \in \mathscr{W}_{h}. \tag{6.18}$$

Note that the right-hand side in the first equation of (6.18) simplifies to $-a(\rho, \varphi) - \mathring{b}_h(\varphi, g)$, where $\mathring{b}_h(\varphi, v) := b_h(\varphi, v) - (\varphi^{\rm nn}, \mathbf{n} \cdot \nabla_{\Gamma} v)_{\Sigma_0}$ (i.e. it has no boundary term).

Similarly, the corresponding (intermediate) discrete problem (5.13), on the exact domain, is replaced by finding $(\sigma_h, w_h) = (\mathring{\sigma}_h + \rho_h, \mathring{w}_h + g_h)$, with $\mathring{\sigma}_h \in V_h$, $\mathring{w}_h \in W_h$ such that

$$a\left(\mathring{\boldsymbol{\sigma}}_{h},\boldsymbol{\varphi}_{h}\right)+b_{h}\left(\boldsymbol{\varphi}_{h},\mathring{\boldsymbol{w}}_{h}\right)=-a\left(\boldsymbol{\rho}_{h},\boldsymbol{\varphi}_{h}\right)-\mathring{b}_{h}\left(\boldsymbol{\varphi}_{h},g_{h}\right)\\-\left(\boldsymbol{\varphi}_{h}^{\mathrm{nn}},\boldsymbol{n}\cdot\nabla_{\Gamma}g_{h}\right)_{\Sigma_{c}}+\left(\boldsymbol{\varphi}_{h}^{\mathrm{nn}},\boldsymbol{n}\cdot\nabla_{\Gamma}g\right)_{\Sigma_{c}},\ \forall\boldsymbol{\varphi}_{h}\in\boldsymbol{V}_{h},\\b_{h}\left(\mathring{\boldsymbol{\sigma}}_{h},\boldsymbol{v}_{h}\right)=-\left\langle f,\boldsymbol{v}_{h}\right\rangle_{\Gamma}-b_{h}\left(\boldsymbol{\rho}_{h},\boldsymbol{v}_{h}\right)-\left(\varsigma_{f},\boldsymbol{v}_{h}\right)_{\Sigma_{f}}-\sum_{\boldsymbol{p}\in\mathscr{V}_{\Sigma_{f}}}\varsigma_{\boldsymbol{p}}\boldsymbol{v}_{h}(\boldsymbol{p}),\ \forall\boldsymbol{v}_{h}\in\boldsymbol{W}_{h},\end{aligned}$$

$$(6.19)$$

where $\rho_h = P_h \rho$, and $P_h : H_h^0(\Gamma) \to V_h$ is the $L^2(\Gamma)$ projection, i.e. ρ_h satisfies

$$(\boldsymbol{\rho}_h - \boldsymbol{\rho}, \boldsymbol{\varphi}_h)_{\mathcal{T}_h} + \langle \boldsymbol{n}^T [\boldsymbol{\rho}_h - \boldsymbol{\rho}] \boldsymbol{n}, \varphi_h^{\text{nn}} \rangle_{\mathcal{E}_h} = 0, \text{ for all } \boldsymbol{\varphi}_h \in V_h,$$
(6.20)

and $g_h = \mathscr{I}_h g$. An error estimate between the solutions of (6.18) and (6.19), analogous to Theorem 6.1, follows similarly with the following additional steps. First, estimate $b_h \left(\rho - \rho_h, v_h \right) \leq \| \rho - \rho_h \|_{0,h} \| v_h \|_{2,h}$, note $\| \rho - \rho_h \|_{0,h} \leq \| \rho - \Pi_h \rho \|_{0,h}$ and use the approximation properties of Π_h (Brezzi & Raviart, 1976; Brezzi *et al.*, 1980; Arnold & Walker, 2020). Next, estimate $\mathring{b}_h \left(\varphi_h, g - g_h \right)$ and $\left(\varphi_h^{\text{nn}}, \boldsymbol{n} \cdot \nabla_{\Gamma} (g - g_h) \right)_{\Sigma_c}$ with (5.9).

Finally, the discrete problem on the discrete domain is to find $(\hat{\boldsymbol{\sigma}}_h, \hat{w}_h) = (\mathring{\hat{\boldsymbol{\sigma}}}_h + \hat{\boldsymbol{\rho}}_h, \mathring{w}_h + \hat{g}_h)$, with $\mathring{\hat{\boldsymbol{\sigma}}}_h \in V_h^m$, $\mathring{w}_h \in W_h^m$ such that

$$a^{m}\left(\mathring{\boldsymbol{\sigma}}_{h}, \hat{\boldsymbol{\varphi}}_{h}\right) + b_{h}^{m}\left(\hat{\boldsymbol{\varphi}}_{h}, \mathring{\hat{w}}_{h}\right) = -a^{m}\left(\hat{\boldsymbol{\rho}}_{h}, \hat{\boldsymbol{\varphi}}_{h}\right) - \mathring{b}_{h}^{m}\left(\hat{\boldsymbol{\varphi}}_{h}, \hat{\boldsymbol{g}}_{h}\right) - \left(\hat{\boldsymbol{\varphi}}_{h}^{nn}, \hat{\boldsymbol{n}} \cdot \left[\nabla_{\Gamma^{m}}\hat{\boldsymbol{g}}_{h} - \tilde{\boldsymbol{\xi}}\right]\right)_{\Sigma_{c}^{m}}, \ \forall \hat{\boldsymbol{\varphi}}_{h} \in V_{h}^{m},$$

$$b_{h}^{m}\left(\mathring{\boldsymbol{\sigma}}_{h}, \hat{\boldsymbol{v}}_{h}\right) = -\left\langle\tilde{\boldsymbol{f}}, \hat{\boldsymbol{v}}_{h}\right\rangle_{\Gamma^{m}} - b_{h}^{m}\left(\hat{\boldsymbol{\rho}}_{h}, \hat{\boldsymbol{v}}_{h}\right) - \left(\tilde{\boldsymbol{\xi}}_{f}, \hat{\boldsymbol{v}}_{h}\right)_{\Sigma_{f}^{m}} - \sum_{p \in \mathscr{V}_{\Sigma_{f}}} \boldsymbol{\xi}_{p}\hat{\boldsymbol{v}}_{h}(p), \ \forall \hat{\boldsymbol{v}}_{h} \in W_{h}^{m},$$

$$(6.21)$$

where $\hat{\rho}_h := P_h^m \tilde{\rho}$, with $\tilde{\rho}$ given by $\rho \circ \Psi^m = \text{Piola}(\tilde{\rho})(\tilde{\mathbf{x}})$ (recall (4.12)), and $P_h^m : H_h^0(\Gamma^m) \to V_h^m$ is the $L^2(\Gamma^m)$ projection on Γ^m , $\hat{g}_h := \mathscr{S}_h^m \tilde{g}$, with $\tilde{g} := g \circ \Psi^m$, $\tilde{\xi} := (\nabla_{\Gamma} g) \circ \Psi^m$ and $\tilde{\zeta}_f := \zeta_f \circ \Psi^m$. To

obtain an analogous result to Theorem 6.4 we need to generalize Lemma 6.2, i.e. we need to show that

$$a^{m}\left(\mathring{\tilde{\boldsymbol{\sigma}}}_{h}-\mathring{\hat{\boldsymbol{\sigma}}}_{h},\hat{\boldsymbol{\varphi}}_{h}\right)+b_{h}^{m}\left(\hat{\boldsymbol{\varphi}}_{h},\mathring{\tilde{\boldsymbol{w}}}_{h}-\mathring{\hat{\boldsymbol{w}}}_{h}\right)+b_{h}^{m}\left(\mathring{\tilde{\boldsymbol{\sigma}}}_{h}-\mathring{\hat{\boldsymbol{\sigma}}}_{h},\hat{\boldsymbol{v}}_{h}\right)=\mathrm{E}_{1}(\hat{\boldsymbol{\varphi}}_{h},\hat{\boldsymbol{v}}_{h}),\tag{6.22}$$

for all $\hat{\boldsymbol{\varphi}}_h \in V_h^m$ and $\hat{v}_h \in W_h^m$, where

$$\begin{aligned} |\mathbf{E}_{1}(\hat{\boldsymbol{\varphi}}_{h}, \hat{\boldsymbol{v}}_{h})| &\leq Ch^{s} \left(\|\boldsymbol{\varphi}_{h}\|_{0,h} + \|\boldsymbol{v}_{h}\|_{2,h} \right) \\ &\cdot \left(\|\boldsymbol{\rho}\|_{W^{t-2,p}(\Gamma; \mathbf{S})} + \|\boldsymbol{g}\|_{W^{t,p}(\Gamma)} + \|\boldsymbol{\varsigma}_{f}\|_{L^{1}(\Sigma_{f})} + \|\mathring{\boldsymbol{\sigma}}_{h}\|_{0,h} + \|\mathring{\boldsymbol{w}}_{h}\|_{2,h} \right), \end{aligned}$$
(6.23)

where s is the exponent appearing in (6.12). This also follows the same outline, but we note the following: (1) Estimating $\mathring{b}_h^m \left(\hat{\boldsymbol{\varphi}}_h, \tilde{g} - \hat{g}_h \right)$ with (4.17) is simpler because the last boundary term in (4.17) does not appear; then use Lemma 5.1; (2) noting that $\hat{g}_h = g_h \circ \boldsymbol{\Psi}^m$, $\left(\varphi_h^{\text{nn}}, \boldsymbol{n} \cdot \nabla_{\Gamma} (g_h - g) \right)_{\Sigma_c}$ is mapped to $\left(\hat{\varphi}_h^{\text{nn}}, \hat{\boldsymbol{n}} \cdot \nabla_{\Gamma^m} (\hat{g}_h - \tilde{g}) \right)_{\Sigma_c^m}$ (plus residual terms) and is compared against $\left(\hat{\varphi}_h^{\text{nn}}, \hat{\boldsymbol{n}} \cdot [\nabla_{\Gamma^m} \hat{g}_h - \tilde{\boldsymbol{\xi}}] \right)_{\Sigma_c^m}$; (3) finally, estimate $\left(\hat{\varphi}_h^{\text{nn}}, \hat{\boldsymbol{n}} \cdot [\nabla_{\Gamma^m} \tilde{g} - \tilde{\boldsymbol{\xi}}] \right)_{\Sigma_c^m}$ using similar arguments as in the proof of Theorem 4.8. With this, generalizing Theorems 6.3 and 6.4, and Corollary 6.5, is immediate and we obtain the following.

THEOREM 6.6 (Inhomogeneous boundary conditions). Adopt the hypotheses of Theorem 6.4, except assume that (σ, w) satisfies (6.18) and $(\hat{\sigma}_h, \hat{w}_h)$ solves (6.21). If $m \ge r+1$ then (σ, w) and $(\hat{\sigma}_h, \hat{w}_h)$ satisfy the same estimates as in (6.12). In addition, if Γ and Σ are smooth, and the data and solution (σ, w) are smooth, then if $r \ge 0$ is the degree of V_h , then (σ, w) and $(\hat{\sigma}_h, \hat{w}_h)$ satisfy the same estimates as in (6.16).

7. Numerical results

We present numerical results for several different domains, both with and without boundary. The discrete domains were generated by either interpolating charts on a sequence of uniformly refined grids, or by creating an initial piecewise linear triangulation of the implicit, closed surface (using Walker, 2013) and interpolating the closest point map. As above, the finite element spaces V_h and W_h are of degree r and r+1, respectively, where $r\geqslant 0$ and the geometric approximation degree is denoted m. All computations were done with the Matlab/C++ finite element toolbox FELICITY (Walker, 2018), where we used the 'backslash' command in Matlab to solve the linear systems.

From (5.17) recall that $\mathbf{F}^m := \mathscr{I}_h^{1,m} \mathbf{\Psi}^1$, which is possible to implement, but inconvenient. Instead, we first compute \mathbf{F}^{m+1} by standard nodal interpolation, then we define $\mathbf{F}^m := \mathscr{I}_h^{1,m} \mathbf{F}^{m+1}$, which is easy to implement over the piecewise linear triangulation of Γ^1 . Moreover, the accuracy is not affected.

As for the boundary data \hat{g}_h , $\tilde{\xi}$ and $\hat{\rho}_h$ only need to be computed on the boundary Σ^m ; in fact only the boundary part of the L^2 projection P_h^m needs to be computed. For the free conditions, ς_p is implemented exactly since a corner coincides with a fixed vertex in the mesh. The other free condition ς_f can be computed exactly at any point on Σ_f using the manufactured solution, so that $\dot{\mathcal{F}}_h^{m+1,m+1}\varsigma_f$ on Σ_f^{m+1} , where $\dot{\mathcal{F}}_h^{m+1,m+1}$ is the standard nodal interpolation onto degree m+1 polynomials, is well defined because Σ_f^{m+1} interpolates Σ_f . Then, we define $\tilde{\varsigma}_f := \varpi_h \left(\dot{\mathcal{F}}_h^{m+1,m+1}\varsigma_f\right) \circ \Phi^{m,m+1}$ on Σ_f^m , where ϖ_h denotes the (local) change in length between Σ_f^m and Σ_f^{m+1} .

Table 1 EoC for the saddle square with simply-supported boundary conditions. N_T is the number of triangles in the final mesh after multiple uniform refinements. Italics indicate the case m = r + 1, which is the optimal case proven in this paper

$\overline{N_T}$	m	r	$\ \hat{w}_h\ _{L^2}$	$ \hat{w}_h _{H^1}$	$\ \hat{w}_h\ _{2,h}$	$\ \hat{\pmb{\sigma}}_h\ _{0,h}$
2^{21}	1	0	2.00	1.98	0.00	1.00
2^{21}	1	1	2.00	1.01	0.00	0.57
2^{19}	1	2	2.00	1.02	0.01	0.63
2^{21}	2	1	3.93	2.93	1.84	2.00
2^{19}	2	2	3.63	2.02	1.03	2.24
2^{17}	2	3	6.27	2.00	1.00	1.69
2^{17}	3	2	6.23	3.99	2.98	2.95
2^{17}	3	3	6.89	6.08	3.97	3.93
2^{15}	3	4	11.00	7.59	4.22	3.88
2^{17}	4	3	6.89	6.67	3.99	4.00
2^{15}	4	4	10.84	10.66	5.00	5.02
2^{15}	5	4	10.83	10.66	5.00	5.02

For convenience, the errors we compute are $\|w - \hat{w}_h\|_{L^2(\Gamma^m)}$, $\|\nabla_{\Gamma^m}(w - \hat{w}_h)\|_{L^2(\Gamma^m)}$, $\|w - \hat{w}_h\|_{2,h,m}$, $\|\sigma - \hat{\sigma}_h\|_{0,h,m}$, where the exact solution has been extended by analytic continuation. These errors can be related to the ones in (6.16) by basic arguments and a triangle inequality; a similar approach was used in Arnold & Walker (2020, Sec. 6.1). The estimated order of convergence (EoC) is computed by using the ratio of the error between two successive uniform refinements for the final mesh size.

7.1 Saddle surface

7.1.1 Square. The domain is given by (U, χ) , where $U = [0, 1] \times [0, 1]$ and $\chi(u_1, u_2) = (u_1, u_2, \cos(2\pi(u_2 - 0.5)) - \cos(2\pi(u_1 - 0.5)))$. The exact solution, on the reference domain, is

$$w \circ \chi(u_1, u_2) = \sin(6.5u_1)\cos(5.9u_2). \tag{7.1}$$

Table 1 shows the EoC for the case of simply-supported boundary conditions; the clamped case gave similar numbers and free boundary conditions had slightly better rates. The optimal orders of convergence, based on the degree of the elements, is r+1 for the three quantities $\|\hat{w}_h\|_{H^1}$, $\|\hat{\sigma}_h\|_{0,h}$ and r for $\|\hat{w}_h\|_{2,h}$. The convergence is a bit better than expected. For example, when m=1 and r=1,2, the convergence rate for $\|\hat{\sigma}_h\|_{0,h}$ is reduced, but not as much as our analysis suggests (see Remark 6.1). Similarly, when m=2 and r=3, the EoC for $\|\hat{\sigma}_h\|_{0,h}$ is reduced. However, \hat{w}_h is not so adversely affected.

7.1.2 Three-leaf domain. The domain is given by (U, χ) , where the boundary of U is parametrized by

$$x(t) = [1 + 0.4\cos(3t)]\cos(t), \quad y(t) = [1 + (0.4 + 0.22\sin(t))\cos(3t)]\sin(t), \tag{7.2}$$

Table 2 EoC for the saddle three-leaf domain with simply-supported boundary conditions. N_T is the number of triangles in the final mesh after multiple uniform refinements. Italics indicate the case m = r + 1, which is the optimal case proven in this paper

$\overline{N_T}$	m	r	$\ \hat{w}_h\ _{L^2}$	$ \hat{w}_h _{H^1}$	$\ \hat{w}_h\ _{2,h}$	$\ \hat{\pmb{\sigma}}_h\ _{0,h}$
2^{18}	1	0	1.99	1.45	0.00	1.00
2^{16}	1	1	1.15	1.07	0.07	0.54
2^{16}	1	2	1.04	1.02	0.02	0.47
2^{16}	2	1	3.27	2.14	1.13	1.99
2^{16}	2	2	3.00	3.03	1.94	1.58
2^{14}	2	3	2.94	2.54	1.53	1.71
2^{16}	3	2	4.07	3.04	2.03	2.99
2^{14}	3	3	5.06	4.03	2.99	2.54
2^{14}	3	4	4.85	3.56	2.52	2.39
2^{14}	4	3	5.06	4.04	3.03	4.00
2^{14}	4	4	6.03	5.01	3.95	3.67
2^{14}	5	4	6.03	5.02	4.01	4.99

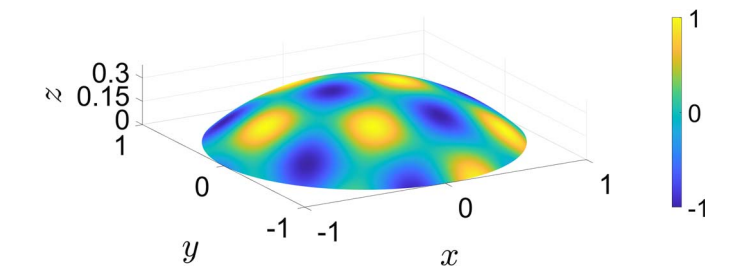


Fig. 4. The surface Kirchhoff plate problem on a spherical cap.

for $0 \le t \le 2\pi$; this choice of domain avoids any spurious symmetries (e.g. the unit disk; see Arnold & Walker, 2020, Sec. 6.2). The surface parametrization is given by $\chi(u_1, u_2) = (u_1, u_2, (u_2 - 0.5)^2 - (u_1 - 0.5)^2)$. The exact solution, on the reference domain, is

$$w \circ \chi(u_1, u_2) = \sin(2\pi u_1)\cos(2\pi u_2). \tag{7.3}$$

The curved element mapping is composed from two maps (recall (5.17)). The first map is a Lenoir-type map (Lenoir, 1986) described in Arnold & Walker (2020) that creates a curved triangulation that optimally approximates U; the second map is the parametrization χ . We then apply (5.17) to the composed map.

Table 2 shows the EoC for the case of simply-supported boundary conditions; the clamped case gave similar numbers and free boundary conditions had slightly better rates. The optimal orders of convergence, based on the degree of the elements, is r+1 for the three quantities $\|\hat{w}_h\|_{H^1}$, $\|\hat{\sigma}_h\|_{0,h}$ and r for $\|\hat{w}_h\|_{2,h}$. The convergence is a bit better than expected. For example, whenever m < r+1, the convergence rate for $\|\hat{\sigma}_h\|_{0,h}$ is roughly $O(h^{m-1/2})$, which is not as bad as our analysis suggests (see Remark 6.1). However, \hat{w}_h is not so adversely affected.

Table 3 EoC for the spherical cap with simply-supported boundary conditions. N_T is the number of triangles in the final mesh after multiple uniform refinements. Italics indicate the case m = r + 1, which is the optimal case proven in this paper

N_T	m	r	$\ \hat{w}_h\ _{L^2}$	$ \hat{w}_h _{H^1}$	$\ \hat{w}_h\ _{2,h}$	$\ \hat{\pmb\sigma}_h\ _{0,h}$
2^{20}	1	0	2.00	1.00	0.00	1.00
2^{18}	1	1	1.21	1.09	0.15	0.57
2^{18}	1	2	1.12	1.02	0.02	0.52
2^{18}	2	1	3.00	2.00	1.00	2.00
2^{18}	2	2	3.51	2.68	1.76	2.46
2^{16}	2	3	3.03	2.03	1.06	2.01
2^{18}	3	2	4.00	3.00	2.00	3.00
2^{16}	3	3	4.96	3.97	2.98	3.73
2^{14}	3	4	4.08	3.15	2.23	2.65
2^{16}	4	3	5.00	4.00	3.00	4.00
2^{14}	4	4	5.99	5.00	4.00	4.98
2^{14}	5	4	5.99	5.00	4.00	4.99

Table 4 Eigenvalues for the spherical cap with free boundary conditions for m=3 and r=2 (the results were similar for other choices of m=3 and r=2). Level refers to the refinement level. The eigenvalue λ_1 (not shown) is machine precision $\approx 10^{-14}$. Note that λ_2 , λ_3 are not zero, but are much smaller than the other eigenvalues listed

level	λ_2	λ_3	λ_4	λ_5	λ_6
$\ell = 1$	$4.29 \cdot 10^{-3}$	$4.49 \cdot 10^{-3}$	$8.13 \cdot 10^{-1}$	$9.00 \cdot 10^{-1}$	$9.97 \cdot 10^{-1}$
$\ell = 2$	$1.28 \cdot 10^{-3}$	$1.35 \cdot 10^{-3}$	$2.90 \cdot 10^{-1}$	$3.45 \cdot 10^{-1}$	$5.37 \cdot 10^{-1}$
$\ell = 3$	$3.51 \cdot 10^{-4}$	$3.72 \cdot 10^{-4}$	$7.84 \cdot 10^{-2}$	$9.44 \cdot 10^{-2}$	$1.33 \cdot 10^{-1}$
$\ell = 4$	$9.19 \cdot 10^{-5}$	$9.78 \cdot 10^{-5}$	$2.07 \cdot 10^{-2}$	$2.52 \cdot 10^{-2}$	$3.50 \cdot 10^{-2}$
$\ell = 5$	$2.35 \cdot 10^{-5}$	$2.51 \cdot 10^{-5}$	$5.31 \cdot 10^{-3}$	$6.51 \cdot 10^{-3}$	$9.01 \cdot 10^{-3}$
$\ell = 6$	$5.96 \cdot 10^{-6}$	$6.35 \cdot 10^{-6}$	$1.35 \cdot 10^{-3}$	$1.66 \cdot 10^{-3}$	$2.29 \cdot 10^{-3}$
$\ell = 7$	$1.50 \cdot 10^{-6}$	$1.60 \cdot 10^{-6}$	$3.39 \cdot 10^{-4}$	$4.18 \cdot 10^{-4}$	$5.76 \cdot 10^{-4}$

7.2 Spherical cap

The domain is given by (U, χ) , where U is the unit disk, centered at the origin, and $\chi(u_1, u_2) = (u_1, u_2, [(1.5)^2 - (u_1^2 + u_2^2)]^{1/2} - [(1.5)^2 - 1^2]^{1/2})$. The exact solution, on the reference domain, is

$$w \circ \chi(u_1, u_2) = \sin(6.7u_1)\cos(6.1u_2). \tag{7.4}$$

The curved element mapping is composed from two maps analogous to Section 7.1.2. The numerical solution \hat{w}_h is shown in Fig. 4 for the case of simply-supported boundary conditions; Table 3 shows the corresponding EoC. The clamped case gave similar rates and free boundary conditions had better rates. The format is similar to Section 7.1. The convergence is again better than expected. For example, when m=1 and r=1,2, the convergence rate for $\|\hat{\sigma}_h\|_{0,h}$ is reduced, but not as much as our analysis

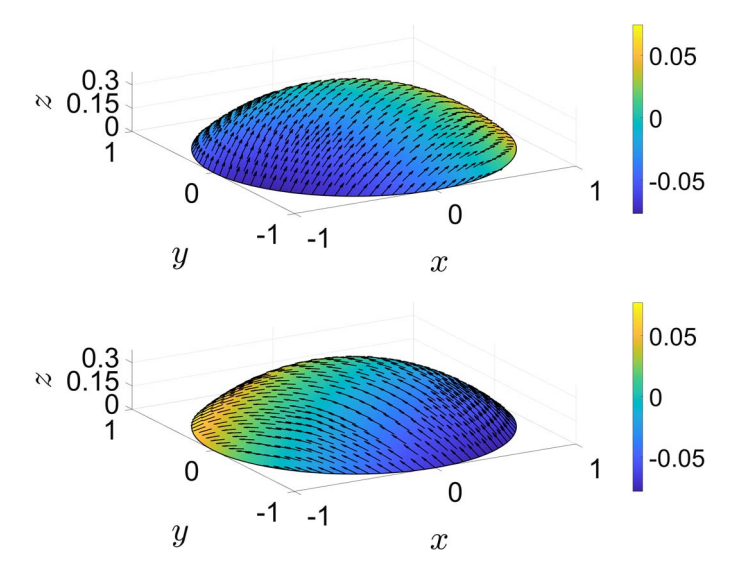


Fig. 5. Killing fields on a spherical cap. Top shows z_2 (in color) with gradient (Killing) field $\nabla_{\Gamma} z_2$ as black arrows. Bottom shows z_3 .

Table 5 EoC for the torus; same format as earlier EoC tables

N_T	m	r	$\ \hat{w}_h\ _{L^2}$	$ \hat{w}_h _{H^1}$	$\ \hat{w}_h\ _{2,h}$	$\ \hat{\pmb\sigma}_h\ _{0,h}$
2 ²¹	1	0	2.00	1.00	0.00	1.00
2^{21}	1	1	2.00	2.00	1.00	1.00
2^{19}	1	2	2.00	2.00	1.00	1.00
2^{21}	2	1	3.98	2.00	1.00	2.01
2^{19}	2	2	3.96	2.00	1.00	2.01
2^{17}	2	3	4.03	2.00	1.00	2.00
2^{19}	3	2	4.70	3.00	2.00	2.99
2^{17}	3	3	5.82	3.00	2.00	2.99
2^{17}	3	4	4.17	3.00	2.01	2.99
2^{17}	4	3	6.04	4.02	3.00	4.05
2^{17}	4	4	5.30	4.00	3.00	4.05
2^{17}	5	4	7.66	5.00	3.99	4.96

suggests (see Remark 6.1). For the other cases there is no reduction below the rate given by m; e.g. the rate for $\|\hat{w}_h\|_{2,h}$ is always at least $O(h^{m-1})$. In addition, \hat{w}_h is not so adversely affected.

When uniformly free boundary conditions are used on the spherical cap domain, the null-space $\mathscr{Z}(\Gamma)$ of the covariant Hessian contains three linearly independent functions $\{z_i\}_{i=1}^3$: the constant function z_1 and two of the isometric rotations of the sphere, z_2 , z_3 , which are illustrated in Fig. 5. Note that the other rotation (not present) cannot be represented as the gradient of a function. Eigenvalues of the discrete finite element system were computed with Matlab and are shown in Table 4, where $\{\lambda_i\}_{i=1}^3$ are the corresponding eigenvalues of $\{z_i\}_{i=1}^3$. The first three eigenvalues of the continuous problem are

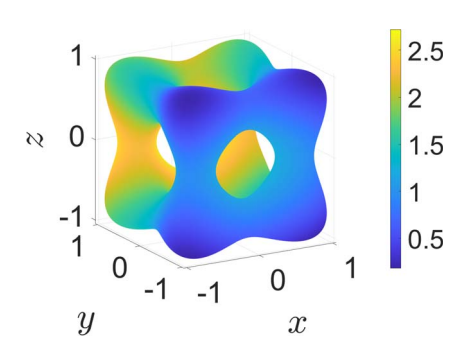


Fig. 6. The surface biharmonic problem on a genus-5 surface.

Table 6 EoC for the genus-5 surface; same format as earlier EoC tables

$\overline{N_T}$	m	r	$\ \hat{w}_h\ _{L^2}$	$ \hat{w}_h _{H^1}$	$\ \hat{w}_h\ _{2,h}$	$\ \hat{\boldsymbol{\sigma}}_h\ _{0,h}$
2^{20}	1	0	1.99	1.17	0.00	1.05
2^{20}	1	1	2.00	2.00	1.00	1.06
2^{18}	1	2	1.99	1.99	0.99	1.07
2^{20}	2	1	3.98	2.00	1.00	2.02
2^{18}	2	2	3.95	2.20	1.06	2.47
2^{18}	2	3	3.97	2.21	1.06	2.41
2^{18}	3	2	6.64	3.01	2.00	2.97
2^{18}	3	3	5.87	3.02	2.01	2.99
2^{16}	3	4	5.82	3.44	2.16	3.06
2^{18}	4	3	5.58	4.09	3.00	4.06
2^{16}	4	4	5.17	4.05	3.06	4.12
2^{16}	5	4	4.70	5.17	4.03	5.07

zero, but for the numerical approximation, only λ_1 is machine precision; λ_2 , λ_3 are not zero, but are much smaller than the other eigenvalues and appear to converge to zero (cf. Reusken, 2018, Sec. 6).

7.3 Torus

The domain is a torus described by the zero level set of the function: $b(x, y, z) = (x^2 + y^2 - (6/10))^2 + (3/2)z^2 - (1/4)$. The exact solution, extended everywhere, is

$$w(x, y, z) = \sin(1.1x) + \cos(1.2y) + \sin(1.3z). \tag{7.5}$$

The 'parametrization' is built from the closest point map. Table 5 shows the EoC. The convergence is better than expected. For instance, the convergence rate for $\|\hat{w}_h\|_{H^1}$ and $\|\hat{\sigma}_h\|_{0,h}$ is $O(h^{\min(m,r+1)})$.

7.4 Biharmonic on a genus-5 surface

The domain is a genus-5 surface described by the zero level set of the function: $b(x, y, z) = (x^4 + y^4 + z^4) - (x^2 + y^2 + z^2) + 0.4$ (see Fig. 6). We solve the biharmonic problem $\Delta_{\Gamma}^2 w = f$ on Γ by modifying the

method in the following way. In terms of index notation one can show that $\int_{\Gamma} (\nabla^{\alpha} \nabla^{\beta} w) \nabla_{\beta} \nabla_{\alpha} z \, dS(g) = \int_{\Gamma} (\nabla_{\beta} \nabla^{\beta} w) \nabla_{\alpha} \nabla^{\alpha} z \, dS(g) - \int_{\Gamma} \kappa_{G}(\nabla^{\alpha} w) \nabla_{\alpha} z \, dS(g)$, where κ_{G} is the Gauss curvature of the manifold (do Carmo, 1992; Berger, 2003; Petersen, 2006). Therefore, solving the biharmonic problem: find $w \in \mathcal{W}(\Gamma)$ such that $\int_{\Gamma} \Delta_{\Gamma} w \Delta_{\Gamma} z = \langle f, z \rangle_{\Gamma}$, for all $z \in \mathcal{W}(\Gamma)$ (recall (2.3)) is equivalent to finding $w \in \mathcal{W}(\Gamma)$ such that (cf. Reusken, 2018, Lem. 5.6)

$$\int_{\Gamma} \nabla_{\Gamma} \nabla_{\Gamma} w : \nabla_{\Gamma} \nabla_{\Gamma} z + \int_{\Gamma} \kappa_{G} \nabla_{\Gamma} w \cdot \nabla_{\Gamma} z = \langle f, z \rangle_{\Gamma}, \text{ for all } z \in \mathcal{W}(\Gamma).$$
 (7.6)

The discrete mixed method for (7.6) is the following modification of (5.13): find $\sigma_h \in V_h^m$, $w_h \in W_h^m$ such that

$$a^{m}\left(\boldsymbol{\sigma}_{h},\boldsymbol{\varphi}\right) + b_{h}^{m}\left(\boldsymbol{\varphi},w_{h}\right) = 0, \ \forall \boldsymbol{\varphi} \in V_{h}^{m},$$

$$b_{h}^{m}\left(\boldsymbol{\sigma}_{h},v\right) - c^{m}\left(w_{h},v\right) = -\langle f,v\rangle_{\Gamma^{m}}, \ \forall v \in W_{h}^{m},$$

$$(7.7)$$

where $c^m(w,v) := \int_{\Gamma^m} \kappa_G \nabla_{\Gamma} w \cdot \nabla_{\Gamma} z$. When $\kappa_G \ge 0$ the convergence of this scheme can be established by standard mixed finite element theory (Boffi *et al.*, 2013). In fact, if $c^m(\cdot,\cdot)$ is only weakly coercive (κ_G slightly negative), then one can still show convergence; see Kellogg & Liu (1996). However, for general surfaces, convergence is not obvious and is a point of future work.

We now present a numerical example illustrating that convergence seems to hold even for very general surfaces. The exact solution, extended everywhere, is given by (see Fig. 6)

$$w(x, y, z) = \cos(0.9x) + \sin(1.1y) + \cos(1.3z). \tag{7.8}$$

Table 6 shows the EoC. The convergence is better than expected; the convergence rate for $|\hat{w}_h|_{H^1}$ and $\|\hat{\sigma}_h\|_{0,h}$ is at least $O(h^{\min(m,r+1)})$.

8. Conclusion

We have demonstrated that the classic HHJ method for the Kirchhoff plate equation extends to general embedded surfaces in \mathbb{R}^3 either closed or with boundary that have a combination of clamped, simply-supported and free conditions imposed. Moreover, optimal convergence is guaranteed so long as $m \ge r+1$, where m is the degree of surface approximation and r+1 is the degree of the Lagrange displacement variable. If m < r+1 some degradation in convergence occurs. The numerical experiment in Section 7.1.2 gave the best test of the method, but the convergence was still better than our estimates suggest when m < r+1. All other examples had slightly better rates. When m < r+1 the error estimates could be improved in the case of closed surfaces characterized by a signed distance function. Indeed, the closest point map enjoys nice approximation properties. But for surfaces with boundary, the parametric approach is more convenient, though multiple charts may be required.

It is worth noting that the classic Ciarlet–Raviart method for solving the biharmonic problem on flat domains is not appropriate when nonclamped boundary conditions are used, and the same holds for surfaces. This is connected to the classic Babuška paradox (Babuška & Pitkäranta, 1990), which concerns polygonal approximation of the domain. However, as was shown in Arnold & Walker (2020) for flat domains, the lowest order surface HHJ method converges optimally with only piecewise linear approximation of the domain, despite the fact that curvature of the boundary is important for accurately capturing boundary conditions (e.g. simply-supported conditions). This is a manifestation

of the *geometrically nonconforming* aspect of the HHJ method, originally noted in Arnold & Walker (2020).

Adapting the surface HHJ method to solve the surface biharmonic problem on closed surfaces requires an extra (lower order) term in the formulation involving the Gauss curvature (see Section 7.4). The theory here extends readily to surfaces of positive, or slightly negative, Gauss curvature. For general surfaces it is not obvious; however, the method appears to perform optimally.

REFERENCES

- AGMON, S. (1965) Lectures on Elliptic Boundary Value Problems. Van Nostrand Mathematical Studies: no. 2. Van Nostrand.
- ARNOLD, D. N. & WALKER, S. W. (2020) The Hellan–Herrmann–Johnson method with curved elements. *SIAM J. Numer. Anal.*, **58**, 2829–2855.
- ARNOLD, D. N. & Brezzi, F. (1985) Mixed and nonconforming finite element methods: implementation, postprocessing and error estimates. *ESAIM M2AN*, **19**, 7–32.
- Babuška, I., Osborn, J. & Pitkäranta, J. (1980) Analysis of mixed methods using mesh dependent norms. *Math. Comput.*, **35**, 1039–1062.
- BABUŠKA, I. & PITKÄRANTA, J. (1990) The plate paradox for hard and soft simple support. SIAM J. Math. Anal., 21, 551–576.
- BÄNSCH, E., MORIN, P. & NOCHETTO, R. H. (2005) A finite element method for surface diffusion: the parametric case. *J. Comput. Phys.*, **203**, 321–343.
- BARRETT, J. W., GARCKE, H. & NÜRNBERG, R. (2007) A parametric finite element method for fourth order geometric evolution equations. *J. Comput. Phys.*, **222**, 441–467.
- BARRETT, J. W., GARCKE, H. & NÜRNBERG, R. (2010) On stable parametric finite element methods for the Stefan problem and the Mullins–Sekerka problem with applications to dendritic growth. *J. Comput. Phys.*, **229**, 6270–6299.
- BARRETT, J. W., GARCKE, H. & NÜRNBERG, R. (2015) A stable parametric finite element discretization of two-phase Navier–Stokes flow. *J. Sci. Comput.*, **63**, 78–117.
- BARRETT, J. W., GARCKE, H. & NÜRNBERG, R. (2016) A stable numerical method for the dynamics of fluidic membranes. *Numer. Math.*, **134**, 783–822.
- Bartels, S., Bonito, A. & Nochetto, R. H. (2017) Bilayer plates: model reduction, gamma-convergent finite element approximation, and discrete gradient flow. *Commun. Pure Appl. Math.* **70**, 547–589. https://doi.org/10.1002/cpa.21626.
- Bartels, S., Dolzmann, G. & Nochetto, R. H. (2012) Finite element methods for director fields on flexible surfaces. *Interfaces Free Boundaries*, **14**, 231–272.
- BERGER, M. (2003) A Panoramic View of Riemannian Geometry, 1st edn. Berlin Heidelberg:Springer.
- Blum, H. & Rannacher, R. (1980) On the boundary value problem of the biharmonic operator on domains with angular corners. *Math. Methods Appl. Sci.*, **2**, 556–581.
- Blum, H. & Rannacher, R. (1990) On mixed finite element methods in plate bending analysis. part 1: the first Herrmann scheme. *Comput. Mech.*, **6**, 221–236.
- Boffi, D., Brezzi, F. & Fortin, M. (2013) Mixed Finite Element Methods and Applications. *volume 44 of Springer Series in Computational Mathematics*. New York, NY: Springer-Verlag.
- BONITO, A., NOCHETTO, R. & PAULETTI, M. (2011) Dynamics of biomembranes: effect of the bulk fluid. *Math. Model. Nat. Phenom.*, **6**, 25–43.
- BONITO, A., NOCHETTO, R. H. & SEBASTIAN PAULETTI, M. (2010) Parametric FEM for geometric biomembranes. *J. Comput. Phys.*, **229**, 3171–3188.
- Brenner, S. C. & Scott, L. R. (2008) *The Mathematical Theory of Finite Element Methods*. Texts in Applied Mathematics, vol. **15**, 3rd edn. New York, NY: Springer.
- Brezzi, F. & Marini, L. D. (1975) On the numerical solution of plate bending problems by hybrid methods. *R.A.I.R.O. Anal. Numér.*, **9**, 5–50.

- Brezzi, F., Marini, L. D., Quarteroni, A. & Raviart, P. A. (1980) On an equilibrium finite element method for plate bending problems. *Calcolo*, **17**, 271–291.
- BREZZI, F. & RAVIART, P. A. (1976) Mixed finite element methods for 4th order elliptic equations. *Topics In Numerical Analysis III: Proceedings of the Royal Irish Academy Conference on Numerical Analysis* (J. J. H. Miller ed.). London; New York: Academic Press, pp. 33–56.
- CIARLET, P. G. (2002) *The Finite Element Method for Elliptic Problems*. Classics in Applied Mathematics, 2nd edn. Philadelphia, PA: SIAM. ISBN: 978-0898715149.
- CIARLET, P. G. (2013) Linear and Nonlinear Functional Analysis with Applications, 1st edn. Philadelphia: SIAM.
- COMODI, M. I. (1989) The Hellan–Herrmann–Johnson method: some new error estimates and postprocessing. *Math. Comput.*, **52**, 17–29.
- DAVIS, C. B. & WALKER, S. W. (2015) A mixed formulation of the Stefan problem with surface tension. *Interfaces Free Boundaries*, **17**, 427–464.
- Davis, C. B. & Walker, S. W. (2017) Semi-discrete error estimates and implementation of a mixed method for the Stefan problem. *ESAIM Math. Model. Numer. Anal.*, **51**, 2093–2126.
- DECKELNICK, K., DZIUK, G. & ELLIOTT, C. M. (2005) Computation of geometric partial differential equations and mean curvature flow. *Acta Numer.*, **14**, 139–232.
- DEMLOW, A. (2009) Higher-order finite element methods and pointwise error estimates for elliptic problems on surfaces. *SIAM J. Numer. Anal.*, **47**, 805–827.
- DEMLOW, A. & DZIUK, G. (2007) An adaptive finite element method for the Laplace–Beltrami operator on implicitly defined surfaces. *SIAM J. Numer. Anal.*, **45**, 421–442.
- DO CARMO, M. P. (1976) Differential Geometry of Curves and Surfaces. Upper Saddle River, New Jersey: Prentice Hall
- Do CARMO, M. P. (1992) *Riemannian Geometry*. Mathematics: Theory and Applications, 2nd (English) edn. Boston: Birkhäuser.
- Du, Q., Liu, C., Ryham, R. & Wang, X. (2005) A phase field formulation of the Willmore problem. *Nonlinearity*, **18**, 1249.
- Du, Q., Liu, C. & Wang, X. (2004) A phase field approach in the numerical study of the elastic bending energy for vesicle membranes. *J. Comput. Phys.*, **198**, 450.
- DZIUK, G. (1988) Finite elements for the Beltrami operator on arbitrary surfaces. *Partial Differential Equations* and *Calculus of Variations*, vol. **1357** (S. Hildebrandt & R. Leis eds). Berlin, Heidelberg: Springer, pp. 142–155.
- DZIUK, G. (2008) Computational parametric Willmore flow. Numer. Math., 111, 55–80.
- DZIUK, G. & ELLIOTT, C. M. (2013) Finite element methods for surface PDEs. Acta Numer., 22, 289–396.
- EISENHART, L. P. (1926) Riemannian Geometry. Princeton, New Jersey: Princeton University Press.
- ELLIOTT, C. M. & RANNER, T. (2015) Evolving surface finite element method for the Cahn-Hilliard equation. *Numer. Math.*, **129**, 483–534.
- ELLIOTT, C. M. & STINNER, B. (2010) Modeling and computation of two phase geometric biomembranes using surface finite elements. *J. Comput. Phys.*, **229**, 6585–6612.
- ELLIOTT, C. M., STINNER, B. & VENKATARAMAN, C. (2012) Modelling cell motility and chemotaxis with evolving surface finite elements. *J. Royal Soc. Interface*, **9**, 3027–3044.
- EVANS, L. C. (1998) Partial Differential Equations. Providence, Rhode Island: American Mathematical Society.
- GERBEAU, J.-F. & LELIÈVRE, T. (2009) Generalized Navier boundary condition and geometric conservation law for surface tension. *Comput. Methods Appl. Mech. Eng.*, **198**, 644–656.
- HEBEY, E. (1996) Sobolev Spaces on Riemannian Manifolds. Lecture Notes in Mathematics. Berlin, Heidelberg: Springer.
- Kellogg, R. B. & Liu, B. (1996) A finite element method for the compressible Stokes equations. *SIAM J. Numer. Anal.*, **33**, 780–788.
- Krendl, W., Rafetseder, K. & Zulehner, W. (2016) A decomposition result for biharmonic problems and the Hellan–Herrmann–Johnson method. *Electron. Trans. Numer. Anal.*, **45**, 257–282.
- Kreyszig, E. (1991) Differential Geometry. New York: Dover.

- Larsson, K. & Larson, M. G. (2017) A continuous/discontinuous Galerkin method and a priori error estimates for the biharmonic problem on surfaces. *Math. Comput.*, **86**, 2613–2649.
- LASIECKA, I., TRIGGIANI, R. & YAO, P. F. (2003) Carleman Estimates for a Plate Equation on a Riemann Manifold with Energy Level Terms. Boston, MA: Springer US, pp. 199–236.
- LENOIR, M. (1986) Optimal isoparametric finite elements and error estimates for domains involving curved boundaries. SIAM J. Numer. Anal., 23, 562–580.
- LI, L. (2018) Regge finite elements with applications in solid mechanics and relativity. Ph.D. Thesis, University of Minnesota (Dept of Mathematics).
- PETERSEN, P. (2006) Riemannian Geometry. Graduate Texts in Mathematics, 2nd edn. New York: Springer.
- RAFETSEDER, K. & ZULEHNER, W. (2018) A decomposition result for Kirchhoff plate bending problems and a new discretization approach. *SIAM J. Numer. Anal.*, **56**, 1961–1986.
- REUSKEN, A. (2018) Stream function formulation of surface Stokes equations. IMA J. Numer. Anal., 40, 109-139.
- SMEREKA, P. (2003) Semi-implicit level set methods for curvature and surface diffusion motion. *J. Sci. Comput.*, **19**, 439–456.
- STENBERG, R. (1991) Postprocessing schemes for some mixed finite elements. *ESAIM Math. Model. Numer. Anal.*, **25**, 151–167.
- TIMOSHENKO, S. & WOINOWSKY-KRIEGER, S. (1959) *Theory of Plates and Shells*, 2nd edn. London: McGraw-Hill College.
- WALKER, S. W. (2013) Tetrahedralization of isosurfaces with guaranteed-quality by edge rearrangement (TIGER). *SIAM J. Sci. Comput.*, **35**, A294–A326.
- WALKER, S. W. (2015) The Shapes of Things: A Practical Guide to Differential Geometry and the Shape Derivative. Advances in Design and Control, vol. 28, 1st edn. Philadelphia: SIAM.
- WALKER, S. W. (2018) FELICITY: A Matlab/C++ toolbox for developing finite element methods and simulation modeling. *SIAM J. Sci. Comput.*, **40**, C234–C257.
- WALKER, S. W. (2021) Poincaré inequality for a mesh-dependent 2-norm on piecewise linear surfaces with boundary. *Comput. Methods Appl. Math.*, accepted .
- WALKER, S. W., SHAPIRO, B. & NOCHETTO, R. H. (2009) Electrowetting with contact line pinning: computational modeling and comparisons with experiments. *Phys. Fluids*, **21**, 102103.
- ZHONG-CAN, O.-Y. & HELFRICH, W. (1989) Bending energy of vesicle membranes: general expressions for the first, second and third variation of the shape energy and applications to spheres and cylinders. *Phys. Rev. A*, **39**, 5280–5288.

A. Appendix

A.1 *Intrinsic differential geometry*

We review the differential geometry tools needed for working on manifolds (Hebey, 1996; do Carmo, 1976, 1992; Kreyszig, 1991; Ciarlet, 2013). Specifically, we review the basic notation of covariant, contravariant and other differential geometry concepts.

Consider a d-dimensional Riemannian manifold $(\Gamma, g_{\mathfrak{ab}})$, where $g_{\mathfrak{ab}}$ is the given metric tensor (discussed below) defined over a (reference) domain $U \subset \mathbb{R}^d$. A point in U is denoted by $(u^1, u^2, ..., u^d)$; in the special case of d = 2 that we are mainly concerned with, we may use $(u, v) \in U$. We refer to variables defined on U as *intrinsic* quantities.

Tensor index notation. We use lower-case *Greek* indices $(\alpha, \beta, \gamma, \text{ etc.})$, which take values in $\{1, 2, ..., d\}$ when referring to intrinsic variables. For example, ∂_{α} is the partial derivative with respect to the coordinate u^{α} for $\alpha \in \{1, 2, ..., d\}$. Covariant vectors are denoted with *lower* indices, e.g. $(v_1, v_2, ..., v_d)$, and contravariant vectors are denoted with *upper* indices, e.g. $(v^1, v^2, ..., v^d)$. The β th component of a covariant (contravariant) derivative is denoted by ∇_{β} (∇^{β}). Similar considerations hold

for *tensors*. Furthermore, we use the letters \mathfrak{a} - \mathfrak{h} (with a different font for emphasis) as a *nonnumerical* label to indicate a covariant, contravariant or mixed tensor. For example, $v_{\mathfrak{a}}$ refers to a covariant vector (not just a single component), i.e. $v_{\mathfrak{a}} \equiv (v_1, ..., v_d)$. When convenient, we use bold-face for vector and tensor quantities instead of writing out indices.

Main concepts. The given metric $g_{\mathfrak{a}\mathfrak{b}}$ is a symmetric, covariant tensor with component functions $g_{\alpha\beta}:U\to\mathbb{R}$, for $1\leqslant\alpha,\beta\leqslant d$, which we assume are at least C^1 , and is uniformly positive definite. We write $g:=\det g_{\mathfrak{a}\mathfrak{b}}$ and the inverse metric tensor $g^{\mathfrak{a}\mathfrak{b}}$ is contravariant with components denoted $g^{\alpha\beta}$, where $g_{\alpha\gamma}g^{\gamma\beta}=\delta^{\beta}_{\alpha}$. Note that $v^{\mathfrak{a}}$ may be converted to $v_{\mathfrak{b}}$ via $v_{\beta}=g_{\beta\alpha}v^{\alpha}$; similarly, $w_{\mathfrak{b}}$ may be converted to $w^{\mathfrak{a}}$ by $w^{\alpha}=g^{\alpha\beta}w_{\beta}$. When convenient, we write $g_{\mathfrak{a}\mathfrak{b}}\equiv \mathbf{g}=[g_{\alpha\beta}]_{\alpha,\beta=1}^2$ and $g^{\mathfrak{a}\mathfrak{b}}\equiv \mathbf{g}^{-1}=[g^{\alpha\beta}]_{\alpha,\beta=1}^2$ in standard matrix notation for the metric and inverse metric, respectively. Let $T_2=T_2(\Gamma)$ ($T^2=T^2(\Gamma)$) be the set of covariant (contravariant) 2-tensors on Γ . Moreover, $S_2\subset T_2$ and $S^2\subset T^2$ are subsets of symmetric tensors; so then $g_{\mathfrak{a}\mathfrak{b}}\in S_2$ and $g^{\mathfrak{a}\mathfrak{b}}\in S^2$.

The Christoffel symbols Γ_{ii}^{k} (of the second kind) are defined by

$$\Gamma^{\gamma}_{\alpha\beta} := \frac{1}{2} g^{\mu\gamma} \left(\partial_{\alpha} g_{\beta\mu} + \partial_{\beta} g_{\mu\alpha} - \partial_{\mu} g_{\alpha\beta} \right), \quad 1 \leqslant \alpha, \beta, \gamma \leqslant 2, \tag{A.1}$$

where $\Gamma_{\alpha\beta}^{\gamma} = \Gamma_{\beta\alpha}^{\gamma}$ (do Carmo, 1976, 1992). With this we recall the definition of covariant (contravariant) derivatives, denoted ∇_{α} (∇^{α}), where f is a scalar, $v_{\mathfrak{b}}$ is a covariant vector and $v^{\mathfrak{c}}$ is a contravariant vector:

$$\begin{split} \nabla_{\alpha}f &= \partial_{\alpha}f, \qquad \nabla_{\alpha}\nabla_{\beta}f = \partial_{\alpha}\partial_{\beta}f - (\partial_{\gamma}f)\Gamma_{\alpha\beta}^{\gamma}, \\ \nabla_{\alpha}v_{\beta} &= \partial_{\alpha}v_{\beta} - v_{\gamma}\Gamma_{\beta\alpha}^{\gamma}, \quad \nabla_{\alpha}v^{\gamma} = \partial_{\alpha}v^{\gamma} + v^{\beta}\Gamma_{\beta\alpha}^{\gamma}, \quad \nabla_{\alpha}v^{\alpha} = (\sqrt{g})^{-1}\partial_{\alpha}(v^{\alpha}\sqrt{g}), \end{split} \tag{A.2}$$

and for a contravariant tensor r^{ab} :

$$\nabla_{\rho} r^{\alpha\beta} = \partial_{\rho} r^{\alpha\beta} + r^{\gamma\beta} \Gamma^{\alpha}_{\gamma\rho} + r^{\alpha\gamma} \Gamma^{\beta}_{\gamma\rho}, \qquad \nabla_{\beta} \nabla_{\alpha} r^{\alpha\beta} = (\sqrt{g})^{-1} \partial_{\beta} (\sqrt{g} \nabla_{\alpha} r^{\alpha\beta}). \tag{A.3}$$

The metric satisfies $\nabla_{\gamma} g_{\alpha\beta} = 0$, $\nabla_{\gamma} g^{\alpha\beta} = 0$, $\nabla_{\gamma} g = 0$, for $1 \leqslant \alpha, \beta, \gamma \leqslant 2$ (do Carmo, 1992).

Let $n_{\mathfrak{a}}$ be the conormal vector of ∂U , and $n^{\mu} = g^{\mu\gamma} n_{\gamma}$. Viewing $n_{\mathfrak{a}}$ as a 'vector' in \mathbb{R}^d it has unit length under the \mathbb{R}^d Euclidean metric. If d=2 let $t^{\mathfrak{a}}$ be the oriented (contravariant) tangent vector of ∂U , which has unit length in the Euclidean metric and satisfies $n_{\alpha}t^{\alpha}=0$. Moreover, $g=t^{\mu}t_{\mu}/(n^{\mu}n_{\mu})$, which implies that $\mathrm{ds}(g):=\sqrt{t^{\mu}t_{\mu}}\,d\mathrm{l}$ for d=2, and we have the following 'orthogonal' decomposition

$$\delta^{\alpha}_{\beta} = \frac{n^{\alpha}n_{\beta}}{n^{\mu}n_{\mu}} + \frac{t^{\alpha}t_{\beta}}{t^{\mu}t_{\mu}}.$$
 (A.4)

A.2 Extrinsic differential geometry

Suppose that the manifold Γ is embedded in \mathbb{R}^n , with $n \ge d$, and that it is represented by a family of charts $\{(U_i, \chi_i)\}$, where a single chart consists of a pair (U, χ) , with $U \subset \mathbb{R}^d$ (reference domain) and $\chi: U \to \mathbb{R}^n$ (do Carmo, 1992). For simplicity of exposition assume there is only one chart (U, χ) , where $\Gamma = \chi(U)$. We refer to variables in \mathbb{R}^n as *extrinsic* quantities.

Tensor index notation. We use lower-case *Latin* letters starting with i (i.e. i, j, k, l, etc.), which take values in $\{1, 2, ..., n\}$, when referring to components of extrinsic (ambient space) quantities. For example, $\mathbf{x} = (\mathbf{x}^1, ..., \mathbf{x}^n)^T \in \mathbb{R}^n$, and $\mathbf{x}^i : U \to \mathbb{R}$ for each $i \in \{1, 2, ..., n\}$. A point $\mathbf{x} \in \mathbb{R}^n$ has its jth coordinate denoted by x^j . Moreover, ∂_k is the partial derivative with respect to coordinate x^k . Repeated indices are

summed over. We typically bold-face extrinsic vectors and tensors, e.g. let \mathbf{w} be a (covariant) 2-tensor in \mathbb{R}^n with components w_{ij} for $i,j \in \{1,2,...,n\}$. The canonical (orthonormal) basis in \mathbb{R}^n is denoted by $\{\mathbf{a}_k\}_{k=1}^n$, where $\mathbf{a}_1 = (1,0,...,0)^T$ (column vector), etc. With the Kronecker delta δ_i^j we have the dual basis $\{\mathbf{a}^k\}$ of $\{\mathbf{a}_k\}$ by the formula $\mathbf{a}_i \cdot \mathbf{a}^j = \delta_i^j$.

Differential geometry in the ambient space. The tangent space $T_{\mathbf{x}}(\Gamma)$, at a point $\mathbf{x} \in \Gamma$, is a subspace of \mathbb{R}^n spanned by $\{\mathbf{e}_1, \mathbf{e}_2, ..., \mathbf{e}_d\}$ (the covariant basis) where

$$\mathbf{e}_{\alpha} = \partial_{\alpha} \mathbf{\chi}(u^{\mathfrak{a}}), \quad 1 \leqslant \alpha \leqslant d, \quad \text{where } u^{\mathfrak{a}} \equiv (u^{1}, ..., u^{d}) = \mathbf{\chi}^{-1}(\mathbf{x}).$$
 (A.5)

In this case the metric tensor $g_{\alpha\beta}$ is given by $g_{\alpha\beta} = \mathbf{e}_{\alpha} \cdot \mathbf{e}_{\beta}$, for $1 \leq \alpha, \beta \leq d$. The contravariant tangent basis is given by $\{\mathbf{e}^1, \mathbf{e}^2, ..., \mathbf{e}^d\}$, where $\mathbf{e}^\beta = \mathbf{e}_\alpha g^{\alpha\beta} = (\partial_\alpha \mathbf{\chi}) g^{\alpha\beta}$ (Ciarlet, 2013). Sometimes, we express $g_{\alpha\beta} \equiv \mathbf{g} = \mathbf{J}^T \mathbf{J}$, where $\mathbf{J} = [\mathbf{e}_1, ..., \mathbf{e}_d]$ is an $n \times d$ matrix.

Given a vector $\mathbf{v} \in \mathbb{R}^n$ it is in the tangent space $T_{\mathbf{x}}(\Gamma)$ if there exists a (contravariant) vector v^{α} such that $\mathbf{v}(\mathbf{x}) = v^{\alpha} \mathbf{e}_{\alpha} \circ \mathbf{\chi}^{-1}(\mathbf{x})$. Alternatively, one can write it in terms of a co-vector v_{α} and the contravariant basis: $\mathbf{v}(\mathbf{x}) = v_{\alpha} \mathbf{e}^{\alpha} \circ \mathbf{\chi}^{-1}(\mathbf{x})$. Moreover, any covariant (contravariant) vector $v_{\alpha}(v^{\alpha})$ has a corresponding extrinsic version given by $\mathbf{v} = v_{\alpha} \mathbf{e}^{\alpha} (\mathbf{v} = v^{\alpha} \mathbf{e}_{\alpha})$. We define the tangent bundle:

$$T(\Gamma) = \{ (\mathbf{x}, \mathbf{v}) \mid \mathbf{x} \in \Gamma, \mathbf{v}(\mathbf{x}) \in T_{\mathbf{x}}(\Gamma) \}, \tag{A.6}$$

thus, we say $\mathbf{v} \in T(\Gamma)$ if $\mathbf{v}(\mathbf{x}) \in T_{\mathbf{x}}(\Gamma)$ for every $\mathbf{x} \in \Gamma$; in this case we write $\mathbf{v} : \Gamma \to T(\Gamma)$. In addition, let $\mathbb{R}^{n \times n}$ be the space of (extrinsic) 2-tensors, and define the subset of tensors on the tangent bundle of Γ :

$$\mathsf{T} = \mathsf{T}(\Gamma) := \{ \mathbf{w} : \Gamma \to \mathbb{R}^{n \times n} \mid \mathbf{w} = w^{\alpha \beta} \mathbf{e}_{\alpha} \otimes \mathbf{e}_{\beta}, \text{ for some } w^{\mathfrak{a}\mathfrak{b}} \in \mathsf{T}^{2}(\Gamma) \}, \tag{A.7}$$

and define the set of symmetric tensors on the tangent bundle of Γ :

$$S = S(\Gamma) := \{ \mathbf{w} \in \mathsf{T}(\Gamma) \mid \mathbf{w} = w^{\alpha\beta} \mathbf{e}_{\alpha} \otimes \mathbf{e}_{\beta}, \text{ for some } w^{\mathfrak{ab}} \in \mathsf{S}^{2}(\Gamma) \}. \tag{A.8}$$

Next, we introduce extrinsic differential operators via their intrinsic counterpart, starting with the surface gradient $\nabla_{\Gamma} f: \Gamma \to T(\Gamma)$ defined in local coordinates by

$$(\nabla_{\Gamma} f) \circ \mathbf{\chi} = (\nabla_{\alpha} f) g^{\alpha \beta} \mathbf{e}_{\beta}^{T} = \partial_{\alpha} (f \circ \mathbf{\chi}) g^{\alpha \beta} (\partial_{\beta} \mathbf{\chi})^{T} \equiv \nabla (f \circ \mathbf{\chi}) g^{-1} \mathbf{J}^{T}, \tag{A.9}$$

for any differentiable function $f: \Gamma \to \mathbb{R}$. The (extrinsic) surface gradient of a tangential vector field $\mathbf{v} \in T(\Gamma)$ is $\nabla_{\Gamma} \mathbf{v} \circ \mathbf{\chi} := \mathbf{e}_{\gamma} g^{\gamma \alpha} (\nabla_{\beta} v_{\alpha}) g^{\beta \mu} \mathbf{e}_{\mu}^{T} = \mathbf{e}_{\gamma} g^{\gamma \alpha} (\partial_{\beta} v_{\alpha} - v_{\omega} \Gamma_{\alpha\beta}^{\omega}) g^{\beta \mu} \mathbf{e}_{\mu}^{T}$, so then $\nabla_{\Gamma} \mathbf{v} \in \mathsf{T}$. Moreover, $(\nabla_{\Gamma} \cdot \mathbf{v}) \circ \mathbf{\chi} := \mathrm{tr}(\nabla_{\Gamma} \mathbf{v} \circ \mathbf{\chi}) = g^{\gamma \alpha} (\nabla_{\beta} v_{\alpha}) g^{\beta \mu} \mathbf{e}_{\mu} \cdot \mathbf{e}_{\gamma} = \nabla_{\beta} (g^{\gamma \alpha} v_{\alpha}) g^{\beta \mu} g_{\mu \gamma} = \delta_{\gamma}^{\beta} (\nabla_{\beta} v^{\gamma}) = \nabla_{\gamma} v^{\gamma}$. The (covariant) surface Hessian, an element of S , is given by

$$(\nabla_{\Gamma}\nabla_{\Gamma}f) \circ \mathbf{\chi} := \mathbf{e}_{\mu}g^{\mu\alpha}[\nabla_{\alpha}\nabla_{\beta}f]g^{\beta\rho}\mathbf{e}_{\rho}^{T} = \mathbf{e}_{\mu}g^{\mu\alpha}[\partial_{\alpha}\partial_{\beta}(f \circ \mathbf{\chi}) - \partial_{\gamma}(f \circ \mathbf{\chi})\Gamma_{\alpha\beta}^{\gamma}]g^{\beta\rho}\mathbf{e}_{\rho}^{T}, \tag{A.10}$$

and using (A.3), the covariant surface divergence and double surface divergence is given by

$$(\operatorname{div}_{\Gamma} \mathbf{r}) \circ \mathbf{\chi} := \mathbf{e}_{\beta}^{T} \nabla_{\alpha} r^{\alpha \beta}, \quad (\operatorname{div}_{\Gamma} \operatorname{div}_{\Gamma} \mathbf{r}) \circ \mathbf{\chi} := \nabla_{\beta} \nabla_{\alpha} r^{\alpha \beta}, \text{ for all } \mathbf{r} \in \mathsf{T}.$$
 (A.11)

Special case of a surface. Suppose d=2 and n=3. Let $\Upsilon=\chi(Y)$, where $Y\subset U$, be a one-dimensional curve embedded in Γ , and let t be the unit tangent vector of Υ and let t be the conormal vector of Υ (t and t are both tangent to Γ). In local coordinates we have

$$t \circ \chi \Big|_{Y} = \frac{t^{\alpha} \mathbf{e}_{\alpha}}{|t^{\alpha} \mathbf{e}_{\alpha}|}, \qquad n \circ \chi \Big|_{Y} = \frac{n_{\beta} \mathbf{e}^{\beta}}{|n_{\beta} \mathbf{e}^{\beta}|},$$
 (A.12)

where $|\mathbf{a}|$ denotes the Euclidean length of the vector $\mathbf{a} \in \mathbb{R}^3$, $t^{\mathfrak{a}}$ is the (contravariant) tangent vector of Y and $n_{\mathfrak{b}}$ is the (covariant) normal vector of Y. Furthermore, let $\mathbf{v} : \Gamma \to \mathbb{R}^3$ be the surface unit normal vector of Γ , which satisfies $\mathbf{n} = \mathbf{t} \times \mathbf{v}$, Walker (2015) on $\partial \Gamma$. With the ambient space \mathbb{R}^3 available the tangent space projection $\mathbf{P} : \mathbb{R}^3 \to \mathbb{R}^3$, defined on Γ , is given by

$$P = I - v \otimes v = t \otimes t + n \otimes n, \tag{A.13}$$

and note that (in local coordinates) $Jg^{-1}J^T = P \circ \chi$ (Walker, 2015).

From Definition 4.6 we have the identity:

$$\begin{aligned} \mathbf{n}^{T}\boldsymbol{\varphi}\mathbf{n} \circ \mathbf{\chi} \Big|_{Y} &= \frac{1}{g} \left(\frac{n_{\rho} \mathbf{e}^{\rho}}{\sqrt{n_{\mu} n^{\mu}}} \right)^{T} \mathbf{e}_{\alpha} \boldsymbol{\varphi}^{\alpha \beta} \mathbf{e}_{\beta} \left(\frac{n_{\omega} \mathbf{e}^{\omega}}{\sqrt{n_{\mu} n^{\mu}}} \right) \\ &= \frac{1}{g n_{\mu} n^{\mu}} n_{\rho} \mathbf{e}^{\rho} \cdot \mathbf{e}_{\alpha} \boldsymbol{\varphi}^{\alpha \beta} \mathbf{e}_{\beta} \cdot \mathbf{e}^{\omega} n_{\omega} = \frac{1}{t_{\mu} t^{\mu}} n_{\alpha} \boldsymbol{\varphi}^{\alpha \beta} n_{\beta} = \frac{1}{|t^{\mu} \mathbf{e}_{\mu}|^{2}} n_{\alpha} \boldsymbol{\varphi}^{\alpha \beta} n_{\beta}, \end{aligned} \tag{A.14}$$

where we used $g = t^{\mu}t_{\mu}/(n^{\mu}n_{\mu})$.

A.3 Parametrization via curved element map

Recall $F_T^l: T^1 \to T^l$ from Section 4.1. It is useful to consider this map as a parametrization of T^l in the following sense. Apply a rigid rotation of coordinates \mathbf{x} to \mathbf{x}' so that $T^s \to T^{s'}$ (for any s) and $T^{1'} \subset \mathbb{R}^2$. In the rotated coordinates we view $\mathbf{F}_T^{l'}$ as a function of two variables, so that $(T^{1'}, \mathbf{F}_T^{l'})$ is a local chart for $T^{l'}$. Next, let $\mathbf{J}' = [\partial_1 \mathbf{F}_T^{l'}, \partial_2 \mathbf{F}_T^{l'}]$ be the 3×2 Jacobian matrix with induced metric $\mathbf{g}' = (\mathbf{J}')^T \mathbf{J}'$. In addition, define the 3×2 matrix $\mathbf{P}_{\mathbf{x}}^{l'} = [\mathbf{a}_1, \mathbf{a}_2]$, where $\{\mathbf{a}_1, \mathbf{a}_2, \mathbf{a}_3\}$ are the canonical basis vectors of \mathbb{R}^3 , $(\mathbf{P}_{\mathbf{x}}^{l'})^T \mathbf{P}_{\mathbf{x}}^{l'} = \mathbf{I}_2$, and $\mathbf{P}_{\mathbf{x}}^{l'} (\mathbf{P}_{\mathbf{x}}^{l'})^T = \mathbf{P}^{l'} := \mathbf{I}_3 - \mathbf{\bar{v}}' \otimes \mathbf{\bar{v}}'$, where $\mathbf{\bar{v}}' \equiv \mathbf{a}_3$ is the unit normal of $T^{1'}$.

All results derived in the rotated coordinates can be mapped back to the original coordinates. For example, let $\bar{P}_{\star} = [\mathbf{b}_1, \mathbf{b}_2]$, where \mathbf{b}_1 , \mathbf{b}_2 are any two orthogonal unit vectors in \mathbb{R}^3 pointing in the plane of T^1 , and note that $\bar{P}_{\star}^T \bar{P}_{\star} = I_2$, and $\bar{P}_{\star} \bar{P}_{\star}^T = \bar{P} := I_3 - \bar{\mathbf{v}} \otimes \bar{\mathbf{v}}$ (see (A.13)), where $\bar{\mathbf{v}} = \mathbf{b}_1 \times \mathbf{b}_2$ is the unit normal of T^1 . Then, $J = (\nabla_{T^1} F_T^1) \bar{P}_{\star}$, $g = J^T J$, and by (4.3),

$$|J - \bar{P}_{\star}| = O(h), \quad g = \bar{P}_{\star}^T \bar{P}^T \bar{P} \bar{P}_{\star} + O(h) = I_2 + O(h),$$
 (A.15)

so \mathbf{g} is invertible for h sufficiently small. Note that, in terms of \mathbf{F}_T^l , the surface gradient (A.9) of $f: T^l \to \mathbb{R}$ can be written as $(\nabla_{T^l} f) \circ \mathbf{F}_T^l = (\nabla_{T^l} \bar{f}) \bar{\mathbf{P}}_{\star} \mathbf{g}^{-1} \mathbf{J}^T$, where $\bar{f} := f \circ \mathbf{F}_T^l$.

A.4 Technical estimates

By elementary geometry we have the following estimate.

LEMMA A.1 Let **a**, **b** be *unit* vectors, with respect to the Euclidean norm, in \mathbb{R}^n . If $|\mathbf{a} - \mathbf{b}| = \gamma \leq \sqrt{2}$ then $|(\mathbf{a} - \mathbf{b}) \cdot \mathbf{b}| \leq (3/4)\gamma^2$.

LEMMA A.2 Let $T \in \mathcal{T}_h$ with unit conormal n, and unit tangent t, vectors (in \mathbb{R}^3) defined on ∂T . Suppose $m > l \geqslant 1$ and consider the corresponding elements $T^m \in \mathcal{T}_h^m$, $T^l \in \mathcal{T}_h^l$ and $T^1 \in \mathcal{T}_h^l$, i.e. $T^s = \mathbf{F}_T^s(T^1)$, for any $m \geqslant s \geqslant 1$ or $s = \infty$ (recall the discussion in Section 4.1). Let $\mathbf{J} = (\nabla_{T^1} \mathbf{F}_T) \bar{\mathbf{P}}_{\star}$,

 $\mathbf{g} = \mathbf{J}^T \mathbf{J}$ and recall (4.4) and the notation introduced there. Then, on T^1 , the following holds

$$\begin{split} \left[(\tilde{\boldsymbol{n}} \circ \boldsymbol{F}_{T}^{m}) - (\hat{\boldsymbol{n}} \circ \boldsymbol{F}_{T}^{l}) \right] \cdot (\tilde{\boldsymbol{n}} \circ \boldsymbol{F}_{T}^{m}) &= O(h^{2l}), \\ \left[(\tilde{\boldsymbol{n}} \circ \boldsymbol{F}_{T}^{m}) - (\hat{\boldsymbol{n}} \circ \boldsymbol{F}_{T}^{l}) \right]^{T} (\tilde{\boldsymbol{P}} \circ \boldsymbol{F}_{T}^{m}) &= \beta \tilde{\boldsymbol{t}}^{T} \tilde{\boldsymbol{P}} + O(h^{2l}) = O(h^{l}), \\ \bar{\boldsymbol{n}}^{T} (\tilde{\boldsymbol{J}} \tilde{\boldsymbol{g}}^{-1} - \hat{\boldsymbol{J}} \hat{\boldsymbol{g}}^{-1}) \bar{\boldsymbol{P}}_{\star}^{T} &= -[\tilde{\boldsymbol{n}} \cdot \nabla_{T^{1}} (\boldsymbol{F}_{T}^{m} - \boldsymbol{F}_{T}^{l})]^{T} \tilde{\boldsymbol{P}} + O(h^{l+1}) = O(h^{l}), \end{split}$$
(A.16)

where $\beta = [(\tilde{t} - \hat{t}) \times v] \cdot \tilde{t}$, $|\beta| = O(h^l)$ and β is continuous across edges of the mesh. Furthermore,

$$(\tilde{\boldsymbol{n}} \circ \boldsymbol{F}_{T}^{m})^{T} \tilde{\boldsymbol{J}} \tilde{\boldsymbol{g}}^{-1} \bar{\boldsymbol{P}}_{\star}^{T} - (\hat{\boldsymbol{n}} \circ \boldsymbol{F}_{T}^{l})^{T} \hat{\boldsymbol{J}} \hat{\boldsymbol{g}}^{-1} \bar{\boldsymbol{P}}_{\star}^{T}$$

$$= \beta \bar{\boldsymbol{t}}^{T} \bar{\boldsymbol{P}} - [\bar{\boldsymbol{n}} \cdot \nabla_{T^{1}} (\boldsymbol{F}_{T}^{m} - \boldsymbol{F}_{T}^{l})]^{T} \bar{\boldsymbol{P}} + O(h^{l+1}) = O(h^{l}), \qquad (A.17)$$

$$(\tilde{\boldsymbol{n}} \circ \boldsymbol{F}_{T}^{m})^{T} \tilde{\boldsymbol{J}} \tilde{\boldsymbol{g}}^{-1} \bar{\boldsymbol{P}}_{\star}^{T} - \bar{\boldsymbol{n}}^{T} = O(h) \boldsymbol{c}^{T} \bar{\boldsymbol{P}} + O(h^{2}), \text{ where } \boldsymbol{c} \in \mathbb{R}^{3} \text{ with } |\boldsymbol{c}| = 1.$$

Proof. Referring to Section A.3 we rotate coordinates so that $T^1 \subset \mathbb{R}^2$ and we simplify notation by dropping '. We also abuse notation and write $\tilde{\boldsymbol{n}} \equiv \tilde{\boldsymbol{n}} \circ \boldsymbol{F}_T^m$ and $\hat{\boldsymbol{n}} \equiv \hat{\boldsymbol{n}} \circ \boldsymbol{F}_T^l$. From (A.12) we have that $\tilde{\boldsymbol{n}} = \tilde{\boldsymbol{J}} \tilde{\boldsymbol{g}}^{-1} \bar{\boldsymbol{F}}_{\star}^{} \bar{\boldsymbol{n}} / |\tilde{\boldsymbol{J}} \tilde{\boldsymbol{g}}^{-1} \bar{\boldsymbol{F}}_{\star}^{} \bar{\boldsymbol{n}}|$ (note that $\bar{\boldsymbol{n}} \cdot \mathbf{a}_3 = 0$).

The first line of (A.16) follows immediately from (4.4) and Lemma A.1. Next, note that $\tilde{J}\tilde{g}^{-1}\tilde{J}^T = \tilde{P} \circ F_T^m \equiv \tilde{P} = I_3 - \tilde{v} \otimes \tilde{v}$ (see (A.13)), i.e. the tangent space projection onto T^m , where $\tilde{v} \equiv \tilde{v} \circ F_T^m$ is the unit normal vector of T^m . Estimating $\mathbf{w}_1^T := (\tilde{\mathbf{n}} - \hat{\mathbf{n}})^T \tilde{P}$ gives $\mathbf{w}_1^T = O(h^{2l}) + [(\tilde{\mathbf{n}} - \hat{\mathbf{n}}) \cdot \tilde{\mathbf{n}}]\tilde{\mathbf{n}}^T \bar{P} + [(\tilde{\mathbf{n}} - \hat{\mathbf{n}}) \cdot \tilde{t}]\tilde{t}^T \bar{P} = O(h^{2l}) + [(\tilde{\mathbf{n}} - \hat{\mathbf{n}}) \cdot \tilde{t}]\tilde{t}^T \bar{P}$, where we used the first line of (A.16). Moreover,

$$(\tilde{n} - \hat{n}) \cdot \tilde{t} = (\tilde{t} \times \tilde{v} - \hat{t} \times \hat{v}) \cdot \tilde{t} = [(\tilde{t} - \hat{t}) \times \hat{v}] \cdot \tilde{t}$$

$$= [(\tilde{t} - \hat{t}) \times v] \cdot \tilde{t} + [(\tilde{t} - \hat{t}) \times (\hat{v} - v)] \cdot \tilde{t} = \beta + O(h^{2l}), \tag{A.18}$$

where $\beta := [\tilde{t} - \hat{t}) \times v] \cdot \tilde{t}$ (and $\beta = O(h^l)$), and we used (4.4); hence, $w_1^T = \beta \tilde{t}^T \bar{P} + O(h^{2l}) = \beta \tilde{t}^T \bar{P} + O(h^{l+1})$ so we obtain the second line of (A.16). Also note that β is *continuous* across element boundaries.

Next, let
$$\mathbf{w}_{2}^{T} := \bar{\mathbf{n}}^{T} (\tilde{\mathbf{J}} \tilde{\mathbf{g}}^{-1} - \hat{\mathbf{J}} \hat{\mathbf{g}}^{-1}) \bar{\mathbf{P}}_{\star}^{T}$$
 and estimate
$$\mathbf{w}_{2}^{T} = \bar{\mathbf{n}}^{T} (\tilde{\mathbf{J}} \tilde{\mathbf{g}}^{-1} - \bar{\mathbf{P}}_{\star}) \bar{\mathbf{P}}_{\star}^{T} - \bar{\mathbf{n}}^{T} (\hat{\mathbf{J}} \hat{\mathbf{g}}^{-1} - \bar{\mathbf{P}}_{\star}) \bar{\mathbf{P}}_{\star}^{T}$$

$$= \bar{\mathbf{n}}^{T} \bar{\mathbf{P}}_{\star} (\bar{\mathbf{P}}_{\star}^{T} - \tilde{\mathbf{J}}^{T}) \tilde{\mathbf{J}} \tilde{\mathbf{g}}^{-1} \bar{\mathbf{P}}_{\star}^{T} - \bar{\mathbf{n}}^{T} \bar{\mathbf{P}}_{\star} (\bar{\mathbf{P}}_{\star}^{T} - \hat{\mathbf{J}}^{T}) \hat{\mathbf{J}} \hat{\mathbf{g}}^{-1} \bar{\mathbf{P}}_{\star}^{T}$$

$$= \bar{\mathbf{n}}^{T} \bar{\mathbf{P}}_{\star} (\bar{\mathbf{P}}_{\star}^{T} - \tilde{\mathbf{J}}^{T}) \hat{\mathbf{J}} \hat{\mathbf{g}}^{-1} \bar{\mathbf{P}}_{\star}^{T} - \bar{\mathbf{n}}^{T} \bar{\mathbf{P}}_{\star} (\bar{\mathbf{P}}_{\star}^{T} - \hat{\mathbf{J}}^{T}) \hat{\mathbf{J}} \hat{\mathbf{g}}^{-1} \bar{\mathbf{P}}_{\star}^{T}$$

$$+ \bar{\mathbf{n}}^{T} \bar{\mathbf{P}}_{\star} (\bar{\mathbf{P}}_{\star}^{T} - \tilde{\mathbf{J}}^{T}) \hat{\mathbf{J}} \hat{\mathbf{g}}^{-1} \bar{\mathbf{P}}_{\star}^{T} + O(h^{l+1}) = \bar{\mathbf{n}}^{T} \bar{\mathbf{P}}_{\star} (\hat{\mathbf{J}}^{T} - \tilde{\mathbf{J}}^{T}) \bar{\mathbf{P}}_{\star} \bar{\mathbf{P}}_{\star}^{T} + O(h^{l+1}), \quad (A.19)$$

where we used (4.3) and (A.15). Again, referring to Section A.3 we find that

$$\mathbf{w}_{2}^{T} = \bar{\mathbf{n}}^{T} [\nabla_{T^{1}} (\mathbf{F}_{T}^{l} - \mathbf{F}_{T}^{m})]^{T} \bar{\mathbf{P}} + O(h^{l+1}), \tag{A.20}$$

so we obtain the third line of (A.16).

As for (A.17) let $\mathbf{z}^T = \tilde{\mathbf{n}}^T \tilde{\mathbf{J}} \tilde{\mathbf{g}}^{-1} \bar{\mathbf{P}}_{\star}^T - \hat{\mathbf{n}}^T \hat{\mathbf{J}} \hat{\mathbf{g}}^{-1} \bar{\mathbf{P}}_{\star}^T$, where $\mathbf{z} \in \mathbb{R}^3$, and expand:

$$\begin{split} \boldsymbol{z}^{T} &= (\tilde{\boldsymbol{n}} - \hat{\boldsymbol{n}})^{T} \tilde{\boldsymbol{J}} \tilde{\boldsymbol{g}}^{-1} \bar{\boldsymbol{P}}_{\star}^{T} + \hat{\boldsymbol{n}}^{T} (\tilde{\boldsymbol{J}} \tilde{\boldsymbol{g}}^{-1} - \hat{\boldsymbol{J}} \hat{\boldsymbol{g}}^{-1}) \bar{\boldsymbol{P}}_{\star}^{T} \\ &= (\tilde{\boldsymbol{n}} - \hat{\boldsymbol{n}})^{T} \tilde{\boldsymbol{J}} \tilde{\boldsymbol{g}}^{-1} \tilde{\boldsymbol{J}}^{T} \bar{\boldsymbol{P}}_{\star} \bar{\boldsymbol{P}}_{\star}^{T} + (\tilde{\boldsymbol{n}} - \hat{\boldsymbol{n}})^{T} \tilde{\boldsymbol{J}} \tilde{\boldsymbol{g}}^{-1} (\bar{\boldsymbol{P}}_{\star}^{T} - \tilde{\boldsymbol{J}}^{T}) \bar{\boldsymbol{P}}_{\star} \bar{\boldsymbol{P}}_{\star}^{T} \\ &+ (\hat{\boldsymbol{n}} - \bar{\boldsymbol{n}})^{T} (\tilde{\boldsymbol{J}} \tilde{\boldsymbol{g}}^{-1} - \hat{\boldsymbol{J}} \hat{\boldsymbol{g}}^{-1}) \bar{\boldsymbol{P}}_{\star}^{T} + \bar{\boldsymbol{n}}^{T} (\tilde{\boldsymbol{J}} \tilde{\boldsymbol{g}}^{-1} - \hat{\boldsymbol{J}} \hat{\boldsymbol{g}}^{-1}) \bar{\boldsymbol{P}}_{\star}^{T} =: \boldsymbol{w}_{1}^{T} \bar{\boldsymbol{P}} + \boldsymbol{z}_{1}^{T} + \boldsymbol{z}_{2}^{T} + \boldsymbol{w}_{2}^{T}. \end{split} \tag{A.21}$$

Since $|z_1| = O(h^{l+1}) = |z_2|$ combining with the above results yields the first line of (A.17).

Now set l = 1, so that the first line of (A.17) simplifies to

$$\tilde{\boldsymbol{n}}^T \tilde{\boldsymbol{J}} \tilde{\boldsymbol{g}}^{-1} \bar{\boldsymbol{P}}_{\star}^T - \bar{\boldsymbol{n}}^T \bar{\boldsymbol{P}}_{\star} \bar{\boldsymbol{P}}_{\star}^T = \beta \bar{\boldsymbol{t}}^T \bar{\boldsymbol{P}} - [\bar{\boldsymbol{n}} \cdot \nabla_{T^1} (\boldsymbol{F}_T^m - \boldsymbol{F}_T^1)]^T \bar{\boldsymbol{P}} + O(h^2), \tag{A.22}$$

and note that $\bar{\boldsymbol{n}}^T \bar{\boldsymbol{P}}_{\star} \bar{\boldsymbol{P}}_{\star}^T = \bar{\boldsymbol{n}}^T$. Since $|\beta| = O(h)$, and $|\nabla_{T^1} (\boldsymbol{F}_T^m - \boldsymbol{F}_T^1)| = O(h)$, we get the second line of (A.17).

A.5 Discrete inf-sup condition

The discrete inf-sup condition for the HHJ method was proved for flat polygonal domains in Blum & Rannacher (1990, pf. of Lem. 5.1). Their proof readily extends to piecewise linear surface triangulations, mutatis mutandis (which we omit). The final result we need is as follows.

LEMMA A.3 Assume Γ^1 is a piecewise linear triangulation in \mathbb{R}^3 that interpolates a surface Γ satisfying the conditions in Section 3.1. Then,

$$\sup_{\varphi \in V_h^1} \frac{|b_h^1(\varphi, v)|}{\|\varphi\|_{0,h,1}} \geqslant C_0 \|v\|_{2,h,1}, \quad \forall v \in W_h^1, \ \forall h > 0, \tag{A.23}$$

holds for any degree $r \ge 0$, where $C_0 > 0$ is independent of h.